AD-A095 366 VISIDYNE INC BURLINGTON MASS F/G 4/1
BALLOONBORNE LIDAR EXPERIMENT.(U)
DEC 80 O SHEPHERD, G AURILIO, R O BUCKNAM F19628-80-C-0094
UNCLASSIFIED VI-577 AFGL-TR-80-0373 NL

1 OF 2
AD A
095366

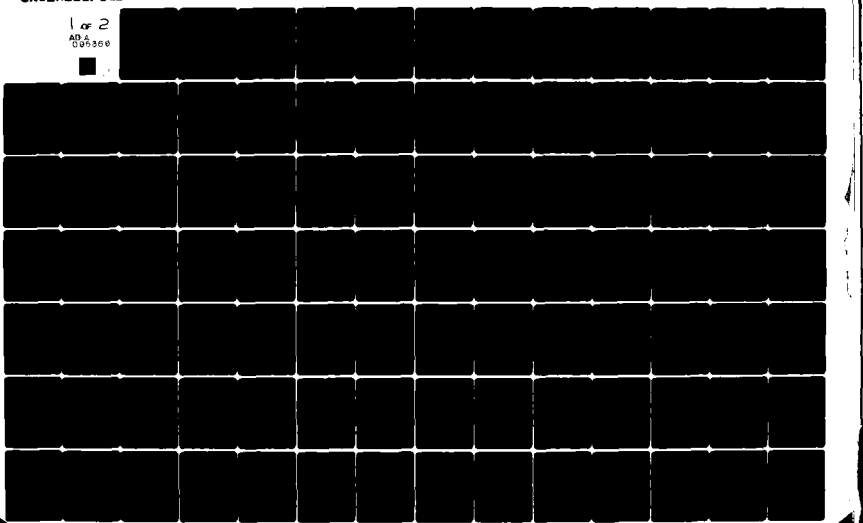

LEVEL II

AFGL-TR-80-0373

BALLOONBORNE LIDAR EXPERIMENT

O. Shepherd
G. Aurilio
R.D. Bucknam
R.W. Brooke
A.G. Hurd
T.F. Zehnpfennig

Visidyne, Inc.
5 Corporate Place
South Bedford Street
Burlington, Massachusetts 01803

24 December 1980

Final Report
9 June 1980 - 9 December 1980

Approved for public release; distribution unlimited

DTIC
ELECTE
FEB 23 1981
S
A

DTIC FILE COPY

AIR FORCE GEOPHYSICS LABORATORY
AIR FORCE SYSTEMS COMMAND
UNITED STATES AIR FORCE
HANSCOM AFB, MASSACHUSETTS 01731

81 2 23 006

Qualified requestors may obtain additional copies from the Defense Technical Information Center. All others should apply to the National Technical Information Service.

UNCLASSIFIED

SECURITY CLASSIFICATION OF THIS PAGE (When Data Entered)

19 REPORT DOCUMENTATION PAGE	READ INSTRUCTIONS BEFORE COMPLETING FORM
1. REPORT NUMBER: AFGL-TR-80-0373 (18)	2. GOVT ACCESSION NO.: AD-A093
	3. RECIPIENT'S CATALOG NUMBER: 366
4. TITLE (and Subtitle): BALLOONBORNE LIDAR EXPERIMENT	5. TYPE OF REPORT & PERIOD COVERED: Final Report, 9 June 1980-9 December 1980
	6. PERFORMING ORG. REPORT NUMBER: VI-577
7. AUTHOR(s): O./Shepherd, R.W./Brooke, G./Aurilio, A.G./Hurd, R.D./Bucknam, T.F. Zehnpfennig (10)	8. CONTRACT OR GRANT NUMBER(s): F19628-80-C-0094
9. PERFORMING ORGANIZATION NAME AND ADDRESS: Visidyne, Inc., 5 Corporate Place, South Bedford Street, Burlington, Massachusetts 01803 (16)	10. PROGRAM ELEMENT, PROJECT, TASK AREA & WORK UNIT NUMBERS: 62101F, 669004AD (17)
11. CONTROLLING OFFICE NAME AND ADDRESS: Air Force Geophysics Laboratory, Hanscom AFN, Massachusetts 01731, Monitor/Donald E. Bedo/LKO (11)	12. REPORT DATE: December 1980
	13. NUMBER OF PAGES: 128 (12)
14. MONITORING AGENCY NAME & ADDRESS (if different from Controlling Office)	15. SECURITY CLASS. (of this report): Unclassified
	15a. DECLASSIFICATION/DOWNGRADING SCHEDULE

16. DISTRIBUTION STATEMENT (of this Report)

Approved for public release; distribution unlimited.

17. DISTRIBUTION STATEMENT (of the abstract entered in Block 20, if different from Report)

18. SUPPLEMENTARY NOTES

19. KEY WORDS (Continue on reverse side if necessary and identify by block number)

Lidar	Neodymium:YAG Laser
Balloonborne Payload	Rayleigh Scattering
Atmospheric Density	Aerosol Scattering

20. ABSTRACT (Continue on reverse side if necessary and identify by block number)

The object of this contract was to design a balloonborne lidar experiment capable of performing nightime atmospheric density measurements in the 10 to 40 km altitude domain with a resolution of 100 meters. The payload includes a frequency-tripled Nd:YAG laser with outputs at 353 and 1064 nm, a telescoped receiver with PMT detectors, a command-controlled optical pointing system, and support systems, including thermal control, telemetry, command, and power. Density measurements would be made using the back-

DD FORM 1 JAN 73 1473 EDITION OF 1 NOV 65 IS OBSOLETE

SECURITY CLASSIFICATION OF THIS PAGE (When Data Entered)

20. ABSTRACT

scattered 353 nm radiation data with aerosol corrections obtained from 1064 nm radiation scatterings.

TABLE OF CONTENTS

TABLE OF CONTENTS (Cont.)

LIST OF ILLUSTRATIONS

LIST OF ILLUSTRATIONS (Cont.)

LIST OF TABLES

LIST OF TABLES (Cont.)

1.0 INTRODUCTION

The objective of this contract was to design a balloonborne lidar experiment capable of performing nighttime atmospheric density measurements in the 10 km to 40 km altitude domain with a resolution of 100 meters.

From the balloonborne lidar system, density measurements would be made by measuring the backscattered 353 nm radiation from a frequency-tripled 1064 nm Nd:YAG laser. Aerosol corrections would be obtained by measurement of the 1064 nm backscattering.

The experiment payload will consist of the following:

1. A frequency-tripled Nd:YAG laser.
2. A telescoped receiver with 353 nm and 1064 nm detectors.
3. A command-controlled optical pointing system.
4. A payload thermal control system.
5. Telemetry, command, and power systems to support the experiment.
6. A payload structure.

The experiment plan provides for the balloonborne payload to be launched during early evening from a site west of White Sands Missile Range (WSMR). As the balloon drifts toward the range, upward looking data will be acquired above 15 km and horizontal look data acquired above 20 km. When the balloon is over the range and above 30 km, downward looking data will be acquired. When the balloon drifts out of the eastern border of the range, horizontal or upward viewing will be resumed.

The experiment design presented is complete in that all systems and their operations are fully specified. This design consists of:

1. The development of a balloon launch and experiment operation plan.
2. Estimates of signal and background count rates using computer simulation.
3. The establishment of environmental specifications pertaining to the experiment hardware.
4. The definition of eye safety criteria with respect to in-flight use.

PRECEDING PAGE BLANK-NOT FILMED

5. The experiment configurations and payload structural layout.

6. The specification of a Nd:YAG laser and the design of the required housings and support electronics.

7. The specification of the receiver detectors and the associated cryogenic system, the design of a telescope and optics, and the design of a PCM data system.

8. Design of a ground controlled pointing mirror.

9. Specification of a cloud monitor.

10. The design of an active thermal control system.

11. The design of the payload electronics.

12. The listing of required ground support equipment.

13. The development of system test procedures.

Items that require additional engineering are the following:

1. The payload structure has been designed consistent with lidar system configuration and balloon environmental specifications. Before fabrication of the payload structure is initialized, it is recommended that a detailed stress analysis be performed. In addition, a thermal analysis of the structure is required to quantify optical alignment tolerances. The assembly of a 1/4 scale model of the payload would provide an excellent look at the structured design.

2. Mounting brackets and clamps for the various system components have not been detailed.

3. The electronic designs, thermal control system design, and receiver optics design are presented in the form of specifications. Packaging for these systems remains to be designed.

4. The payload cabling has been considered but wire run lists and connector specifications will be required prior to fabrication.

5. Engineering change orders may be required for the above if there are interface revisions with respect to procured components.

2.0 EXPERIMENT SCENARIO

The requirement for low background levels in the two spectral bands of interest dictates that the data flights be night flights. Thus the balloon launch (Figure 2.1) would be scheduled for around sunset. The selection of a launch time will depend upon both the low level ground wind conditions, wind shear, and high altitude winds. It is desirable to keep the payload flight path over the controlled airspace of WSMR for as much of the flight as possible. Thus, low velocity winds will be a launch criterion. As long as the payload is over the controlled airspace, the lidar can be directed downward. This will provide the most complete density distribution data (Ref. Section 3.0).

Launching the payload from Holloman AFb and having the lidar system over the restricted area of WSMR when float altitude is reached is highly improbable. This is due to the time it takes to reach float altitude and wind effects on the balloon during ascent. Also, the predictability of the wind velocity at 100,000 feet during the "turnaround" period (winds light and variable, 0-5 knots), is only ±10 knots. In other words, although the wind at 100,000 feet might be predicted to be from the west at 5 knots, when the payload reached float altitude, the wind might be from the east at 5 knots.

For the above reasons, it is suggested that the lidar payload be launched using a five million cubic feet balloon system from a launch area near Truth or Consequences, New Mexico. Because the lidar will operate at nighttime, the launch will occur near sundown. Fall is the optimum time of year for low surface winds in the evening. The payload system will collect and transmit data during the nighttime hours. At sunrise payload recovery operations will begin.

Truth or Consequences is about twenty miles to the west of the western edge of WSMR. The reason for launching from this site is to enable the payload to reach operational altitude while still over the restricted area of WSMR as shown in Figure 2.2.

Launch should take place when the winds at 100,000 to 140,000 feet are predicted to be from the west at 15-20 knots. Upper atmospheric winds of at least this speed are quite steady and predictable.

The balloon will be launched with the lidar in standby mode. When an altitude of 15 km has been attained, the baroswitch will be opened permitting the laser to be armed, in preparation for firing, by an uplinked command.

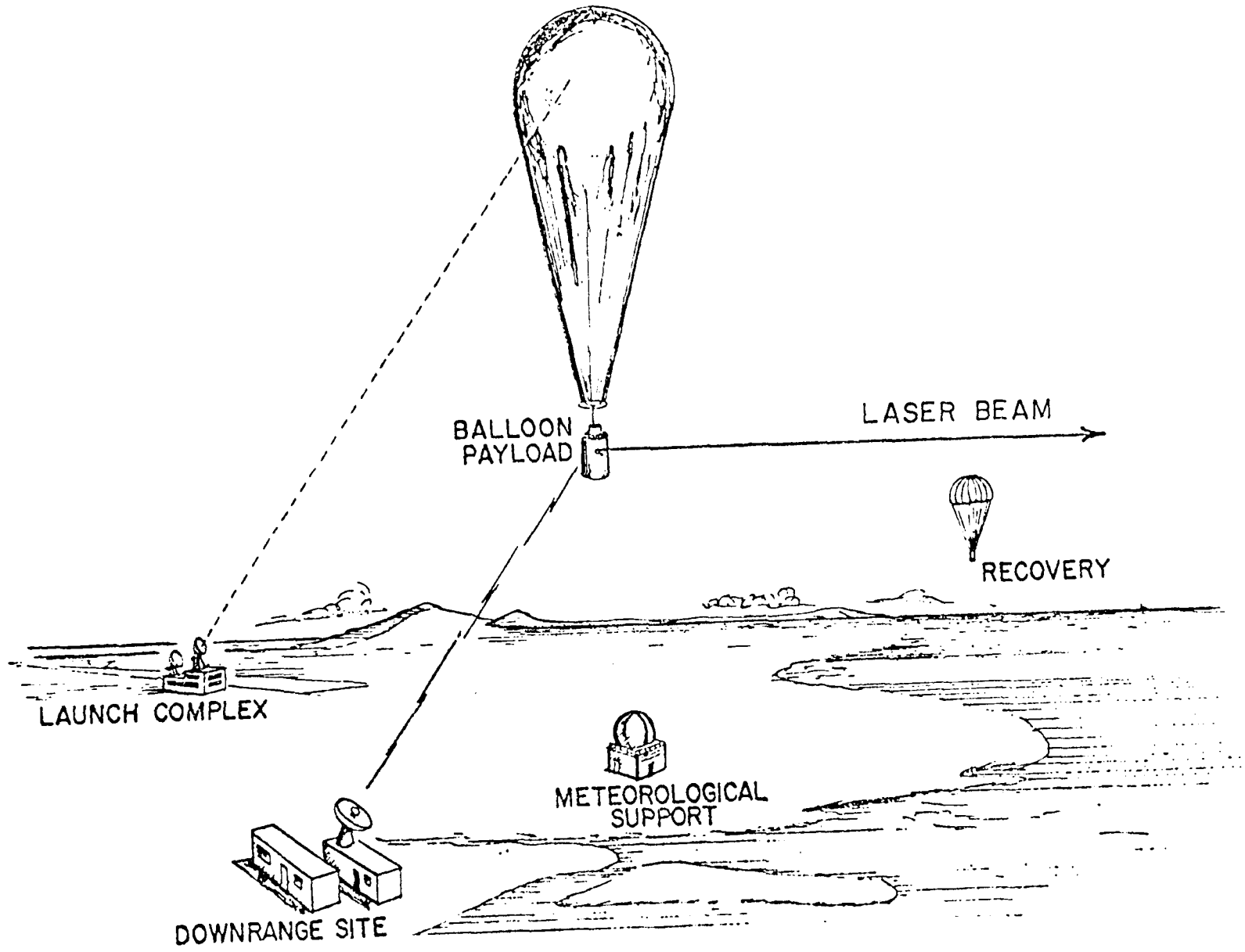

Figure 2.1 Balloonborne Lidar Experiment

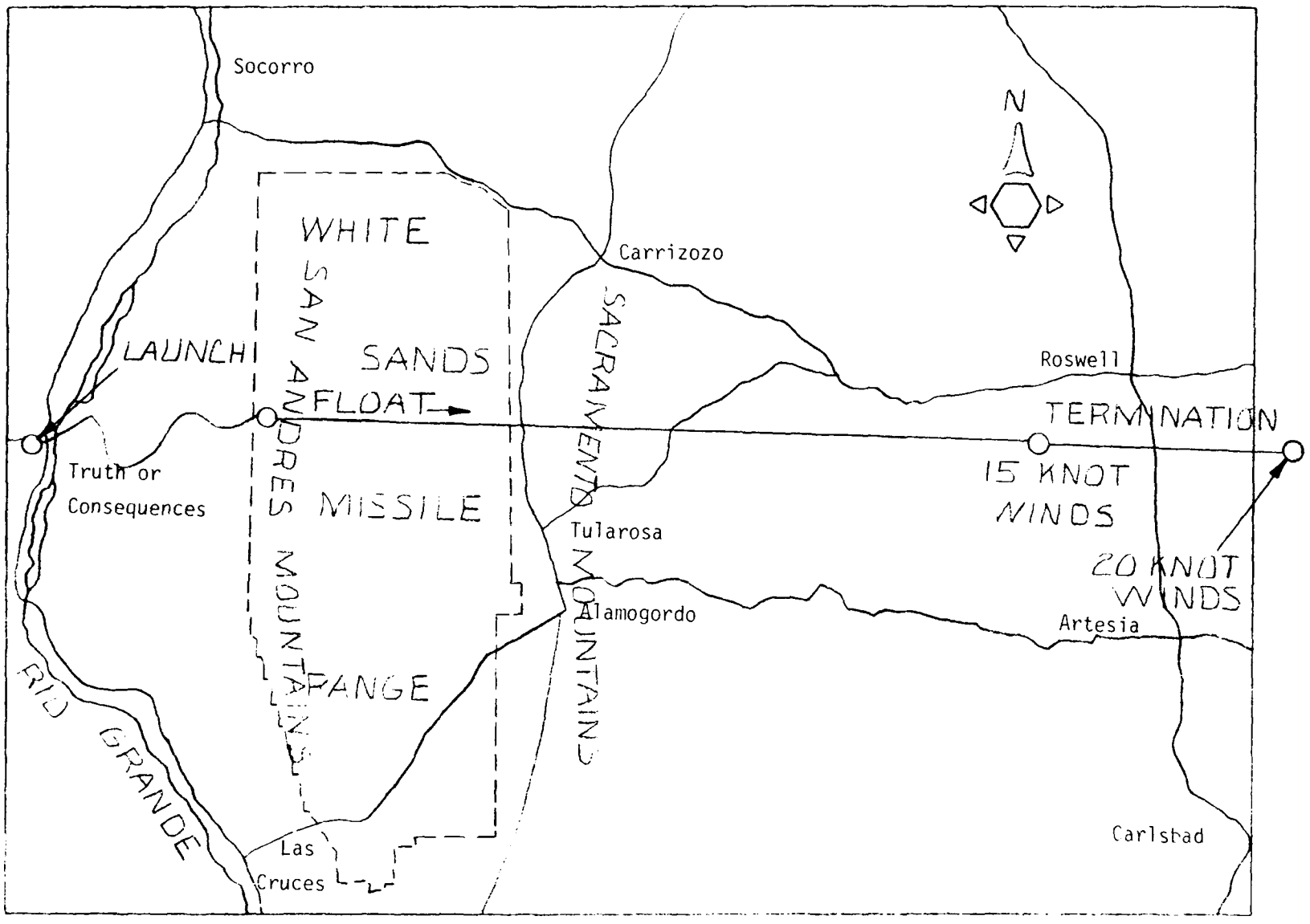

Figure 2.2 Lidar Experiment Flight Plan

From 15 km to 20 km laser firing will be limited to upwards only (30° from zenith). From 20 km to 30 km, horizontal (90°) and upwards laser pointing angles can be utilized. Only when the payload is above 30 km and over controlled ground space (WSMR) will the lidar be operated pointing downward. Data acquisition will continue until it appears that the payload is drifting out of the controlled airspace. At that time, the laser will be turned off and the pointing mirror rotated so that the laser beam will be aligned with the local horizontal. Data acquisition will then resume with the laser being fired continuously.

After a mission operating time of approximately 6 hours, the lidar system will be turned off and the pointing mirror system slewed into a stow configuration. Flight termination will require daylight conditions. The balloon will be valved down to lower altitudes (~80,000 ft) and the balloon ruptured on command. The payload parachute will open and the payload will drift down and impact on the ground. An on-board beacon transmitter will guide a search helicopter to the downed payload and experiment project personnel will land and inspect the payload to determine that it is in a non-hazardous condition. The payload will then be airlifted by helicopter back to the payload build-up area.

During the time of flight, other experiment personnel will be in the balloon mission control center evaluating data quality and instrument performance from the real time read-out of the raw telemetry data. In addition the lidar experiment data will be displayed in real time to provide experiment personnel with sufficient data to permit a preliminary evaluation of the mission's scientific success.

2.1 Ranging and Navigation

The payload is maintained under constant observation by the ranging system. This system determines slant range from the payload to the ground control station, and elevation and azimuth angles. These data are inputted to a computer on the ground where range, elevation, and azimuth are transformed into map coordinates on a plotting table. Figure 2.3 indicates a typical ranging system.

From a series of plotting table coordinates, the payload velocity and direction of drift may be calculated. These functions can also be made available directly from the ranging system.

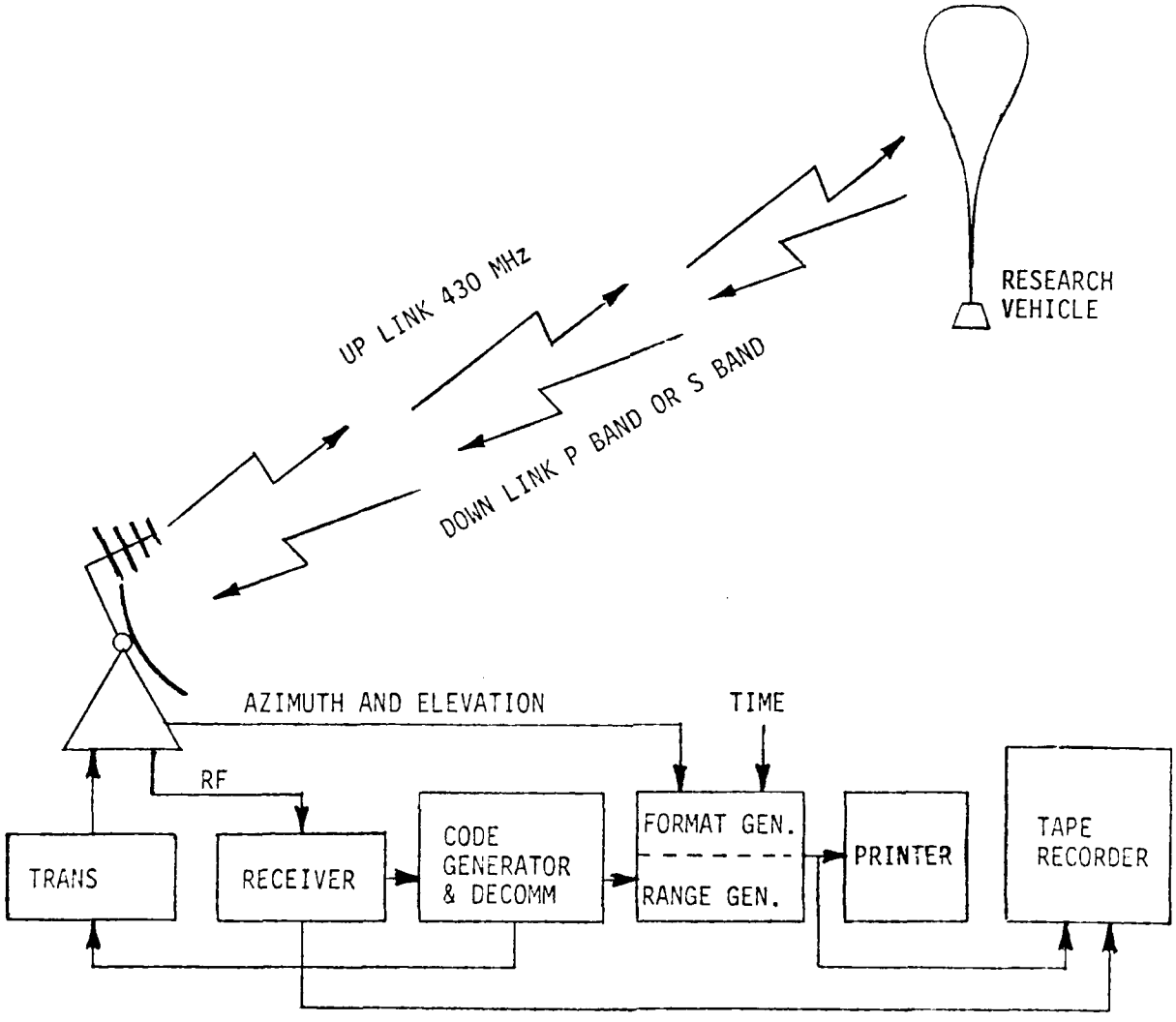

Figure 2.3 Typical Ranging System

2.2 Launch/Recovery Operations

2.2.1 Launch - Balloon payload launch techniques vary with geographical and meterological conditions, but all represent attempts to minimize the effect of winds and dynamic loading on the balloon during inflation and launching.

When there is no surface wind, ideal conditions prevail, and a "zero-wind" ground launch method may be employed. The balloon is inflated while vertically deployed and there is no chance of developing "sail effects".

In reality, however, wind is usually present, so the dynamic ground launch technique is used in wind speeds to 15 knots. Its principal aim is to expose to the wind as little of the balloon as possible by running its top part under a restraining roller arm which can be installed on a variety of vehicles. Inflation of the balloon is an extremely important step and must be carried out precisely according to plan, or failure will occur. The balloon must be handled very carefully while it is being laid out and inflated to prevent abrasions or stresses to the material.

To inflate the balloon, helium is run through the supply hose to a diffuser where its pressure is reduced, then through an inflation tube attached to the upper section of the balloon. Only that part of the balloon that has gone under the roller arm is inflated. The remainder of the balloon is still laid out on the ground on a protective cloth. The amount of helium must be sufficient to create a lifting force equal to the system weight plus free lift. If the amount of free lift is too small, the system could fail either to rise or reach its ceiling altitude. If too much free lift is provided, the ascent velocity may increase to the point of causing the balloon to burst.

As the helium bubble expands, the payload carrying vehicle moves forward, causing more of the balloon to rise above the roller arm. The balloon rises quickly and is pushed forward by the existing winds. The payload is still attached to the launch vehicle. As the balloon swings into its overhead arc, the launch vehicle moves along with the system to the point where the balloon is stretched to its maximum length and is aligned vertically over the payload. The final launch release is then made and the payload is lifted from its cradle with just enough vertical acceleration to ensure its safety from obstacles as it moves downwind.

2.2.2 Float - When the payload reaches an altitude of about 100,000 feet, it is considered to be at float altitude. The amount of time spent at float altitude will depend largely on the direction and speed of the wind at 100,000 feet and the weather conditions at the planned recovery area. The time at float altitude may be extended or shortened, depending on these conditions. Table 2-1 gives the maximum disturbances at float altitude to the payload based on statistical data from many flights.

2.2.3 Recovery - The point where recovery is initiated is determined by a computer-calculated trajectory from 100,000 feet to ground level. The calculations take into account the wind velocities at the various altitudes. Recovery is initiated by releasing helium from the balloon such that the payload altitude is reduced to about 80,000 feet. At this altitude, the balloon is released and the payload descends on the parachute. When the balloon release actuates, panels are torn from the balloon, destroying it so that it will not be a hazard to aviation. On landing, impact switches are triggered releasing the parachute so that the ground winds will not drag the payload.

TABLE 2-1

MAXIMUM DISTURBANCES AT FLOAT ALTITUDE

CONDITION	MOTION	ACCELERATION	VELOCITY
1) Payload Spin Rate	360° in 4 minutes	---	---
2) Wind Turbulence	From 30-35 mph in a few minutes (Assume 2 min.)	Horizontal $\pm.06'/sec^2$ ($\pm.002$ g)	Horizontal (Average) $\Delta V = 7.33'/sec$
3) Vertical Movement	200-300 feet over minutes	Vertical $\pm 1/100$ g	Vertical $\pm 7.85'/sec$
4) Pendular Movement for 300' Cable	Amplitude .1° or $\pm.25$ feet	Horizontal 8.4×10^{-4} g	Horizontal $\pm.087'/sec$

3.0 SIGNAL AND BACKGROUND MEASUREMENTS

The basic scattering geometry of the Balloonborne Lidar Experiment System for measurements of atmospheric density is shown in Figure 3.1. The balloon floats at an altitude h_o as laser pulses are fired into the atmosphere at a zenith angle θ. The laser pulse propagates through the atmosphere and in each volume element, $\delta V = \Omega_L D^2 \delta D$, a small fraction of the photons are Rayleigh scattered by air molecules or suffer other scatterings and absorptions due to aerosols and other constituents. For each laser pulse, the number of photons from δV that are Rayleigh backscattered into the collecting mirror on the balloon package is given by:

$$N_\lambda = \frac{\epsilon_\lambda}{h\upsilon} f \sigma_\lambda n(z) \delta D \frac{A}{4\pi D^2} T_\lambda$$

where ϵ_λ is the energy in the laser pulse at wavelength λ, $h\upsilon$ is the photon energy, f is the fraction of the atmospheric element δV visible to the detection system, σ_λ is the Rayleigh scattering cross section at 180°, $n(z)$ is the atmospheric molecular number density vs. altitude, A is the area of the collecting mirror, and T_λ is the atmospheric transmission for a photon traversing a path length of 2D at the specified altitude and zenith angle.

A model exponential atmosphere was adopted to simplify the computations of expected count rate vs. time delay. With a scale height of 7 km, the atmospheric density between 0 and 80 km, which ranges over 5 orders of magnitude, is reproduced to an rms accuracy of ~20%. The scale height was chosen to yield the correct density at an altitude of 40 km.

Table 3-1 lists the various illustrative instrument parameters that were adopted for the calculation of the expected count rate vs. time delay. It should be noted that the listed instrument parameters may differ slightly from the actual design specification because of engineering changes incorporated into the final system design. Laser pulse energies of 30 and 380 millijoules at 353 and 1064 nm respectively, were chosen to represent the output of the Neodymium:YAG laser and frequency tripler described in Section 7.1. The optical system consists of a 50 cm diameter collecting mirror with a dichroic beam splitter and photomultiplier detectors (see Section 8.2). Specified values of the quantum efficiencies of the photomultipliers were used, as well as transmission and reflection efficiencies of the optics. The field of view

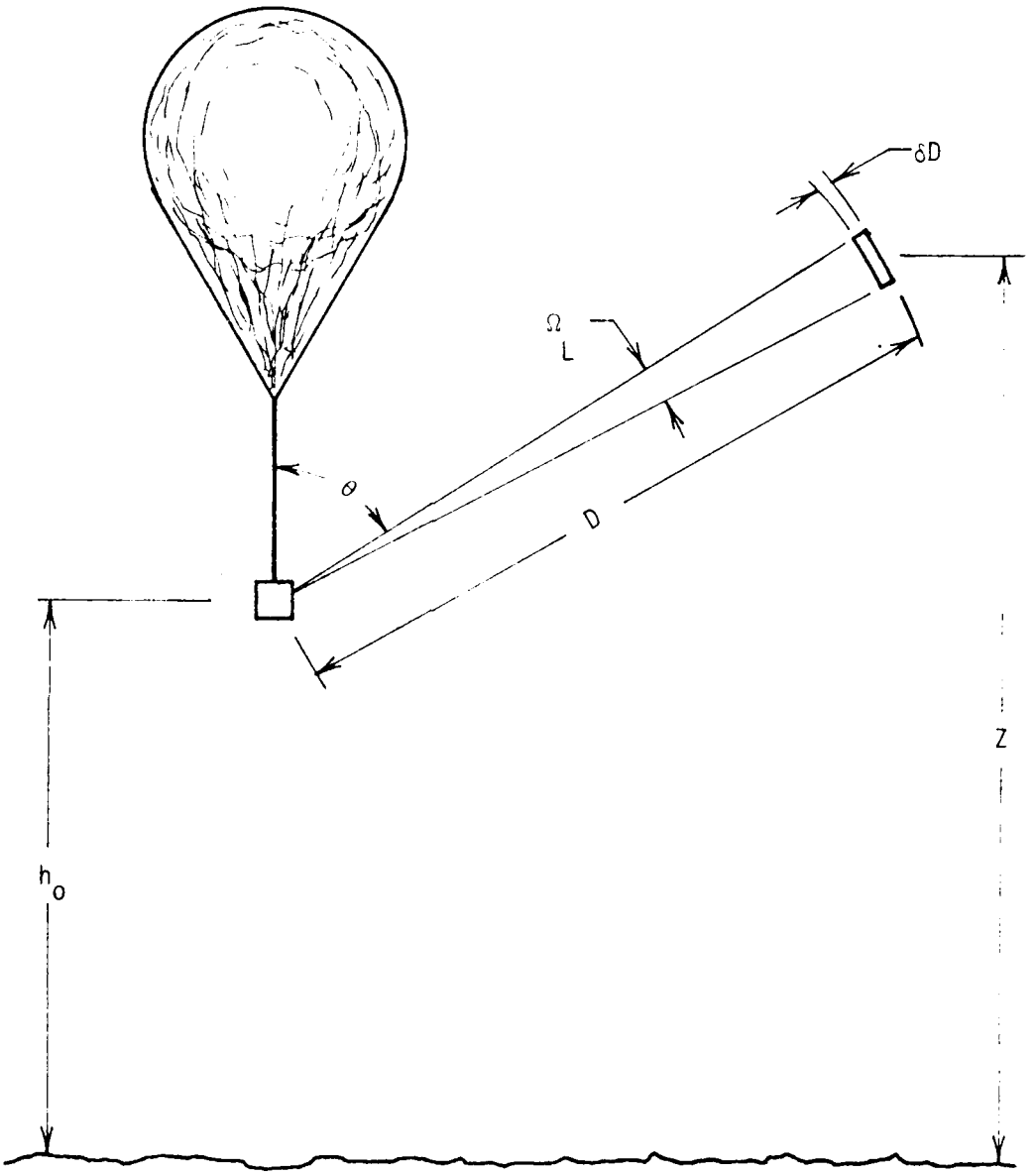

Figure 3.1 Predicted Signal Level Calculation Geometry

TABLE 3-1

LIDAR CODE INPUTS

Mirror Radius	RM	25.4	cm
Laser Wavelengths	WAVE (1)	10640	Å
	WAVE (2)	3530	Å
Separation of Mirror and Laser	S	100	cm
Atmospheric Interval	DELD	10^4	cm
Atmospheric Scale Height	ZO	7×10^5	cm
Laser Energy			
10640 A	E1	.380	Joules
3530	E2	.030	Joules
Receiver Field of View	THM	.004/2	Radian
Laser Field of View	THL	.004/2	Radian
Atmospheric Transmission			
10640	T1	85	Percent
3530	T2	42	Percent
Rayleigh Cross-Section			
10640	$[9.6 \times 10^{-27} \times 1.5(4580/\lambda)^4]4\pi$		cm^2
3530			
Detector Efficiencies			
10640	EFFD (1)	2	Percent
3530	EFFD (2)	10	Percent
Optical Transmission			
10640	TRAN (1)	30	Percent
3530	TRAN (2)	30	Percent
Balloon Altitude	HO		cm
Sea Level Density	DENO	2.67×10^{19}	cm^{-3}
Receiver Spectral Bandwidth			
10640		10	Å
3530		30	Å

of the detection system was chosen to match the angular divergence of the laser beam although, in the actual lidar, the detector field of view is slightly larger.

Calculations of the return signal from the laser pulse at two wavelengths were carried out for balloon float altitudes of 40 km and 20 km for various zenith angles. The experimental acquisition plan is summarized in Table 3-2. The results of the calculations are shown in Figures 3.2 through 3.5. In each case, the number of counts that are recorded for photons scattered in an atmospheric interval of length 100 meters as a function of slant range from the payload are plotted. In all cases, the count rate rises to a maximum within a fraction of a kilometer; this results from the fact that the 1 meter separation between the axes of the laser beam and detection system is rapidly overcome by the divergence of the beams. This overlap function is plotted in Figure 3.6. The rapid decline in the count rate curves for distances between 1 and 10 km results from the b^{-2} fall off in the return signal with increasing distance. For larger distances (>10 km) the curves, representing different zenith angles, are qualitatively very different. Here the change in atmospheric density with slant range from the payload is the dominant effect in determining the amplitude of the return signal. For $\theta = 30°$ (nearly vertically up), the decline in atmospheric density with altitude causes the return signal to drop sharply with altitude. By contrast, for $\theta = 180°$ (viewing directly down), the return signal remains nearly constant with distance.

An inspection of the absolute numbers of counts expected from the scattered laser pulse allows one to separate the density measurements into two regimes. For those distances (corresponding to specific altitudes) where the return signal yields counts in excess of ~10 per 100 m atmospheric bin, density measurements may be obtained from a single laser pulse. These measurements are, of course, limited in accuracy by the $1/\sqrt{n}$ counting statistics, the background flux, and the modeling of aerosol contributions to the scattering. When only a small number of photons (or fraction of a photon) are expected from a single laser pulse at a given altitude, the density measurements will be obtainable only after the integration of many pulses. Figure 3.7 is a plot of the estimated statistical error as a function of shots and slant range. The nadir pointed lidar experiment will see backgrounds as shown in Figure 3.8.[11] The receiver count rates from various backgrounds are tabulated in Table 3-3.

TABLE 3-2

DATA ACQUISITION PLAN

OVER UNCONTROLLED LAND SPACE

20 km and ABOVE	SIDE LOOKING
15 km and ABOVE	UPWARD LOOKING

OVER CONTROLLED LAND SPACE (WSMR)

15 km and ABOVE	UPWARD LOOKING
20 km and ABOVE	SIDE LOOKING
30 km and ABOVE	DOWNWARD LOOKING

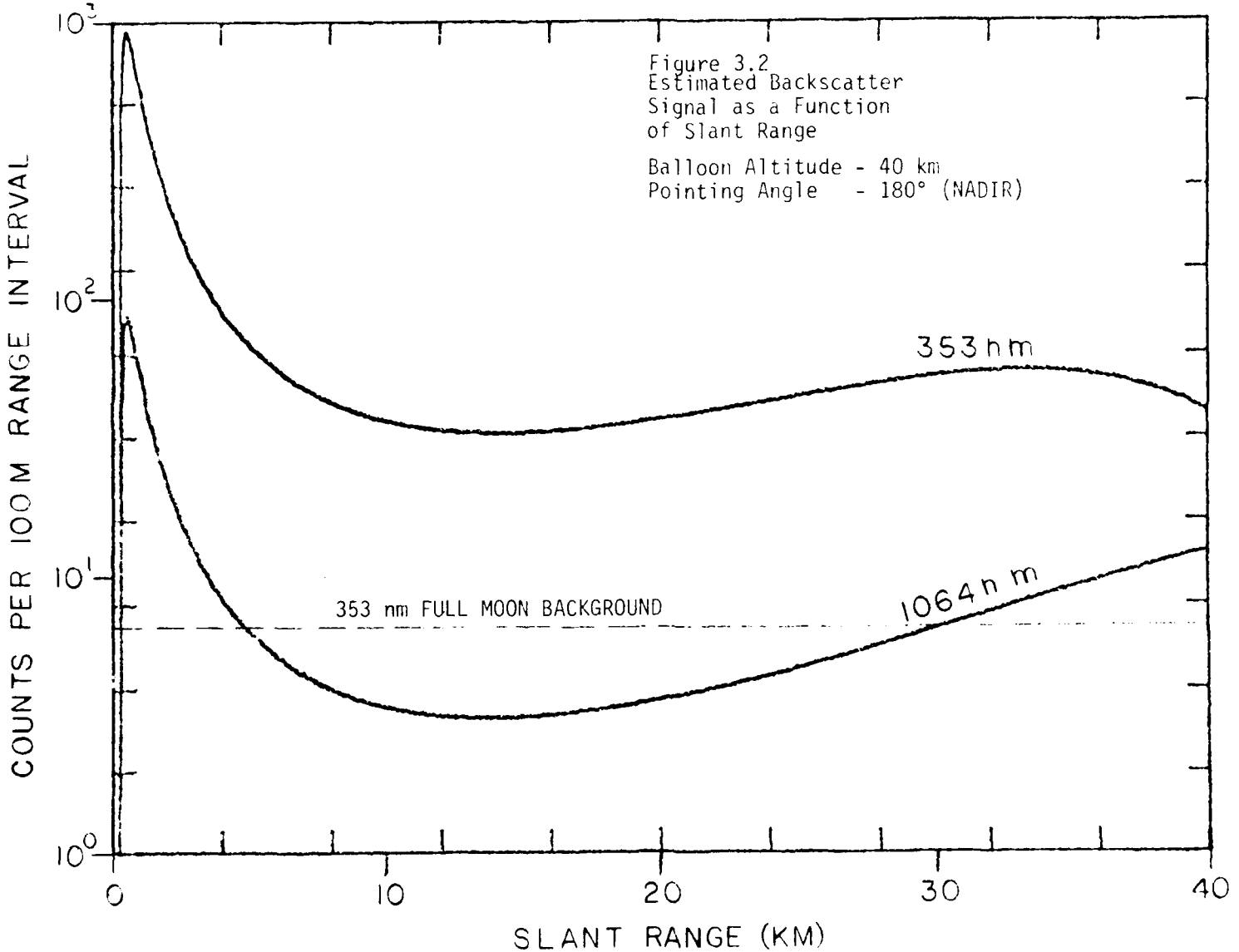
Figure 3.2
Estimated Backscatter
Signal as a Function
of Slant Range
Balloon Altitude - 40 km
Pointing Angle - 180° (NADIR)
353 nm
1064 nm
353 nm FULL MOON BACKGROUND
COUNTS PER 100 M RANGE INTERVAL
SLANT RANGE (KM)
10^3
10^2
10^1
10^0
0
10
20
30
40

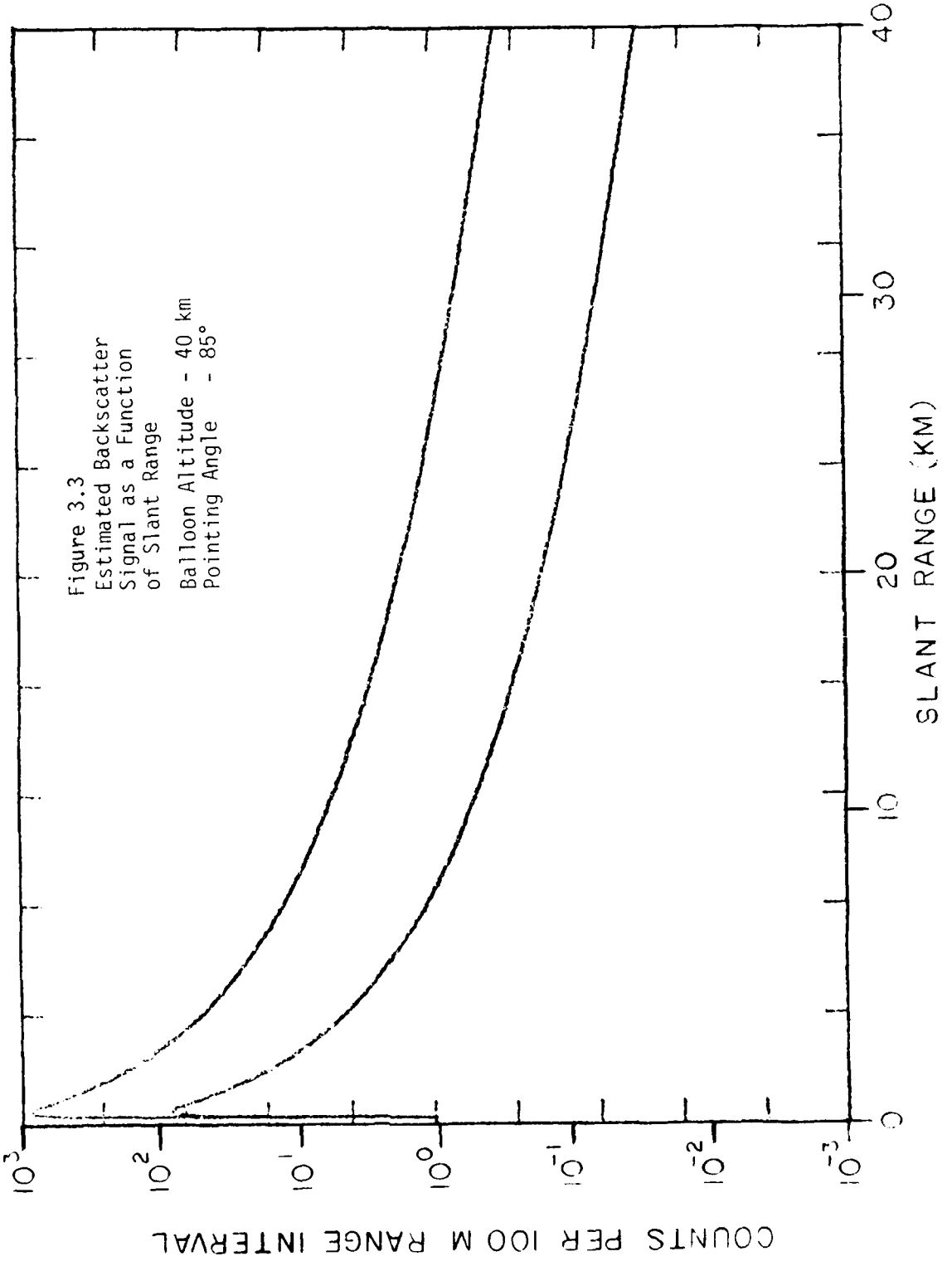

Figure 3.3
Estimated Backscatter
Signal as a Function
of Slant Range

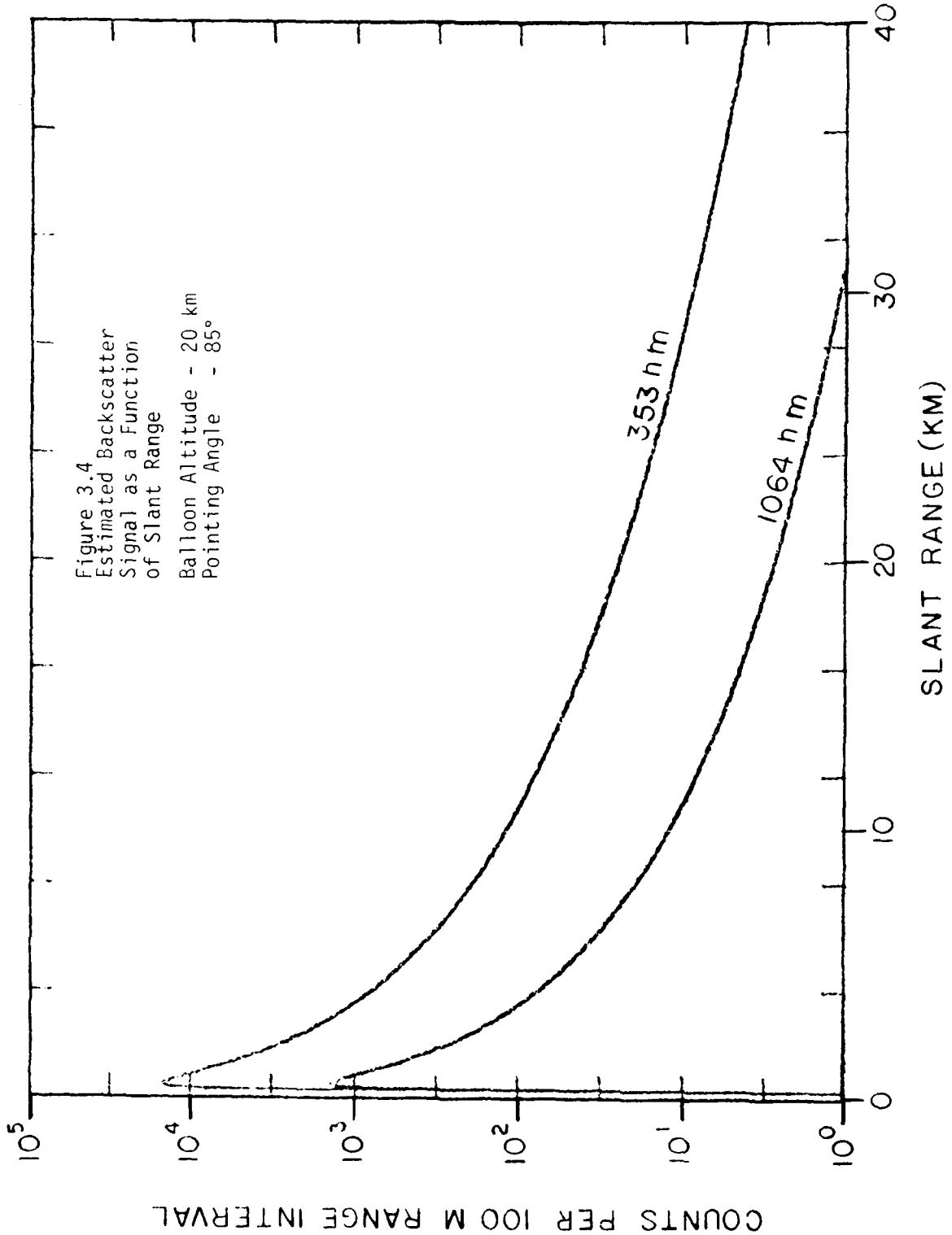
Figure 3.4
Estimated Backscatter
Signal as a Function
of Slant Range
Balloon Altitude - 20 km
Pointing Angle - 85°
353 nm
1064 nm
COUNTS PER 100 M RANGE INTERVAL
SLANT RANGE (KM)
10^5
10^4
10^3
10^2
10^1
10^0
0
10
20
30
40

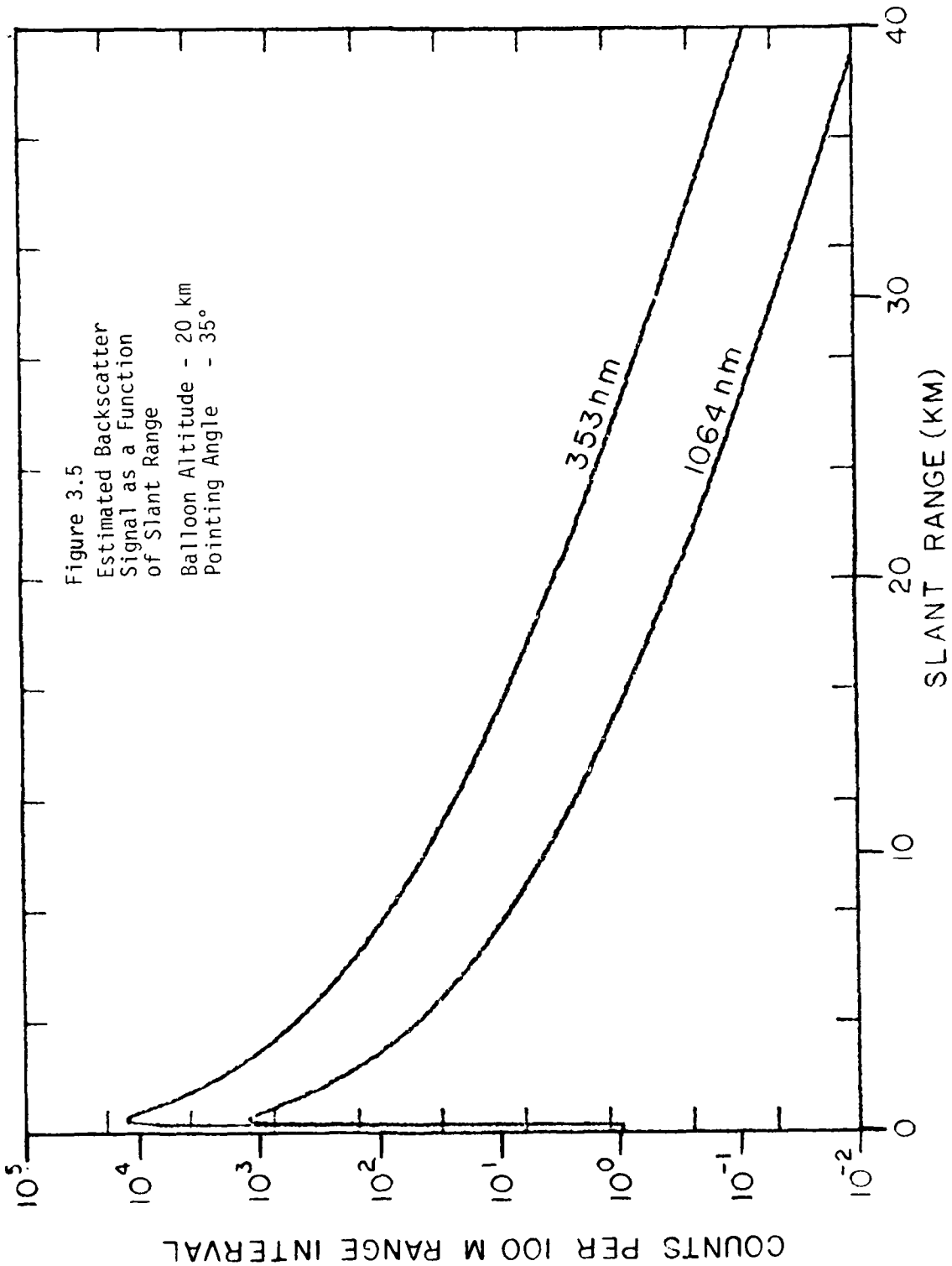

Figure 3.5
Estimated Backscatter Signal as a Function of Slant Range

Balloon Altitude - 20 km
Pointing Angle - 35°

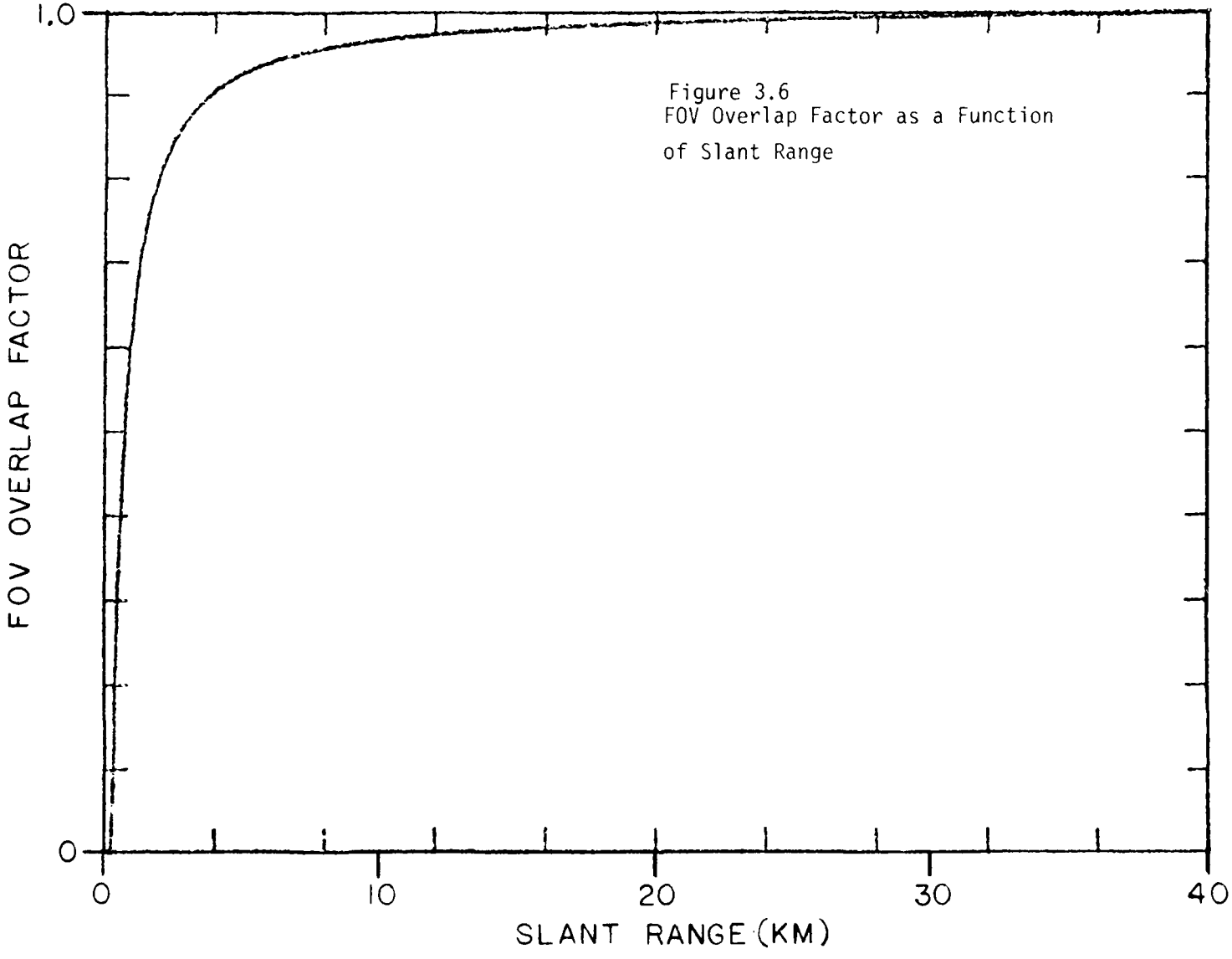

Figure 3.6
FOV Overlap Factor as a Function of Slant Range

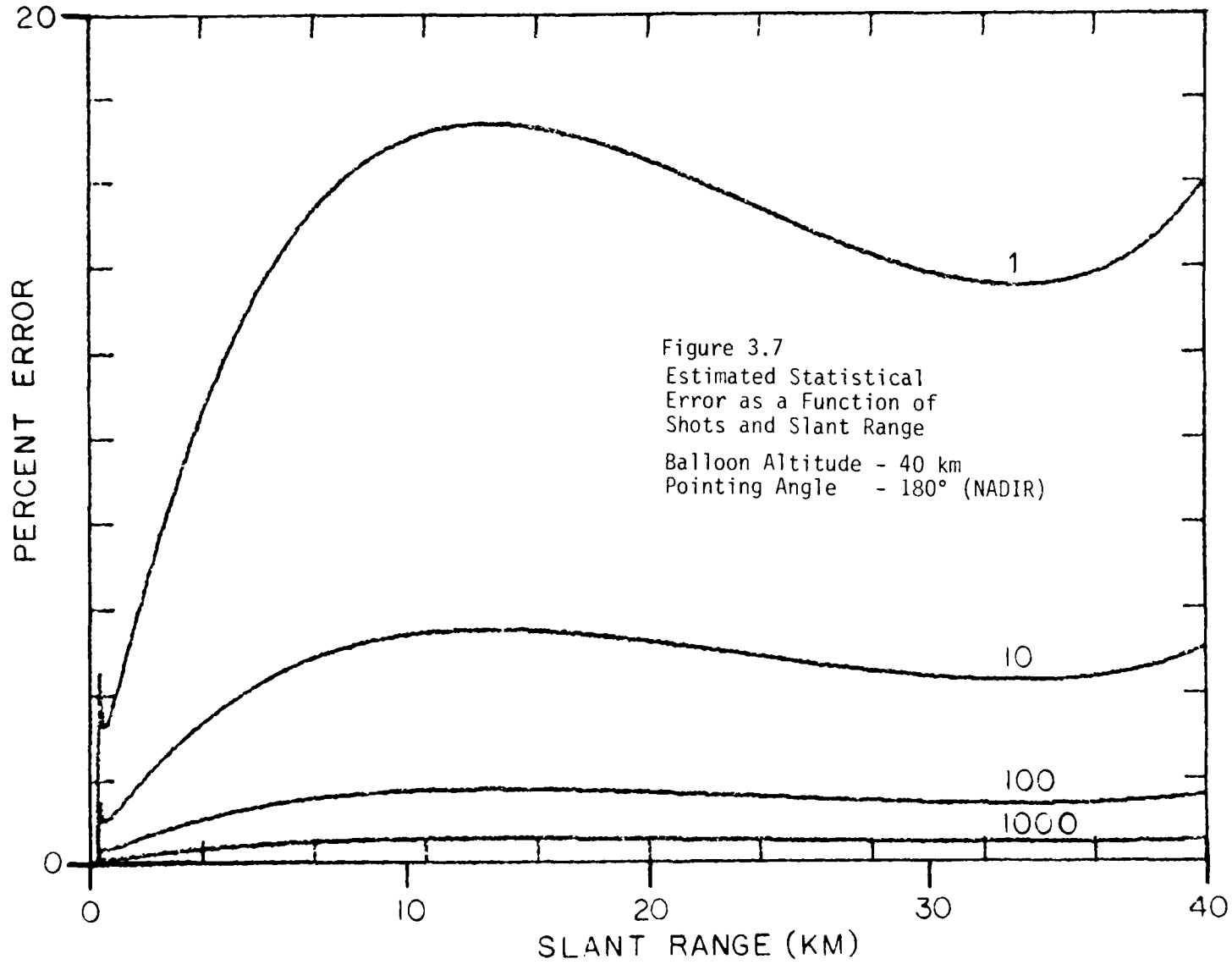

Figure 3.7
Estimated Statistical
Error as a Function of
Shots and Slant Range

Balloon Altitude - 40 km
Pointing Angle - 180° (NADIR)

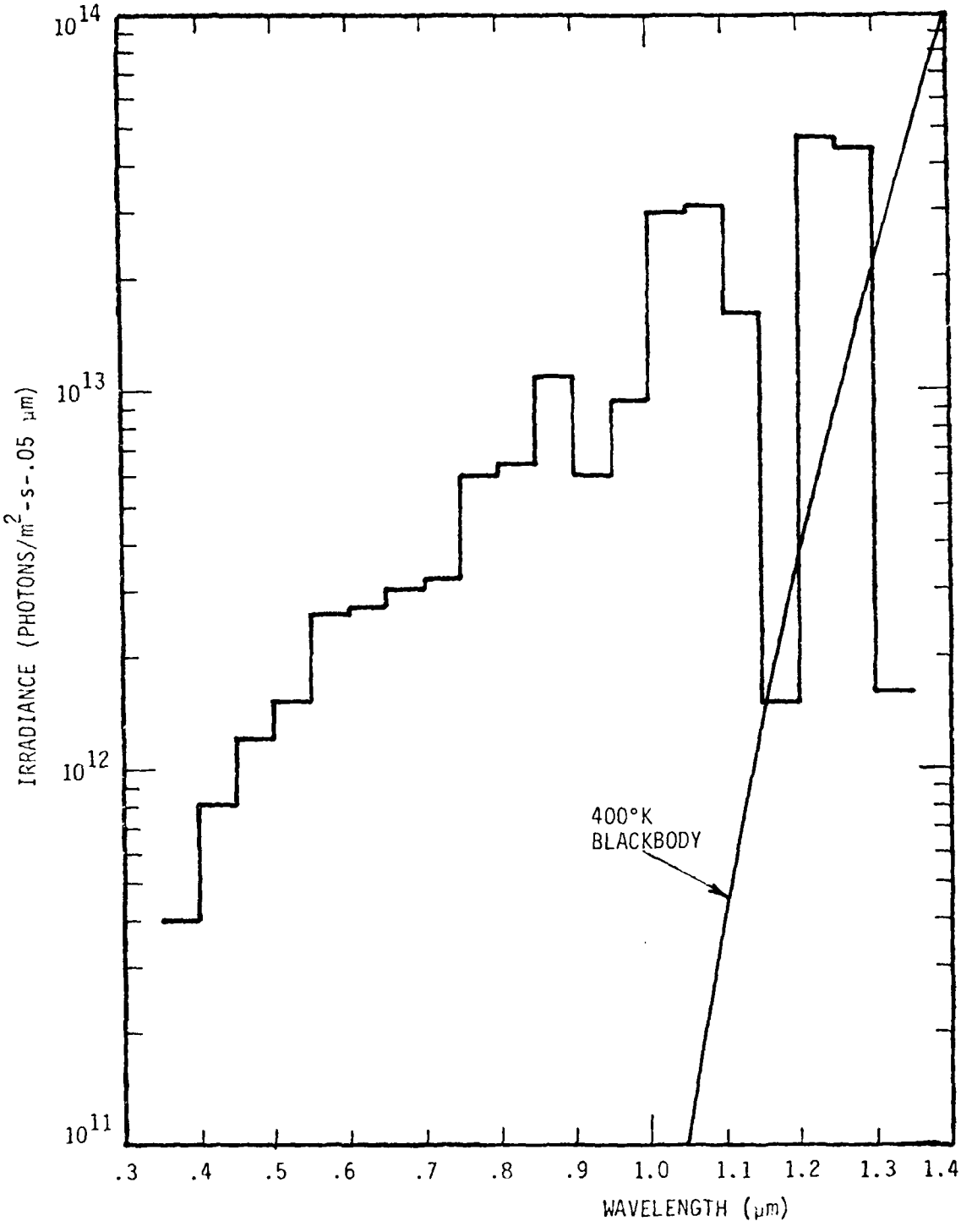

Figure 3.8 Natural Night Sky Spectral Irradiance on Horizontal Earth's Surface

TABLE 3-3

ESTIMATED BACKGROUNDS (NADIR-LOOKING)

	353 nm	1064 nm
NIGHT-SKY	10^{-3} COUNTS/BIN	1.4×10^{-3} COUNTS/BIN
FULL MOON	6 COUNTS/BIN	1.7×10^{-2} COUNTS/BIN
DAYLIGHT	6×10^{5} COUNTS/BIN	1.5×10^{3} COUNTS/BIN

4.0 ENVIRONMENTAL SPECIFICATIONS

The environmental specifications, with respect to pressure, temperature, and mechanical shock, in which the Lidar Experiment and support systems must operate are listed in Tables 4-1, 4-2, and 4-3. These specifications form the basis for the design specifications outlined in this report.

TABLE 4-1

BALLOON PAYLOAD ENVIRONMENTAL SPECIFICATIONS

PRESSURE

EVENT	DEFINITION	COMMENTS
PRE-LAUNCH	14.7 psia ± 4 psia	
BALLOON ASCENT	14.7 psia to 0.029 psia	ABIENT PRESSURE CHANGE WITH ALTITUDE
BALLOON FLIGHT	0.16 psia to 0.029 psia (FOR UP TO 12 HRS)	FLOAT ALTITUDES FROM 100,000 FT. TO 140,000 FT.
TEST	15 psig for 5 HOURS	PRE-LAUNCH PRESSURE TEST IN ALL CHAMBERS

TABLE 4-2

BALLOON PAYLOAD ENVIRONMENTAL SPECIFICATIONS

TEMPERATURE

EVENT	DEFINITION	COMMENT
PRE-LAUNCH	10°C TO 35°C	OPERATIONAL
BALLOON ASCENT	-56°C	AMBIENT AIR TEMPERATURE
	25°C ± 5°C	DESIGN GOAL REQUIRED LASER AND RECEIVER
	10°C to 35°C	OPERATIONAL ELECTRONICS TEMPERATURES
BALLOON FLOAT	-46°C to -20°C	AMBIENT AIR TEMPERATURE
	25°C ± 5°C	DESIGN GOAL REQUIRED LASER AND RECEIVER
	10°C to 35°C	OPERATIONAL ELECTRONICS TEMPERATURES
TEST	SIMULATE BALLOON ASCENT & FLOAT	THERMOVAC TEST

TABLE 4-3

BALLOON PAYLOAD ENVIRONMENTAL SPECIFICATIONS

MECHANICAL SHOCK

EVENT	DEFINITION	COMMENTS
LAUNCH	± 2.0 g, 70 msec, HALF SINE ALL AXES	NO DEGRATION OF EXPERIMENT SYSTEM PERFORMANCE
CHUTE OPENING	± 10 g, 70 msec, HALF SINE ALL AXIS	LASER IS NOT REQUIRED TO MAINTAIN ALIGNMENT. NO PERMANENT DAMAGE IS PERMITTED. OPTICAL MISALIGNMENT IS PERMITTED.
GROUND IMPACT	PROBABLY 10 g IN Z AXIS	AMOUNT OF DAMAGE WILL DEPEND ON TERRAIN, HORIZONTAL IMPACT VELOCITY AND SECOND IMPACT.
TEST	± 2.0 g, 70 msec, HALF SINE Z AXIS ONLY	NO DEGRADATION OF EXPERIMENT SYSTEM PERFORMANCE.

5.0 SAFETY CONSIDERATIONS

5.1 Introduction

Two principal types of hazards are associated with laser operation: the laser radiation itself and the high voltages present in the laser power supply. Few serious eye injuries due to lasers have been reported since the introduction of commercial models. The accident rate has been low because the possibility of exposure of the eye to a collimated beam is extremely remote if a few rudimentary precautions are followed. On the other hand, electrical hazards have proved to be far more serious and a number of guidelines should be followed to prevent electric shock.

Applicable parts of the following documents, or their most recent revisions, shall form a part of the safety considerations:

1. Brehm, W.L., and J.L. Buckley "Design Study of a Laser Radar System for Spaceflight Applications," Final Report, Contract F19628-78-C-0204, General Electric Space Division, AFGL-TR-79-0264, (December 1979).

2. "American National Standard for the Safe Use of Lasers," ANSI Z136.1-1976, American National Standards Institute, Inc., New York, NY 10018 (1976).

3. "Laser Safety Evaulation and Approval," STEWS-NR-P SOP, No. 40-A, Range Programs Division, National Range Operations Directorate, WSMR, NM (November 1978).

4. "Safety Standing Operating Procedures," WSMR Regulation No. 385-15, Department of the Army, WSMR, NM (April 1972).

5. "Control of Potential Hazards to Health from Nonionizing Radiation," WSMR Regulation No. 40-9, Department of the Army, WSMR, NM (January 1975).

5.2 Radiation Hazards

The laser proposed for this experiment emits electromagnetic radiation at two widely spread wavelengths: 355 and 1064 nm. In addition, it will radiate in the visible to some extent at 532 nm. The radiation at 355 nm, if incident on the unprotected human eye will be absorbed in the lens and may contribute to some forms of cataract. At high irradiances, it can also produce "sunburn" or erythema of the skin. Radiation at 532 and 1064 nm would be transmitted through the ocular media of the eye with little loss and is usually focused on the retina where it can damage a spot size area. A similar hazard is caused by viewing a specular, or mirror-like, reflection, and to a lesser degree the reflection from a diffuse surface at close proximity.

The problem of protective eyeware is compounded by the three radiation wavelengths of the neodymmium:YAG laser at 1064, 532, and 353 nm. However, it can be readily solved by combining two filters, such as Schott Color Filter Glass KG3 and American Cyanamid Argon filter plastic, or by using a broad spectrum filter designed for a neodymium double frequency lasers and available from Glendale Optical Co. The luminous transmittance of these combinations is 45%, which is more than adequate for laboratory work.

The Bureau of Radiological Health (BRH) has classified lasers according to their potential hazards. The proposed laser system would be in Class IIIb, which consists of lasers which can produce accidental injury to the eye if viewed either directly or from specular reflections. Accordingly, a warning label must be affixed to the laser identifying it as a Class IV laser product and carry the legend "Danger: Laser Radiation - Avoid Eye or Skin Exposure to Direct or Scattered Radiation". The label will also list the radiating wavelengths and their respective output energies. The Occupational Health and Safety Administration (OHSA) has proposed standards for laser safety, and these must be adhered to.

5.3 Electrical Hazards

As previously noted, in the past history of laser operations, the frequency of accidents due to electrical hazards has been far greater than those due to radiation hazards. The following is a list of guidelines to prevent electrical shock[12]:

1. General precautions.

a. Avoid wearing rings, metallic watchbands, and other metallic objects.

b. When possible, use only one hand in working on a circuit or control device.

c. Never handle electrical equipment when hands, feet, or body are wet or perspiring or when standing on a wet floor.

d. With high voltages, regard all floors as conductive and grounded unless covered with well-maintained dry rubber matting of a type suitable for electrical work.

e. Learn rescue procedures for helping victims of apparent electrocution: Kill the circuit; remove the victim with a non-conductor if he is still in contact with the energized

circuit; initiate mouth-to-mouth resuscitation immediately and continue until relieved by a physician; have someone call for emergency aid.

2. Precautions with high-power lasers

   a. Provide fault-current-limiting devices, such as fuses or resistors, capable of clearing or dissipating total energy, and emergency shutoff switches.

   b. Provide protection against projectiles that may be produced during faults by the use of suitable enclosures and barriers.

   c. Provide enclosures designed to prevent accidental contact with terminals, cables, or exposed electrical contacts. Provide a grounded metal enclosure that is locked and/or interlocked.

   d. Prevent or contain fires by keeping combustible material away from capacitors.

   e. Automatically dump, or crowbar, capacitors before opening any access door.

   f. Where feasible, wait 24 hours before working on circuits involving high-energy capacitors.

   g. Provide a sufficiently short discharge time constant in the grounding system.

   h. Check that each capacitor is discharged, shorted, and grounded before allowing access to capacitor areas.

   i. Provide reliable grounding, shorting, and interlocking.

   j. Install crowbars, grounding switches, cables, and other safety devices to withstand the mechanical forces that could exist when faults occur or crowbar currents flow.

   k. Provide suitable warning devices, such as signs and lights.

   p. Place shorting straps at each capacitor during maintenance and while capacitors are in storage.

   m. Provide manual grounding equipment that has the connecting cable visible for its entire length.

   n. Supply such safety devices as safety glasses, rubber gloves, and insulating mats.

   o. Provide metering, control, and auxiliary circuits that are protected from possible high potentials even during fault conditions.

   p. Inspect routinely for deformed or leaky capacitor containers.

q. Provide a grounding stick that has a discharge resistor at its contact point, an insulated ground cable (transparent insulation preferred), and a grounding cable permanently attached to ground. Such a grounding stick should not be used to ground an entire large bank of capacitors. Large-capacity shorting bars, with resistors, should be part of the stationary equipment. Final assurance of discharge should be accomplished with a solid-conducting grounding rod.

5.4 Range Safety Requirements

5.4.1 Introduction - Operation of the laser in the field prior to launch or after payload recovery would require guidelines as given above for use in the laboratory. However, once the payload is aloft, the possibility arises that the laser radiation may be viewed by someone not using protective eyewear. The standards for the use of lasers, such as those set by the American National Standard Institute (ANSI), and which are usually adopted or modified by BRH and OSHA, define the permissible exposure limits.

The laser firing after launch will be controlled by three separate and independent methods, as follows:

1. The laser firing will be enabled only when an uplink Laser Fire command is being received.

2. A barometric pressure switch will disable the laser firing below a preset altitude.

3. A clock timer will automatically disable the laser firing after a preset time from launch has elapsed.

In addition to the above, the pointing mirror, in the stow position, will cover the laser beam aperture.

5.4.2 Calculation of Maximum Permissible Exposure - Criteria for the Maximum Permissible Exposure (MPE) values for laser spectral wavelengths are set forth in the document "American National Standard for the Safe Use of Lasers".[4] It also includes the step by step procedures and examples of MPE determination and laser classification. MPE is given in terms of the irradiance, H, in joules/cm^2.

Maximum permissible exposure (MPE) values are below known hazardous levels, but still may be uncomfortable to view. Thus, it is good practice to maintain exposure levels as far below the MPE values as is practicable. When a laser emits radiation at several widely different wavelengths, computation of the MPE is complex. Exposure from several wavelengths in the same

time domain are additive on a proportional basis of spectral effectiveness with due allowance for all correction factors. An appropriate aperture is used for measurements and calculations with all MPE values. This is the limiting aperture and is the maximum circular area over which irradiance and radiant exposure can be averaged. To determine the MPE applicable for an exposure to a repetitively pulsed laser such as proposed for this experiment, one must know the wavelength, pulse repetition frequency (prf), duration of a single pulse, and duration of a complete exposure. In every instance this process requires two analyses,or approaches, and a conclusion, Steps 1 and 2 and Step 3, respectively, as follows:

Step 1. Individual Pulse Limitation. This requires the calculation of the MPE based upon the limitation that a single-pulse exposure shall not exceed the single-pulse MPE for pulses greater than 10^{-5} second and may not exceed this single pulse MPE multiplied by an appropriate correction factor for pulses less than or equal to 10^{-5} second.

Step 2. Average Irradiance or Average Radiant Exposure Limitation. The average-power limitation requires the calculation of the average irradiance or total radiant exposure for the entire pulse train for comparison with the MPE applicable for the duration of the entire exposure.

Step 3. Conclusion. Compare the results of Step 1 and Step 2; the limitation which provides the lowest total exposure is applied.

We have rigorously followed these steps for each of the three laser radiations and have used the appropriate Figures and Tables of "American National Standard for the Safe Use of Lasers". Our results and conclusions are given below.

1064 nm Radiation

Step 1. Individual Pulse Limitation for 1064 nm

MPE/Pulse: $H \leq$ (fig. 12 Correction)(Figure 8 correction for 1064 nm)(Tabulated Value)

Tabulated Value: 5×10^{-6} J/cm^2

Figure 8 Correction: 5

Figure 12 Correction: .32

Then MPE/Pulse:

$$H \leq (5 \times 10^{-6})(5)(.32) = 8.0 \times 10^{-6} \text{ J/cm}^2$$

And MPE for a 1000 second pulse train would be

$$H \leq (8.0 \times 10^{-6})(1 \times 10^{3} \text{ sec})(10 \text{ Hz})$$
$$= 8.0 \times 10^{-2} \text{ J/cm}^2$$

Step 2. Average Power Limitation

MPE (avg.) (from Figure 10):

$$E \leq 1.5 \times 10^{-3} \text{ W/cm}^2$$

or

$$H \leq (1.5 \times 10^{-3})(1000 \text{ sec})$$

$$H \leq 1.5 \text{ J/cm}^2$$

Step 3. Conclusion

Clearly, the limitation in Step 1 determines the MPE. Thus the MPE per pulse is 8.0×10^{-6} J/cm^2.

532 nm Radiation

For this calculation, we have assumed no natural aversion response.

Step 1. Individual Pulse Limitation

MPE/Pulse: $H \leq$ (Figure 12 Correction)(Tabulated Value in Table 5)

Tabulated Value: 5×10^{-7} J/cm^2

Figure 12 Correction: .32

Then MPE/Pulse:

$$H \leq (5 \times 10^{-7})(.32) = 1.6 \times 10^{-7} \text{ J/cm}^2$$

And MPE for the entire train would be

$$H \leq (1.6 \times 10^{-7})(1 \times 10^{3} \text{ sec})(10 \text{ Hz})$$
$$= 1.6 \times 10^{-3} \text{ J/cm}^2$$

Step 2. Average Power Limitation

MPE (avg.)(from Figure 10):

$$E = 1 \times 10^{-5} \text{ W/cm}^2$$

or

$$H \leq (1 \times 10^{-5})(1000 \text{ sec})$$

$$H \leq 1 \times 10^{-2} \text{ J/cm}^2$$

Step 3. Conclusion

Clearly, the limitation in Step 1 determines the MPE. Thus, the MPE per pulse is 1.6×10^{-7} J/cm^2.

353 nm Radiation

Step 1. Individual Pulse Limitation

MPE/Pulse: $H \leq$ (Figure 12 Correction)(Tabluated Value in Table 5)

Tabulated Value: $0.56\ t^{1/4}$ J/cm^2

where $t = 2 \times 10^{-8}$ sec, then $t^{1/4} = 1.2 \times 10^{-2}$ sec

Figure 12 Correction: .32

Then MPE/Pulse:

$$H \leq (0.56)(1.2 \times 10^{-2})(.32) = 2.15 \times 10^{-3}\ \text{J/cm}^2$$

And MPE for the entire train would be

$$H \leq (2.15 \times 10^{-3})(1 \times 10^{3}\ \text{sec})(10\ \text{Hz}) = 2.15 \times 10^{1}\ \text{J/cm}^2$$

Step 2. Average Power Limitation

MPE (avg.) is not specified in Figure 10. However, Table 5 gives an MPE for 10^{-3} to 3×10^{4} seconds of 1×10^{-3} W/cm^2, or

$$H \leq (1 \times 10^{-3})(1000\ \text{sec}) = 1\ \text{J/cm}^2$$

Step 3. Conclusion

It appears that the limitation in Step 2 determines the MPE. Working backwards to find the required maximum H per pulse:

$$H \leq \frac{(1\ \text{J/cm}^2)}{(1000\ \text{sec})(10\text{Hz})} = 1 \times 10^{-4}\ \text{J/cm}^2 \text{ per pulse}$$

Table 5-1 summarizes the MPE's for the three laser wavelengths. It also lists the energies per pulse as specified by the laser manufacturer. Dividing these energies by the appropriate MPE's yields areas which are the minimum values over which the laser energy must be spread. From this we conclude that the 532 nm radiation is more than an order of magnitude less safe than the total of the other radiations, which we can safely neglect as long as we do not decrease the 532 nm radiation.

Several factors must be considered in order to relate the above area to the actual experiment. These factors and their values are listed in Table 5-2. The area, A, over which the laser energy must be spread should be modified as follows:

$$A = (1.25 \times 10^6)(.9)(.86)(2) = 1.9 \times 10^6 \text{ cm}^2$$

The most important factor not yet considered is the effect of atmospheric scintillation on the laser beam intensity. In its study,[5] General Electric Space Division stated that scintillation effects might provide hot spots on the ground up to ten times the normal energy density. However, the effects are far more complex than this. The next section is devoted exclusively to a discussion of this problem.

5.4.3 Atmospheric Scintillations - Theoretical and experimental studies of laser beam scintillations in the atmosphere have been intensively researched for more than a decade, and because of their complexity, these scintillations are still not understood completely. Parts of the following discussion are taken from several sources.[6],[7],[8]

Measured fluctuations in the intensity of laser beams propagating through a turbulent atmosphere depend on meteorological conditions, optical length of the beam path, diameter of the source and receiving apertures, time constant of the receiver, measuring time (exposure), emitted wavelength, and beam focusing.

The index of refraction, n, is the ratio of propagation velocity in a vacuum to that in the medium, which in this case is the turbulent atmosphere. Since at optical frequencies

$$n \approx 1 + 7.9 \times 10^{-5} \, P/T$$

TABLE 5-1

SUMMARY OF MAXIMUM PERMISSIBLE EXPOSURES AND AREAS

Laser Wavelength (nm)	MPE/pulse (J/cm^2)	Energy/pulse (J)	Area (cm^2)
1064	8.0×10^{-6}	7.0×10^{-1}	8.75×10^{4}
532	1.6×10^{-7}	2.0×10^{-1}	1.25×10^{6}
353	1.0×10^{-4}	3.0×10^{-2}	3.0×10^{2}

TABLE 5-2

SAFETY CORRECTION FACTORS FOR 532 nm RADIATION

Category	Correction Factor
Atmospheric Transmission	.9
Pointing Mirror Reflection	.86
Limiting Aperture (7 mm)	No correction required (same aperture as in MPE criteria)
Gaussian beam peak	2
Multimode Inhomogeneities	No correction required (to be filtered out by manufacturer)

where P is the atmospheric pressure in millibars and T is the temperature in °K, then the index of refraction in a turbulent atmosphere is clearly not a constant.

The refractive index variations along a path of propagation modulate the intensity in a multiplicative manner, such that if twice the intensity is transmitted, twice the variation is observed. The variations induced in each subrange of the path then combine multiplicatively to the extent that the effect of the atmosphere in each subrange is independent of the initial degree of coherence. Hence, these refractive index variations modulate the logarithm of the intensity and the amplitude in an additive manner; i.e., the observed variation of log-amplitude is the sum of many random perturbations induced at various places along the path of propagation. As a consequence of the central-limit theorem, the variations of log-amplitude should follow a normal distribution. This result is referred to as the normal distribution of log-amplitude, or equivalently, as the log-normal distribution of amplitude and intensity.

The quantitative measure of fluctuations in the intensity, H, of a beam is usually represented by the quantity

$$\sigma^2 = \overline{(\ln H - \overline{\ln H})^2},$$

or

$$M^2 = \frac{\overline{H^2(t)}}{\overline{H(t)}^2},$$

and the standard deviation of the measured signal, referred to its average value,

$$\sigma_n = \sqrt{M^2}.$$

The experimentally measured quantities are

$$\overline{H} = \frac{1}{N}\sum_{i=1}^{N} H_i,$$

$$\overline{H^2} = \frac{1}{N}\sum_{i=1}^{N} H^2_i,$$

$$\sigma_K^2 = \frac{\overline{H^2} - \overline{H}^2}{\overline{H}^2}$$

When the fluctuations in intensity, H, follow a log-normal distribution, σ_k^2 and σ^2 are related by the expression

$$\sigma^2 = \ln(1 + \sigma_k^2).$$

Measurements have been made of the scintillation of a 6328Å He-Ne laser beam after propagating over an 8-km path near the ground.[18] The measurements were made with collection apertures ranging from 1 mm to 1 m in diameter. The probability distribution of the scintillation was found to be log-normal for all collector diameters.

The phase fluctuations produced by turbulence cause various portions of the beam to travel in different directions. Thus, a very narrow, well collimated laser beam can be expected to spread as a result of turbulence. The irregularities near the transmitter are most effective in spreading the beam, contrary to the case of irradiance fluctuations, where irregularities near the middle of the path are most important. Typical beam widths may increase along a 5 km path by over 100 μr from a transmitter located at the ground during the heat of the day. Since in our case, the laser transmitter is located in the upper atmosphere, the beam irregularities near it will be essentially non-existant, so that the beam width increase will be negligible.

5.4.4 Calculation of Beam Divergence Requirements - In section 5.4.2, we calculated that the ground area, A, over which the 532 nm laser energy must be spread is 1.9×10^6 cm^2. Let us take as an example the case where the balloon payload is at an altitude, Z, of 30 km and we have designed the laser beam output divergence, θ, to be 2 mr. Then the area on the ground would be

$$A = \pi (Z \tan \theta/2)^2 = 2.8 \times 10^7 \text{ cm}^2$$

The ratio of these two areas is inversely proportional to the ratio of the safe intensity, or irradiance, H_{safe}, to the average of the actual irradiance, H_{ave}. Thus,

$$\frac{H_{safe}}{H_{ave}} = \frac{A_{actual}}{A_{safe}} = \frac{2.8 \times 10^7}{1.94 \times 10^6} = 14$$

Of the many experimental cases measured by Fried et al,[8] the closest to our case of someone viewing the laser beam with a dark-adapted eye having a 7 mm diameter pupil is the measurement with a 9 mm diameter collector. We have replotted the log-normal probability distribution of the intensities (Figure 3 in Reference 5) for this case in Figure 5.1. The average intensity, H_{ave}, for this case is 1.7 so that H_{safe} would be

$$H_{safe} = 14\ H_{ave} = 24.5$$

From Figure 5.1 we see that the fraction of pulses above the safe level would be about 5×10^{-3}. If we double the laser beam divergence to 4 mr, the area would increase by a factor of four. Then the ratio of intensities would increase to 98 and the fraction decreases to about 1×10^{-4}. Similarly for 6 mr divergence, the area factor is 9, the intensity ratio is 220, and the fraction is about 7×10^{-6}.

A recent study by Shipley and Browell[9] was made which consisted of a review of optical scintillation literature and unpublished results in an effort to characterize the effects of eye safety for space shuttle and airborne lidars. This study included recent experimental results of laser propagation downward to the earth's surface from high altitude U2 aircraft.[10] Such an experiment is much nearer to the conditions of the balloon-borne lidar than those of Fried et al.[8] The study concluded that sufficient information on atmospheric turbulence and scintillation theory verification is presently available to predict the effects on optical scintillation during downward laser radiation propagation from high altitude platforms, and the study proceeds to make several quantitative predictions. For the case of a shuttleborne lidar, the mean Hufnagel model[11] for atmospheric refractive index turbulence predicts a probability $<10^{-6}$ for surface spot intensitites over a 7 mm pupil diameter with $i>5$, where $i=H/H_{ave}$. The "worst case" three standard deviation Hufnagel model for strong refractive index turbulence gives probabilities $<10^{-3}$ and $<10^{-6}$ for surface spot intensities over a 7 mm pupil diameter with $i>5$ and $i>15$, respectively.

If we chose these probabilities, and since we have shown that $H_{safe}/H_{ave}=14=i$, then even in the "worst case", the probability of a pulse resulting in an intensity above the safe level is about 10^{-6}.

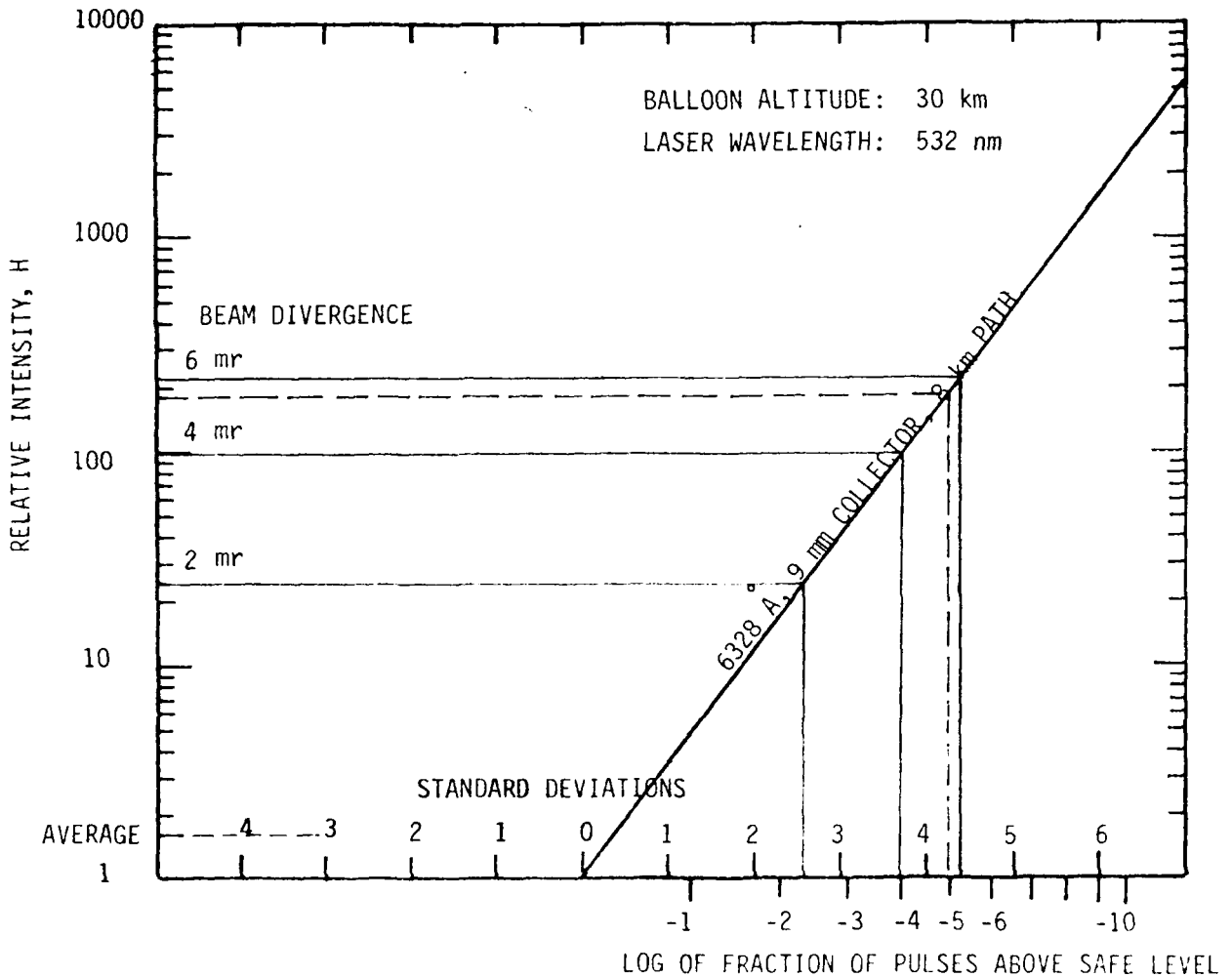

Figure 5.1 Log-normal Probability Distribution of Intensities of Laser Pulses

5.4.5 Summary - We have determined that for range eye safety, the principal danger is from the pulsed 532 nm radiation and that by comparison, the danger from radiation of the other two wavelengths is unimportant. We have also shown that because of the log-normal distribution of the beam irradiance due to atmospheric turbulence-induced scintillations, it is not possible to eliminate entirely the possibility of laser pulses above the maximum permissible exposure level. This possibility exists with the two other radiating wavelengths as well, but with a much lower probability.

A reasonable standard to use as part of our range safety criteria is that the probability of a single laser pulse during the entire mission being above the safe level be less than one. First, let us state that the laser will not be operated in the downward-looking mode unless the payload is over the range and at an altitude of at least 30 km. If we consider that the lidar system is over the range for a maximum of three hours, the total number of laser pulses is

$$(10 \text{ pulses/sec})(3600 \text{ sec/hr})(3 \text{ hr}) = 1.08 \times 10^{5} \text{ pulses.}$$

Then the probability for a pulse during the mission causing an intensity level at ground level above the safe eye limit (MPE) is given by

$$\text{Probability} = (1.08 \times 10^{5} \text{ pulses})(\sim 10^{-6} \text{ per pulse}) \approx 1 \times 10^{-1}$$

which is within our safety standard. If, in addition, we were to include the probability of an individual located in the range who might be looking up at the precise time of such a pulse, then the overall probability becomes vanishingly small.

6.0 PAYLOAD STRUCTURAL DESIGN

The payload is a lightweight, welded aluminum truss structure. The basic design goal is to obtain an unobstructed view for the lidar and the IR cloud monitor. Figure 6.1 is a sketch of the payload indicating locations for the equipment. The basic philosophy was to design a structure that is strong, lightweight, and easily repairable after ground impact at landing. The design also permits the instrumentation to be easily removed.

The payload is suspended through four eyebolts and four steel cables, each capable of reacting to possible ten "g" shock load during the recovery sequence. The cables are attached to a ball bearing swivel which partially isolates the payload from balloon rotational motions.

The gondola is a bird cage type structure with supporting members arranged as a cube inside which all instruments are located. The cube is protected by roll bars which are interconnected to form an impact resistant frame. Crush pads of paper honeycomb are utilized on various parts of the structure to minimize structural damage during landing. The crush pads are designed such that the "g" loads at impact become progressively larger as the honeycomb is crushed.

Because the laser is designed to operate only at near horizontal position, the elevation angle pointing of the lidar transmitter and receiver is achieved by an intermediate pointing system. This pointing system is described in Section 9.0.

6.1 Structural Requirements

To insure the success of the experiment, the following requirements must be met by the payload design:

1. The structure should be built to provide a rigid support to insure alignment of the optical components.

2. The distance from the laser optical axis to the receiver optical axis should be at least one meter.

3. The line of sight should be unobstructed in the nadir direction, in the horizontal direction, and 30° from the zenith direction looking back through the gondola.

4. The alignment of the three pointing mirrors should be maintained within seconds of arc on the ground and at float altitude.

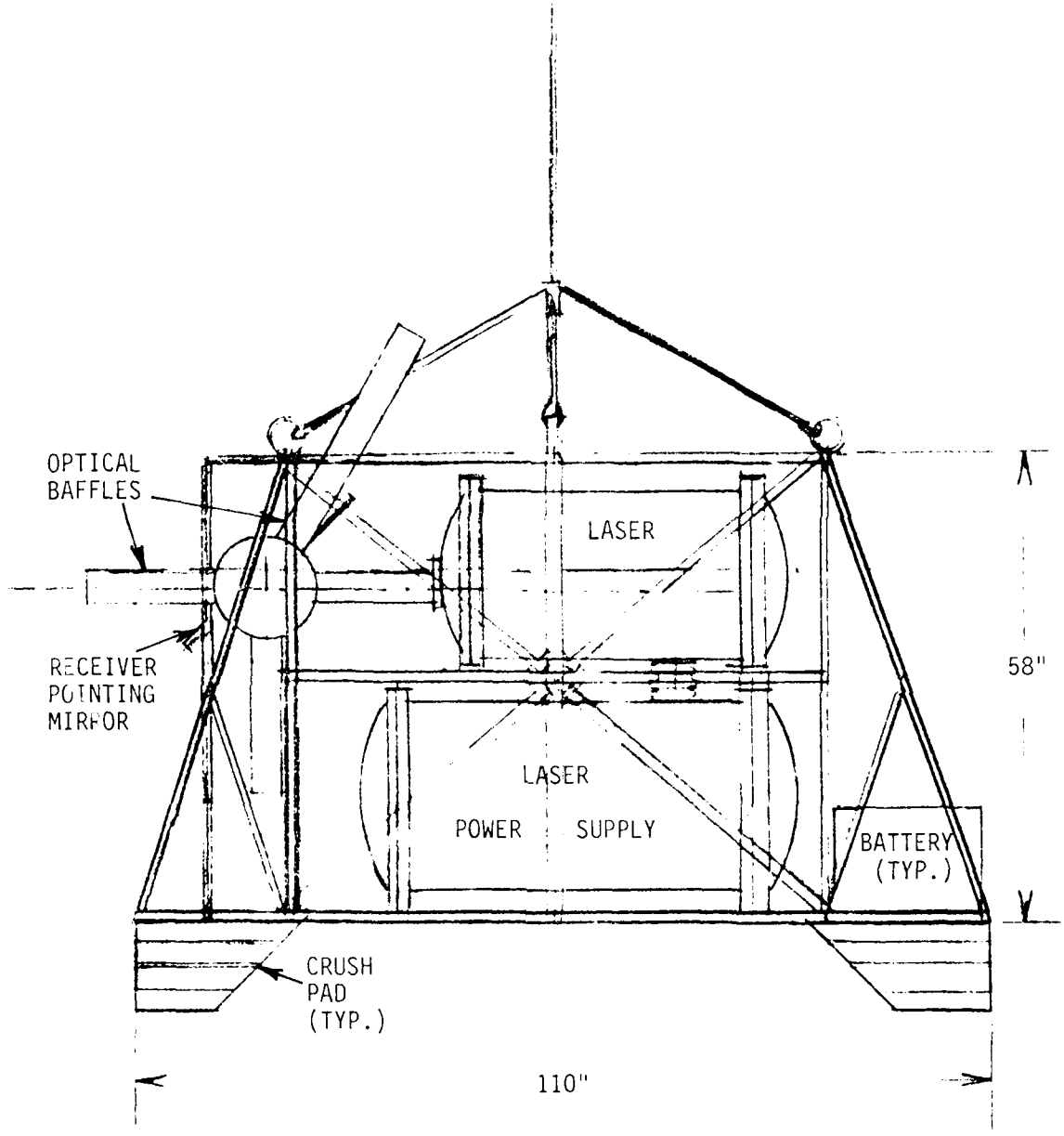

Figure 6.1 Lidar Payload Configuration

5. The electronic components operating at high voltage should be enclosed in pressurized containers capable of maintaining a 1 atm pressure differential.

6. The structure should protect the instruments for a possible launch acceleration of up to 2 g's.

7. The payload should withstand an acceleration on parachute deployment of up to 10 g's in any axis.

8. The payload should survive ground impact (up to 10 g's, any axis) with minor structural damage to the roll bars only.

6.2 Payload Configuration

The configuration of this payload structure is a cube with three decks as shown in Figure 6.2. The middle deck is the one which supports all the optical instrumentation including the transmitter (laser), cloud monitor, receiver, and pointing mirror system.

The bottom deck supports the laser power supply, the cooling system, and the housekeeping and telemetry. The ballast, balloon control, and batteries are also located there.

At the middle of each cube side, a vertical member is joined to the top deck where four eyebolts are mounted. Four cables stretch from the eyebolts to the swivel joint where one cable connects the payload to the parachute and the balloon.

On each side of the cube, the diagonals are designed to be demountable to allow for removal of the instruments. They are fixed in position by pins and bolts. This arrangement allows them to be considered as integral parts of the cube consitituting the structural frame.

6.3 Weight Considerations

Table 6-1 lists the estimated weights of the various payload components.

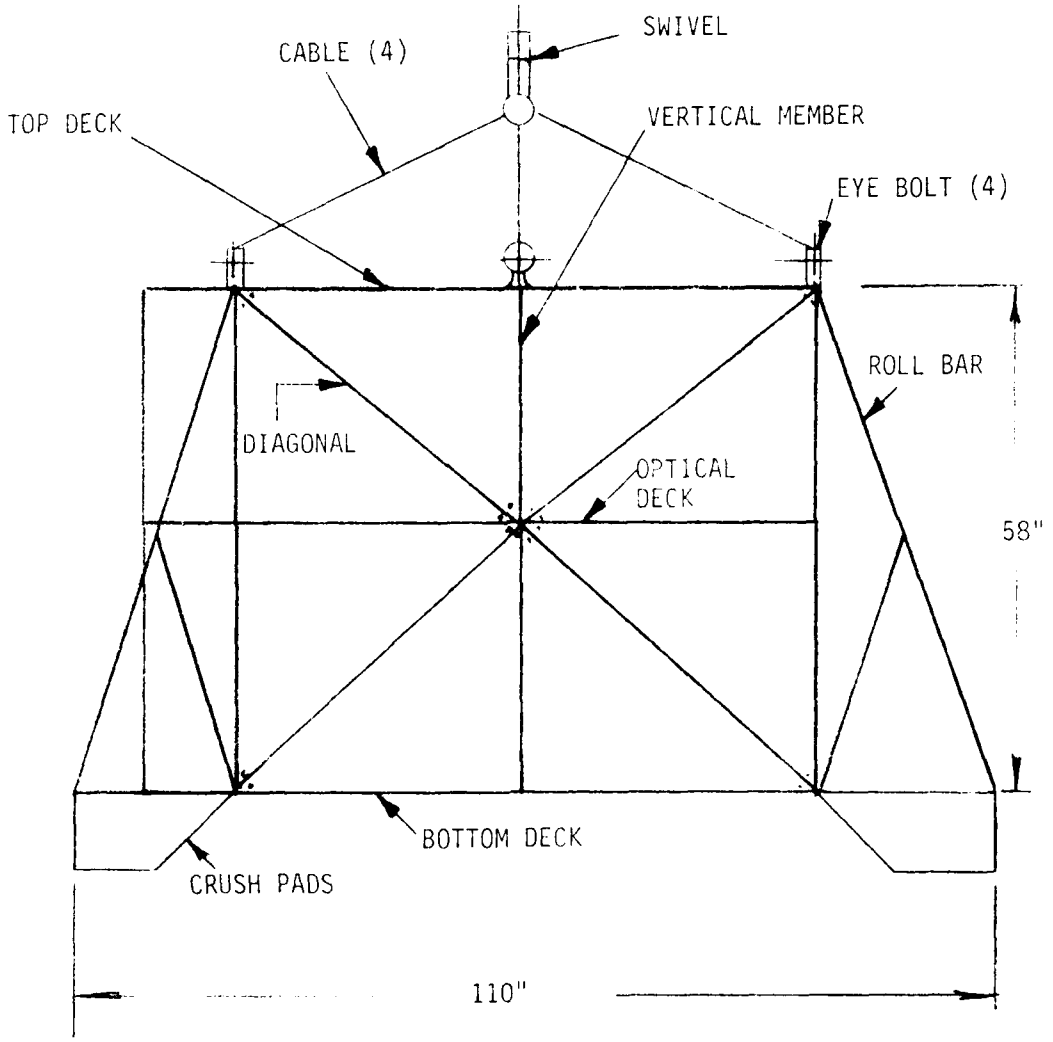

Figure 6.2 Structural Frame, Side View

TABLE 6-1

LIDAR BALLOON EXPERIMENT

WEIGHT ESTIMATES

	Component	Weight Lbs.
1.	LASER	40
2.	LASER CONTAINER	25
3.	POWER SUPPLY	75
4.	POWER SUPPLY CONTAINER	35
5.	RECEIVER BAFFLE AND MIRRORS	20
6.	RECEIVER CONTAINER AND DETECTORS	32
7.	POINTING SYSTEM (MOTOR & GEARS, BEARINGS, ENCODER)	35
8.	FRAME STRUCTURE	400
9.	BATTERIES	500
10.	COOLING SYSTEM AND RADIATORS	85
11.	CRYOGENICS	49
12.	ELECTRONICS	40
13.	CLOUD DETECTOR	30
14.	TELEMETRY	32
15.	HARDWARE	25
16.	EYE BOLTS	12
	TOTAL	1435

7.0 TRANSMITTER DESIGN

7.1 Laser

The balloonborne lidar experiment requires a Nd:YAG laser which is frequency tripled to provide coaxial outputs at 1064 nm, 532 nm, and 355 nm. An industry survey was done and a possible laser selected. The selection criteria were the following:

1. The system must be capable of being powered by 28 vdc.
2. The system must be of a light weight, rugged design with a configuration capable of being packaged for balloonborne operation.
3. The unit should be capable of being modified, as required, for this specific application.

A laser system meeting these criteria, and used to develop this design, was a variation of the ILS-104 system. An optical layout of the laser is shown in Figure 7.1. The detailed specifications are given in Section 7.2.

The laser uses an oscillator and two amplifiers to obtain the specified power levels. The oscillator (and amplifier) rods are powered by a xenon flashlamp. After a preset delay, typically 130 μsec, the Pockels cell Q-switch is triggered. A 15 nsec wide pulse of 1064 nm radiation is dumped from the oscillator through amplifiers 1 and 2 resulting in a 700 mJ pulse of 1064 nm radiation. To generate the 355 nm radiation, a frequency tripler is required. The 1064 nm output from the flashlamp-pumped, Q-switched Nd:YAG laser enters a second harmonic generation (SHG) crystal which outputs orthogonally polarized 1064 nm and 532 nm radiation. A quartz rotator plate brings these two wavelengths back into the same plane before they enter a third harmonic generation (THG) crystal. The THG crystal mixes the 1064 nm second harmonic to produce the desired 355 nm third harmonic. All three wavelengths are present in the coaxial output beam.

In order to achieve maximum efficiency of the tripler, the SHG and THG must be tuned (i.e. peaked) in both angle and temperature. For the balloonborne lidar system, the SHG and THG crystals will be maintained at constant temperature by ovens. Two-axis angle tuning of these crystals will be done by using motor driven micrometers. These will be controlled from a payload controller and, during flight, through the uplink command system.

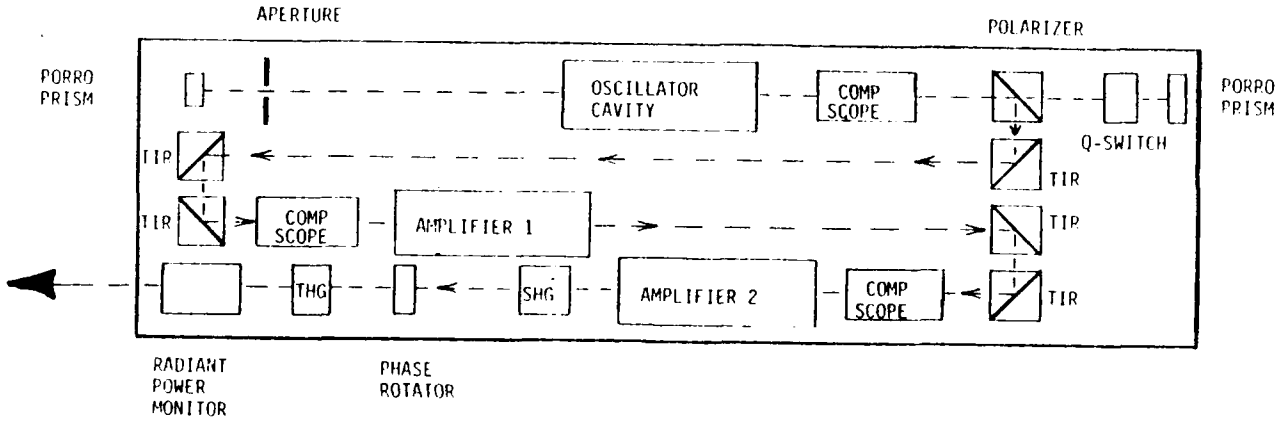

Figure 7.1 Laser Optical Layout

It is required that the radiant output power be monitored at both wavelengths. The monitor system is shown in the schematic of Figure 7.2. A beam sampler, consisting of an uncoated quartz plate, deflects approximately 5 percent of the radiated power to a quartz diffuser. The purpose of this screen is to scramble (integrate) the beam for sensing by the two silicon PIN diode detectors. The PIN diode outputs are amplified and formatted for telemetry transmission.

7.2 Transmitter System

The laser firing will be controlled in flight by a set of independent tuctions:

1. Laser firing will be enabled only when an uplinked laser fire command is being received.

2. A baroswitch will disable laser firing below a preset altitude. The altitude setting will be determined by range/eye safety parameters.

3. A clock timer will automatically disable laser firing after a preset time-from-launch has elapsed.

4. An uplink command will arm/safe the laser high voltage power supply.

5. To prevent laser firing when the pointing mirror is not aligned with the nadir or the local horizontal, interlocks are provided.

The laser safety interlocks are summarized in Table 7-1. The transmitter data requirements are summarized in Table 7-2, and the command requirements are in Table 7-3.

The lidar laser transmitter and power supply will be enclosed in a pressure chamber that will maintain the system at a pressure of 1 atm throughout the flight.

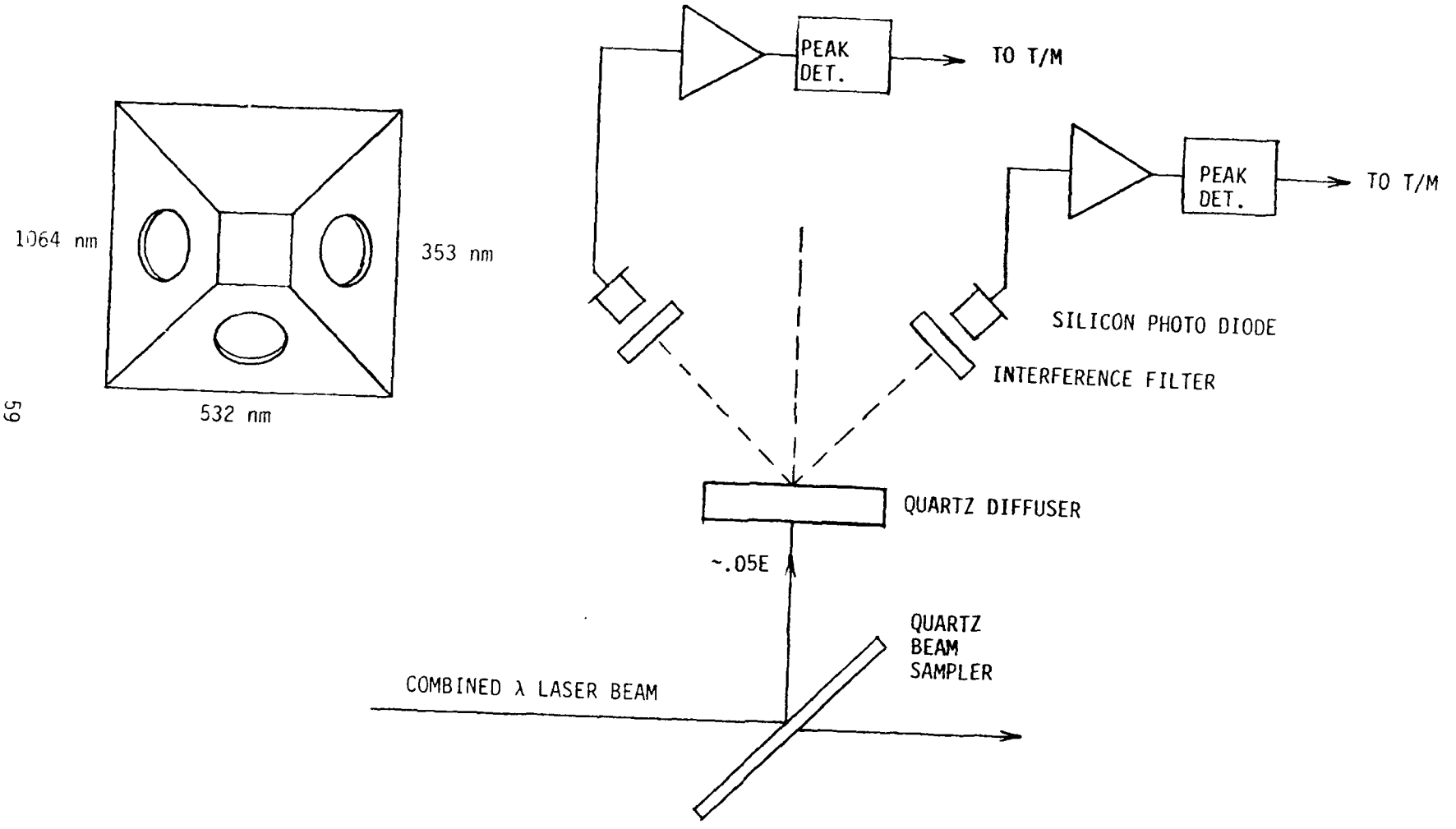

Figure 7.2 Radiant Power Monitor

TABLE 7-1

TRANSMITTER SAFETY INTERLOCKS

In-Flight Operation

- BAROSWITCH
- POINTING MIRROR IN SET POSITION
- COMMANDS
    1) POWER ON (LATCHED)
    2) LASER ARM (LATCHED)
    3) FIRE (CONTINUOUS TRANSMISSION REQUIRED)
- COOLANT TEMPERATURE

Ground Operation

- KEY SWITCH POWER ON
- KEY SWITCH LASER ARM
- VISUAL INDICATION OF LASER STATUS
- AUDIBLE ALARM PRIOR TO LASER FIRING

TABLE 7-2

TRANSMITTER DATA

	T/M Link Number	Resolution (Bits)	Sampling Frequency (Hz)
353 nm Radiant Power Monitor	1	8	10
532 nm Radiant Power Monitor	1	8	10
1064 nm Radiant Power Monitor	1	8	10
Synchronization	2	1	10
Laser Chamber Press Monitor	2	10	1
Power Supply Chamber Press Monitor	2	10	1
28 Vdc Reference	2	10	1
SHG X Reference	2	1	5
SHG Y Reference	2	1	5
THG X Reference	2	1	5
THG Y Reference	2	1	5
SHG Temperature	2	10	1
THG Temperature	2	10	1
Laser ON	2	1	1
Laser OFF	2	1	1
Laser ARM	2	1	1
Laser SAFE	2	1	1
Laser FIRE	2	1	10
Timer Status	2	1	1
Baroswitch	2	1	1
Interlock Override	2	1	1

TABLE 7-3

TRANSMITTER COMMANDS

LASER POWER ON
LASER POWER OFF
LASER ARM
LASER SAFE
LASER FIRE CONTINUOUS 10 PPS
LASER FIRE SINGLE SHOT
XTAL ANGLE CW
XTAL ANGLE CCW
SHG X
SHG Y
THG X
THG Y
INTERLOCK OVERRIDE
TIMER RESET

TOTAL COMMANDS 14

7.3 Laser Specification for a Typical Nd:YAG Laser Chosen for Development of the Lidar System Design

Laser Model:	ILS 104-10 with DC Power Supply		
Type:	Nd:YAG		
Output Wavelengths:	1064 nm	532 nm	355 nm
Minimum Output Energy:	700 mJ	150 mJ	30 mJ
Exit Beam Divergence:	≤2 mr	≤1 mr	≤1 mr (Beams are triaxially aligned)
Amplitude Stability: (Pulse to Pulse)	≤3%	≤5%	≤10%
Repetition Rate:	10 pps		
Pulse Width:	15 nsec		
Pulse Jitter (Sync to Pulse)	≤50 nsec		
Exit Beam Diameter:	6.35 mm		
Head Size:	8.19" x 12.75" x 40.81"		
Head Weight:	40 lbs.		
Coolant:	30% Deionized Water - 70% Glycol		
Coolant Flow:	0.5 gal/min typ. ± .25 gal/min		
Coolant Pressure:	12 psig max.		
Maximum Coolant Temperature at Outlet	55°C		
Minimum Coolant Temperature at Inlet	5°C		
SHG Crystal:	CD*A		
THG Crystal:	KDP		

The THG and SHG crystals are to be mounted in 20 watt ovens to eliminate spectral drift due to temperature tuning of the crystals during operation. Two-axis angle tuning micrometer adjustment mounts will be provided for SGH and

THG crystals. Micrometer type will be Ardel Kinamatic 0.5 inch Motor Mikes and Motor Mike Controller to be provided by contractor.

Operating Temperature Range:	25°C $\pm$ 5°C at full rated radiant output at all wavelengths without adjustment. 10°C to 35°C with minor optical realignment.
Attitude:	Laser will be capable of rated operation with the laser head oriented horizontally $\pm$ 20° degrees.
Altitude:	Sea Level to 10,000 ft.
Relative Humidity:	0 to 90%
Mechanical Shock:	System shall withstand a 2g, 70 msec half sine shock in any axis without degradation in performance. System shall withstand a 10g, 70 msec half sine shock in any axis without damage.
Power Supply Input Voltage:	28 VDC $\pm$ 4 VDC
Input Current:	40 amps average 60 amps peak
	The master power supply will have a TTL compatible synchronization pulse input to permit external control of laser firing. TNC connector is preferred.
Size:	Master - 11" high x 21" wide x 13" deep Slave - 11" high x 21" wide x 13" deep
Weight:	Master - 40 lbs. Slave - 35 lbs.
	Unit is to include three flashlamp simmer power supplies.
Power Supply Operating Temperature:	0°C to 35°C
Power Supply Rated Efficiency:	50% minimum

Accessories Required

3 SS-100 Simmer Power Supplies
1 C1002 Shot Counter

1 C1082 Cooling Supply
A liquid coolant-to-air heat exchanger system will be supplied. The system will be capable of dissipating the thermal load of the laser system during continuous laboratory operation. This unit will not be part of the flight configuration.
Size: 9" x 14" x 20"
Weight: 60 lbs.

1 SHG Crystal (CD*A) w/oven

1 THG (KDP) Crystal w/oven
C1088

1 Line Converter
C1012
This unit, with an input of 115V 60 Hz 10 amps average and an output of 28 VDC power, is required to operate the laser system continuously in the laboratory. This unit will not be part of the flight configuration. The converter will consist of two (2) units each:

Size: 9" x 14" x 20"
Weight: 70 lbs.

Modification Required

1. Laser modifications are required in order to provide up to a maximum of 18 additional tapped holes in the laser optical bench. Hole locations will be defined when order is placed.

2. Two sets of interconnecting cables are to be delivered with the system. One set is to be used when the laser is operated in the laboratory. The second set will be used when the laser system is in the flight configuration. Maximum length of each set will be four (4) meters.

3. System User Manual is to be delivered three weeks ARO. Complete engineering drawings, to commericial standards, are to be delivered with system.

4. Notification is to be given prior to final testing so that a user representative can be present during the final test.

Laser Modification to be Done by Contractor after Delivery of Laser and Acceptance Testing

1. Modify safety interlocks for flight operation.
2. Remove laser head cover.
3. Add temperature sensors to optical bench and coolant lines.
4. Add three wavelengths energy/pulse monitors to optical bench.
5. Add diverging lens to optical bench.
6. Add high voltage monitors to power supply.
7. Add temperature monitors to power supply.
8. Install command angle-tuning mechanism.

6.0 RECEIVER DESIGN

6.1 Receiver Layout

The lidar receiver layout is shown in Figure 6.1. Principal assemblies of the receiver are the following:

a) Cassegrain telescope assembly
b) beamsplitter-filter assembly
c) 1064 nm detector assembly and cryogen supply
d) 355 nm detector assembly

The telescope assembly, including the field stop is on a vertically adjustable mount. All field of view alignments can therefore be made in this one assembly. A flexible, light-tight coupling connects the telescope and beamsplitter-filter assemblies. When this coupling is removed, the receiver field-of-view can be observed during focusing and pointing adjustments by inserting an ocular lens and 45° folding mirror assembly focused on the field stop.

The beamsplitter-filter assembly is hard-mounted to the 1064 nm detector assembly. The first relay lens is mounted ahead of the beamsplitter. It focuses the field stop straight through the beamsplitter onto the 355 nm detector and also reflected at 90° through the beamsplitter onto the second relay lens mounted in the 1064 nm detector housing. The second relay lens focuses the image of the first relay lens onto the small photocathode in the 1064 nm detector.

6.2 Receiver Optical System

The receiver optics, shown in Figure 6.2, consists principally of a large aperture collector, a beamsplitter to separate the 355 nm and 1064 nm wavelengths, and a pair of narrow band interference filters to eliminate the out-of-band background radiation. The lidar receiver optical specifications are listed in Table 6-1.

The collector optics consists of a 50 cm diameter F/1.0 concave paraboloidal primary mirror and a 10 cm diameter convex hyperboloidal secondary. The telescope collecting area is 1875 cm^2. The fact that the spatial resolution required here is modest and the field of view is small, indicates that the aberrations of the collector optics will not be a problem. The modest spatial resolution requirement also allows the use of a lightweight,

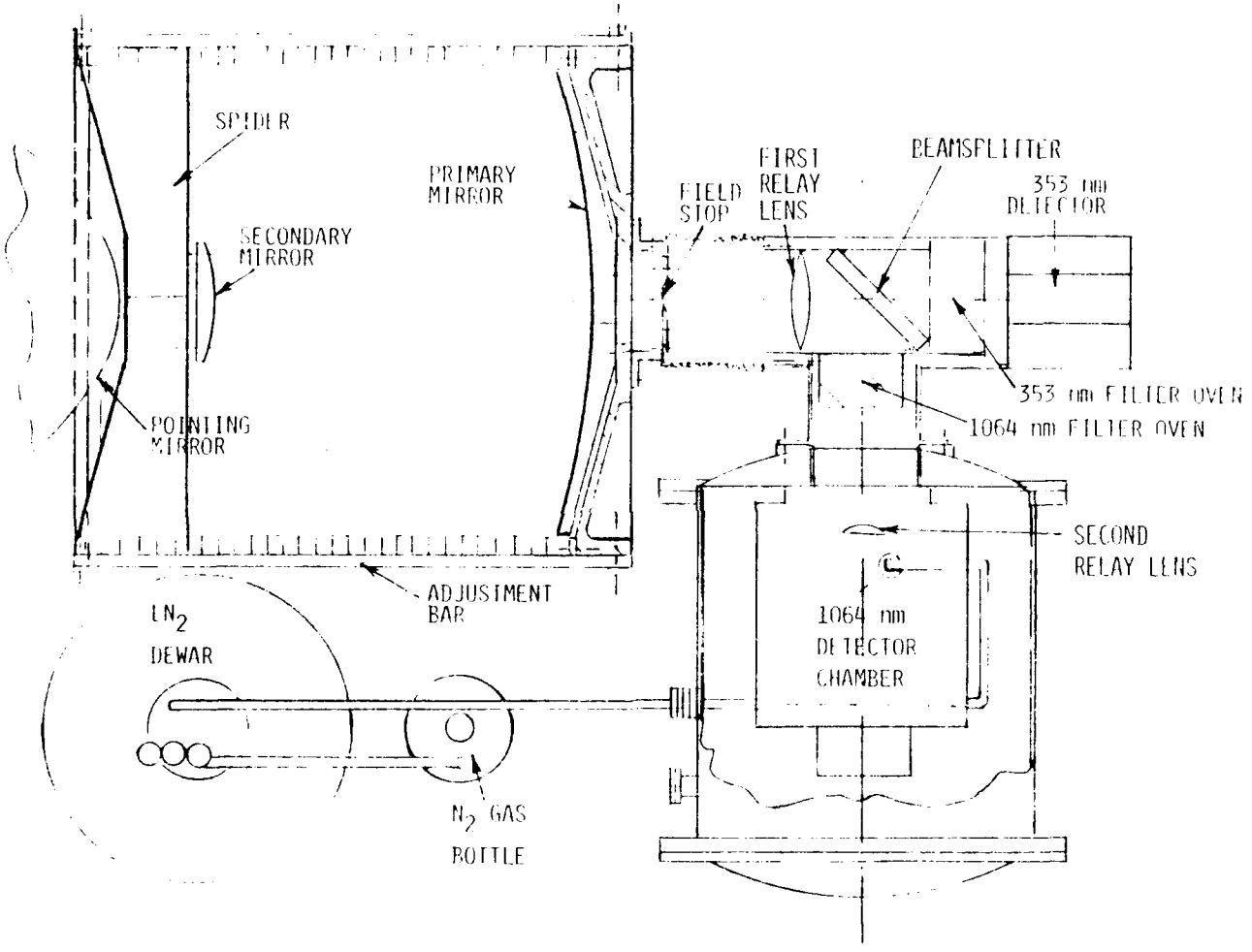

Figure 8.1 Receiver Layout

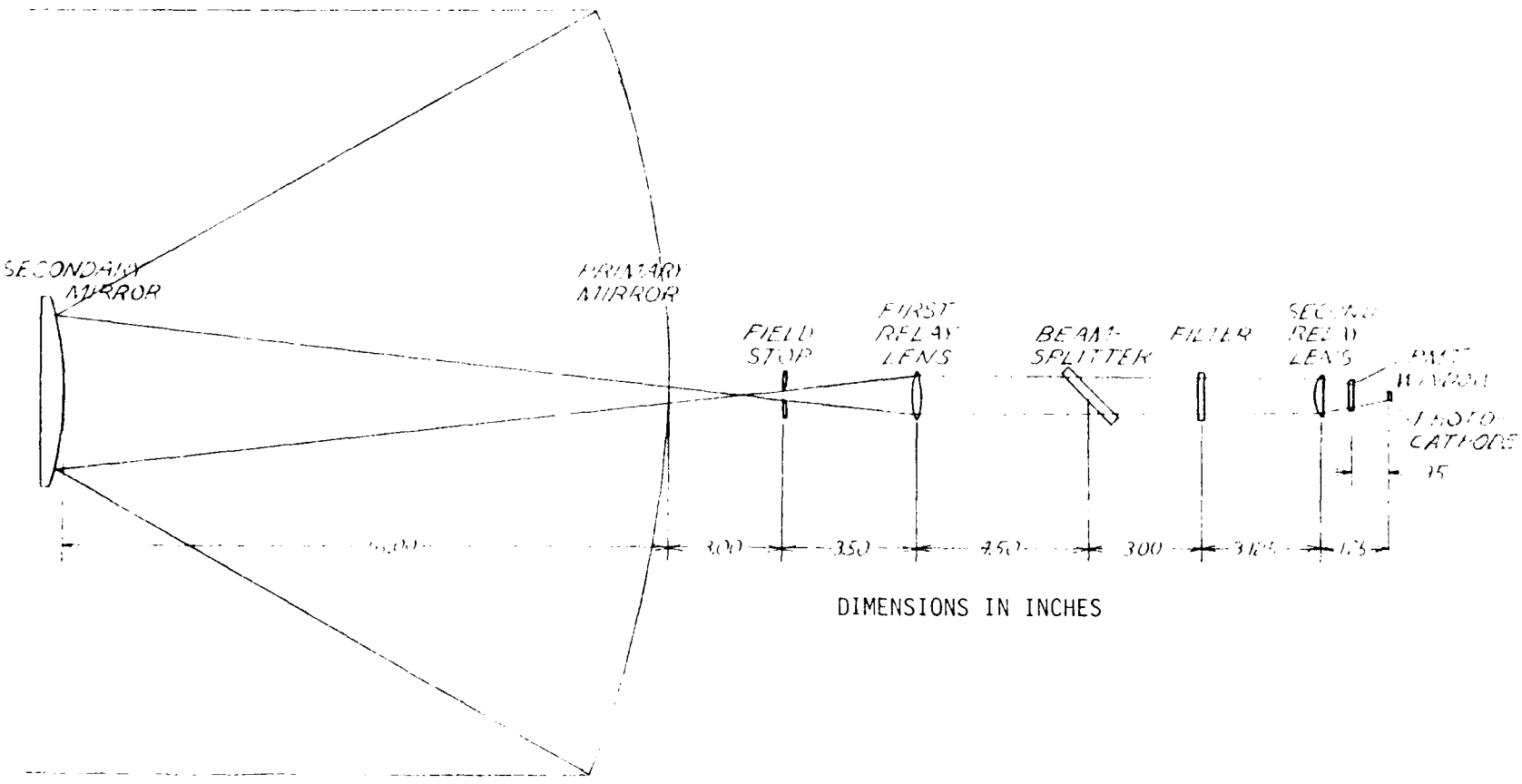

Figure 8.2 Receiver Optics Layout

TABLE 8-1

LIDAR RECEIVER OPTICAL SPECIFICATIONS

Field of View	3 mr
Telescope	
Type	Cassegrain
f/no.	5.0
Primary Mirror	
Material	Aluminum
Diameter	50.4 cm
Coating	Aluminum + SiO
Secondary Mirror	
Material	Aluminum
Diameter	10.1 cm
Coating	Aluminum + SiO
Effective Collecting Area	1875 cm^2
Effective Focal Length	241.3 cm
Reflection	
@ 353 nm	.79
@ 1064 nm	.83
Relay Lenses	
Material	Fused Silica, AR-coated
Lens Number 1	
Type	Biconvex
Focal Length	6.68 cm
Diameter	3 cm
f/no.	2.1
Lens Number 2	
Type	Plano-convex
Focal Length	3.82 cm
Diameter	2.5 cm
f/no.	1.5
Beamsplitter	
Material	Fused Silica, AR-coated
Transmission	
@ 353 nm	>.90
@ 1064 nm	<.05
Reflection	
@ 353 nm	>.05
@ 1064 nm	<.90
Interference Filters	
Clear Aperture	4.5 cm
Bandpass	
353 nm	30Å
1064 nm	10Å
Transmission	
353 nm	.2
1064 nm	.35

ribbed structure for the primary, which will be machined from aluminum. The paraboloidal optical surface will be generated on a numerically-controlled lathe, and then polished with diamond machining. Because of its small size, the weight of the secondary mirror will be negligible regardless of its construction. It would be fabricated in a manner similar to the primary. The secondary will be positioned in the system using a vaned spider support structure.

The choice of coatings for the receiver optics is rather limited because of the wavelengths of the laser lines. Gold can be ruled out because although it can be made to be very durable and is an excellent reflector at 1064 nm, its reflectivity at 355 nm is less than 0.4. Except for silver and aluminum, most other metals have relatively low reflectivities.[12] Multilayer dielectric coatings are not suitable because, in addition to manufacturing difficulties and angular effects, their maximum refectivity is limited to bandwidths of about 200 nm. Reflectivities for protected silver and SiO-overcoated aluminum are shown in Figure 8.3.

Our choice for the mirror coatings is aluminum for the following reasons:

1. Reflectivity for the aluminum is nearly constant with wavelength while that of silver is dropping sharply below 350 nm. If the silver coating should degrade at all, this edge might shift and drastically affect the reflectivity.

2. The protected silver coating meets only the humidity provisions of MIL M-13508C while the aluminum - SiO_2 coating meets or exceeds all requirements of MIL M-13508C.[13] This coincides with our experience.

As shown in Figure 8.2, the beam from the secondary mirror passes through the field stop and first relay lens and strikes the beamsplitter. A beamsplitter is used as part of the receiver optics to separate the backscatter radiation into its two spectral components at 355 and 1064 nm. It is of the single plate type, set at 45° to the incoming radiation, and designed to reflect the 1064 nm signal and transmit the 355 nm signal. The plate will be made of fused silica and its rear surface will be antireflection-coated for 355 nm. Such beamsplitters are commercially available. It should be noted that because the beamsplittter is at an angle to the incoming radiation, its reflectivity can vary depending upon the polarization of the incident radiation. Since the transmitter laser emits a pulse which is polarized, the Rayleigh backscattered signal will be polarized as well. However, if properly

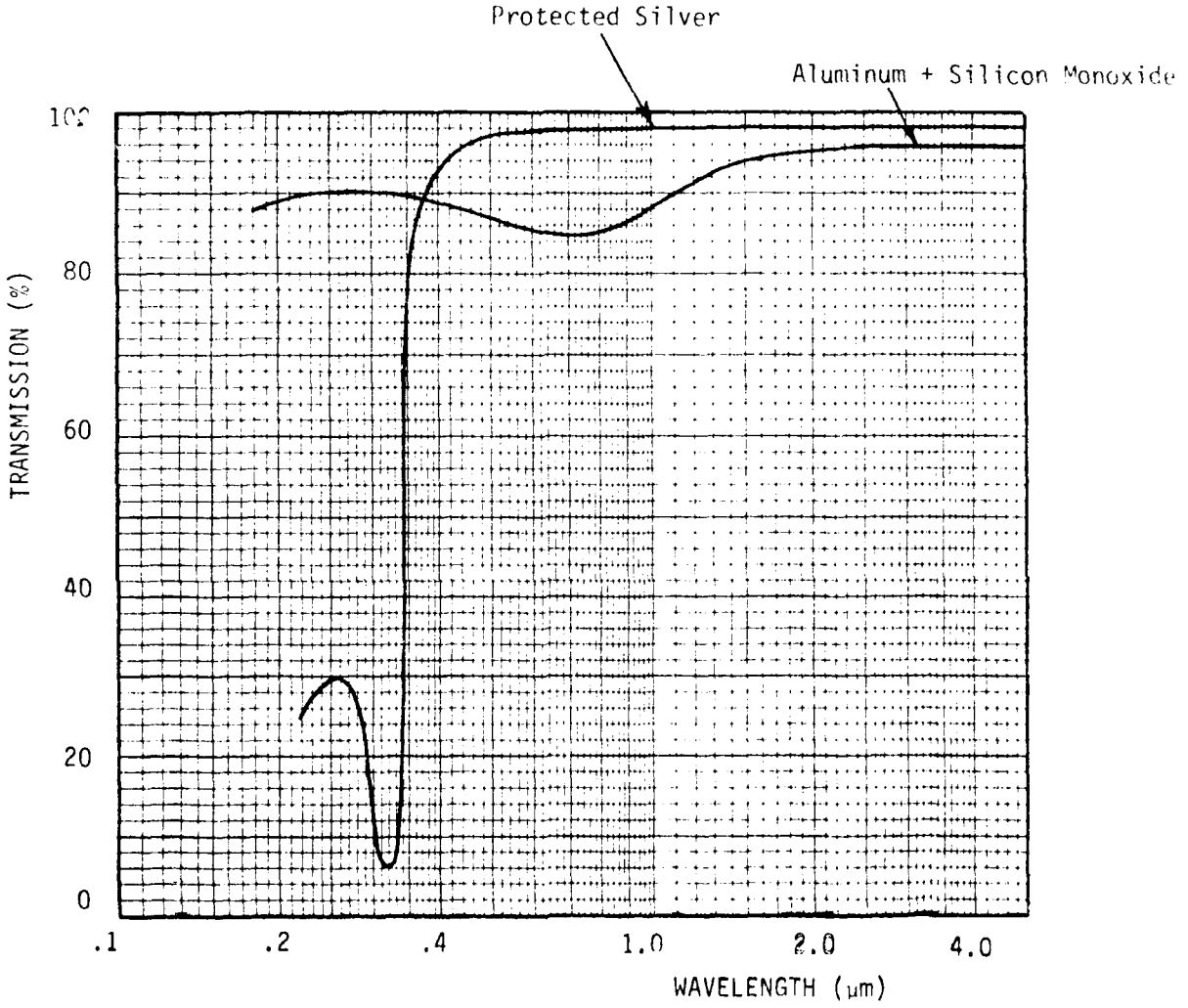

Figure 8.3 Receiver Mirror Coatings

designed, the beamsplitter will reflect better than 96% of the 1064 nm radiation independent of its polarization, and at the same time, transmit better than 96% of the 355 nm radiation. Suitable data curves to be supplied by the manufacturer will verify this specification.

The chosen width of the passbands of the narrowband filters are a compromise between a width narrow enough to reject out-of-band background radiation and one wide enough to guarantee that temperature drifts will never vary the filter transmissions measurably at the wavelengths of the backscattered signals. The wavelengths of the output of the SHG and THG crystals in the transmitter vary with temperature. However, these crystals are temperature stabilized with heaters. The interference filters in the receiver have passband drift coefficients of 0.06% per °C,[14] which is 0.25Å at 355 nm and 0.75Å per °C at 1064 nm. Therefore, the interference filters will be temperature stabilized by mounting them in temperature-controlled ovens.

Table 6.2 lists the diameters and maximum beam sizes for each of the components of the receiver optics. The field stop aperture, by definition, determines the angular field of view and it should be noted that the maximum beam size for each component in the optical path beyond the field stop is less than the corresponding clear aperture. Hence, there is no vignetting of the beam and no resulting loss of signal.

The performance of the telescope optical design of the receiver has been verified using a ray tracing program, RAYTRAC, developed at Visidyne. This is a versatile program which can ray trace optical systems consisting of a wide variety of conventional and unconventional optical components.

6.5 Detector Specifications

The sensor for the 1064 nm radiation will be a Varian VPM-164A photomultiplier which has an indium gallium arsenide phosphide photocathode. This material exhibits a quantum efficiency of approximately 1 percent at 1064 nm. A characteristic of the VPM-164A is that it must be maintained at temperatures lower than -20°C except for the short periods of time required for assembly. Extended periods at higher temperature will result in cathode degradation. Thus, a LN_2 cooling system capable of operating for extended periods was designed. This system uses a Products for Research Inc. TE-166TSRF cooling chamber and temperature controller. The system is shown schematically in Figure 6.4. A lecture cylinder of dry N_2 provides 15 psig N_2, through a regulator, to force the LN_2 from the dewar to the cooling chamber. A temperature

TABLE 8-2

RECEIVER OPTICS DIMENSIONS AND BEAM SIZE

Component	Diameter (in)	Maximum Beam Size (in)
Primary Mirror	20	20
Secondary Mirror	5	4
Field Stop Aperture	0.285	0.285
First Relay Lens	1.250	1.074
Beamsplitter	1.500 (@ 45°)	0.985
Filter	1.250	0.926
Second Relay Lens	1.000	0.865
PMT Window (1064 nm)	0.625	0.550
PMT Photocathode (1064 nm)	0.200	0.177

sensor in the cooling chamber controls a solenoid valve which controls the LN_2 flow into the chamber. A return line vents the gaseous N_2 into the atmosphere. The specified LN_2 usage rate of the chamber is 0.75 liters/hour. Thus, the system hold time, including piping losses, will be greater than 16 hours. For extended periods of operation, an LS-160 will be connected to the cooling chamber. Hold times in excess of seven days are specified for this mode of operation. For shipment of the payload from AFGL to the launch site, an LS-160 of LN_2, connected on the cooling system, will be shipped with the payload. During the post flight payload recovery operation, the detector chamber will be removed from the payload and connected to an LS-160 and shipped back to the launch site.

A small electrically powered food freezer will be used to store the photomultiplier for extended periods when it is not in use.

Since the photomultiplier requires high bias voltages, it is required that the cooling chamber be enclosed in an outer pressure vessel so that the detector is maintained at standard pressure throughout the flight.

The sensor for the 353 nm radiation is an EMR photomultiplier 541-N-14 having a bi-alkali photocathode. This sensor will not require cooling because the dark counts for this tube are typically 1.6×10^2 counts/sec.

8.4 Receiver Data Processing

The return signal from a range cell can be as high as 10^4 counts per 667 nsec, or 1.5×10^{10} counts/sec; thus it is not practical to pulse count. The output current will be measured using an R-C integrator as shown in Figure 8.5. The voltage across capacitor C will be proportional to the charge.

$$C = \frac{e \times G}{V}$$

where

e = electron charge (1.6×10^{-19}c)
G = PMT Gain (10^6)
V = Volts/count (10^{-3})
C = 160 pf

This voltage will decay with the time constant, RC. By setting RC = 667 nsec, which corresponds to the width of a range cell, and sampling the capacitor voltage once each range cell, an accurate representation of the backscatter signal is obtained.

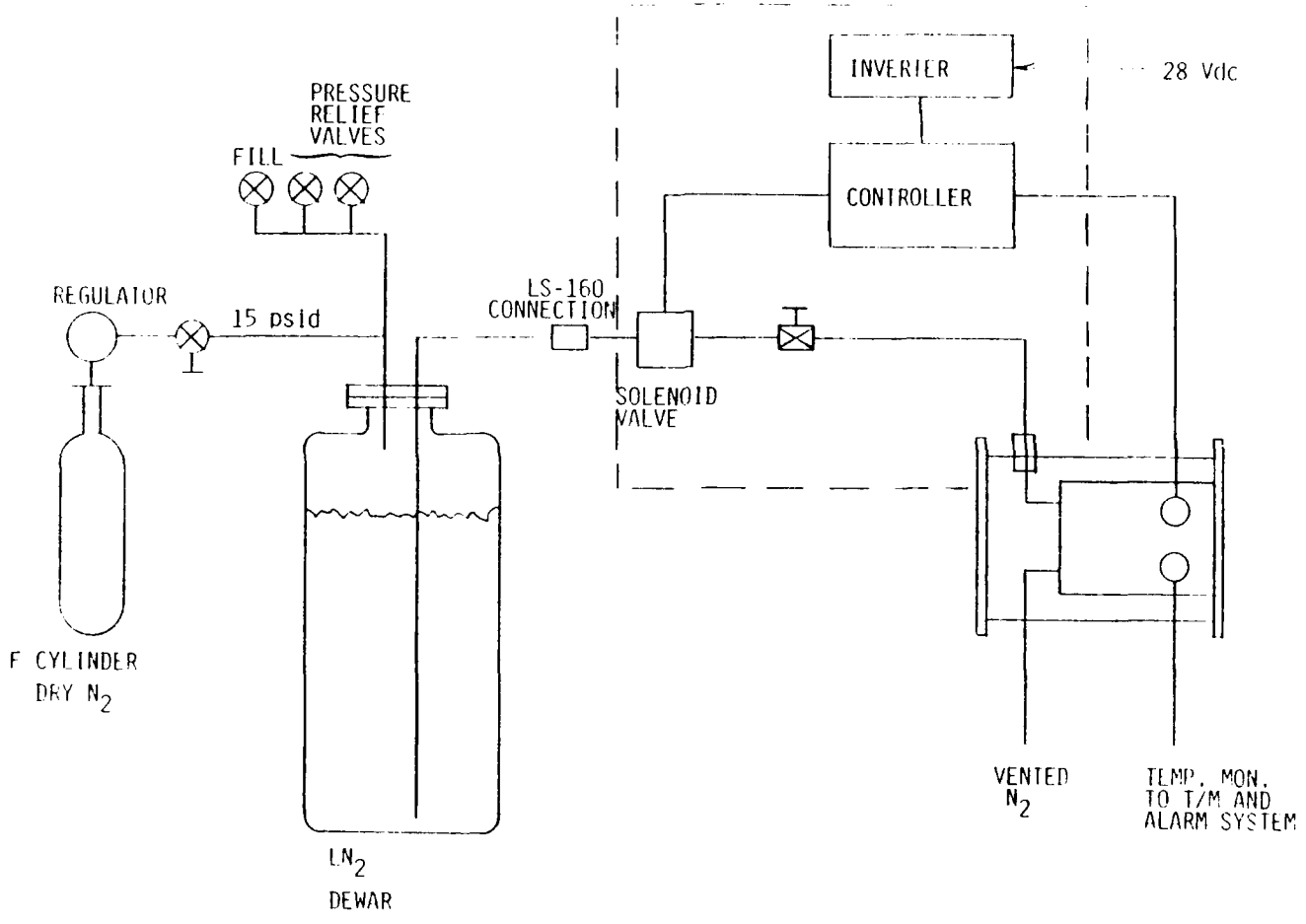

Figure 8.4 1064 nm Detector Cooling System

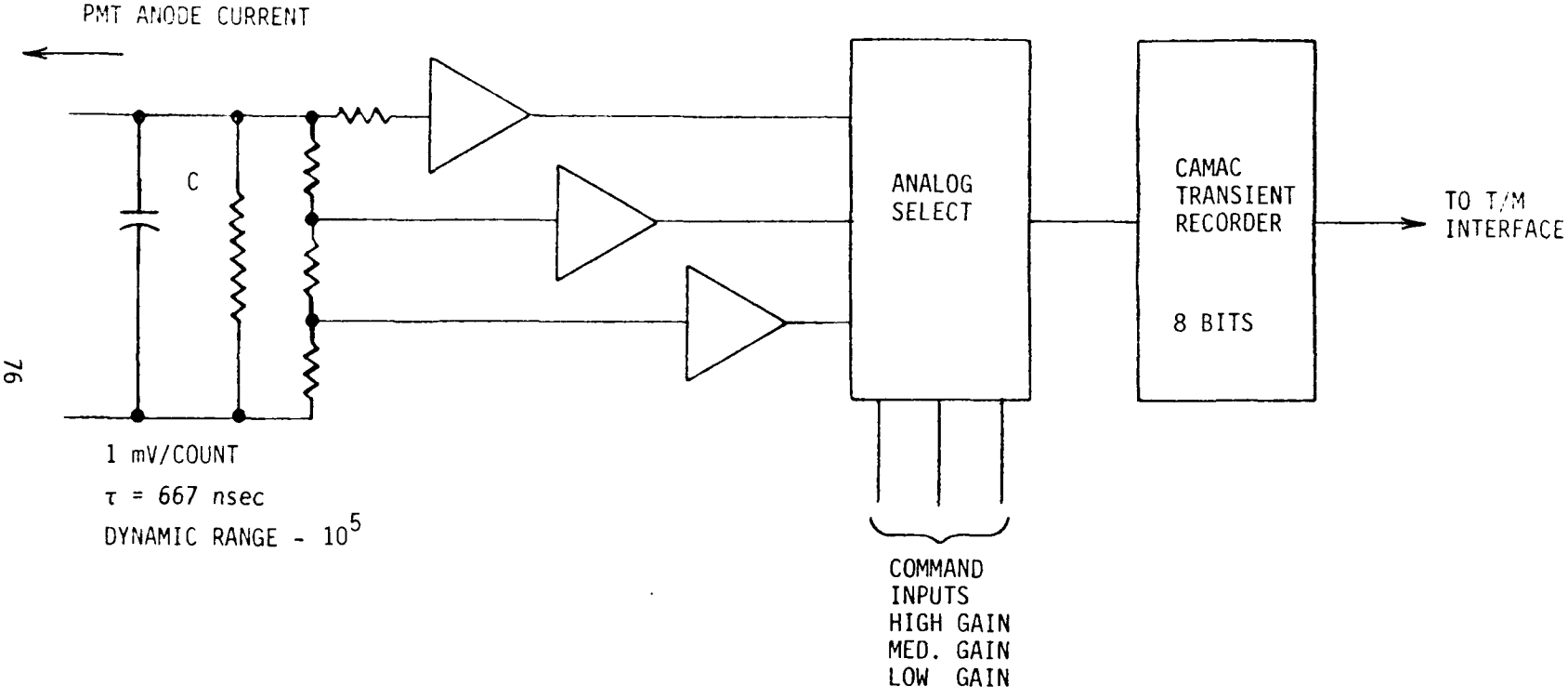

Figure 8.5 Receiver Electronics

The voltage across capacitor C is fed through three high frequency amplifiers chains having gains of -20, -1, and -0.05. This provides full scale output voltages of 5.12 volts for 256 counts, 5120 counts, and 102,400 counts respectively. These analog signals are fed into J-FET switches which are cascaded to provide 100 dB on-off isolation. The appropriate amplifier chain is selected by uplinked commands which select gain switching programs to be run on a microprocessor (8748).

The selected analog signal is sent to the input of a LeCroy Model 2256AS CAMAC[15] waveform digitizer.

A crystal oscillator generates the 1.50 MHz sampling clock. The waveform digitizer is set up in the pretrigger mode and the digitizer is continuously sampling and storing the data. When the q-switch trigger is received from the laser, the memory is loaded with 1024 8-bit data words of which 128 are those sampled prior to the Q-switch trigger (and laser firing) and thus will be used for a measurement of background. When the digitizer memory is full, a signal is sent to the CAMAC controller module.

A block diagram of the digital data handling system is shown in Figure 8.6. A microprocessor controls the read-out of data, via the CAMAC buss, from each of two digitizers. 528 (of 1024 words in memory) 8-bit data words representing 128 background samples and 400 backscatter range bins are read-out of each digitizer. In addition, two data words representing dc offset and panel switch positions are read out with the data. The data from the digitizer is read into a first-in, first-out (FIFO) memory which acts as a buffer between the digitizer system and the pcm encoder.

The PCM encoder reads the data from the FIFO, encodes it with the specified synchronization patterns, formats it into a major frame structure, and converts it into an NRZ-L 100 k bit/sec serial bit stream.[16] The NRZ-L data is converted into BØ-L before being inputted into the transmitter. The bØ-L serial data out of the ground receiver can be direct recorded on a wideband instrumentation recorder running at 15 ips.

System timing is simplified by the following:

1. The use of pre-trigger mode in data digitization.

2. The use of a FIFO in isolating data read-out timing from the PCM encoder timing.

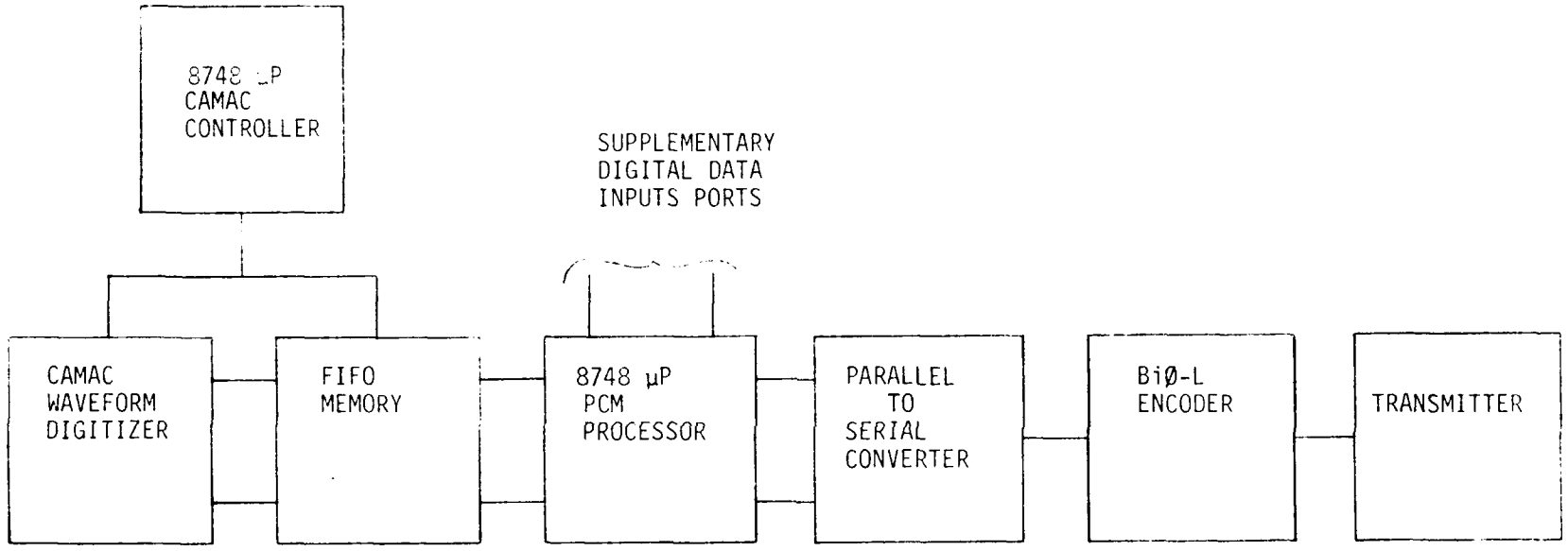

Figure 8.6 Digital Data System

The major timing functions are the following:

1. 100 kHz PCM Clock and 9.77 Hz Laser Firing Clock
2. 1.5 MHz Data Sampling Clock.

The laser Q-switch trigger is used as a laser fire cursor pulse because there is a 120 to 140 μsec time delay between the firing synchronization pulse input to the laser and the laser firing, whereas with the Q-switch trigger, the delay is 150 nsec.

The packaging of the receiver electronics with the exception of the detectors, preamplifiers, and high voltage power supplies, will be CAMAC modules or in an auxiliary card rack chasis. The detectors and their electronics will be located in their respective pressure housings.

To prevent excessive photocathode current in the photomultipliers, it will be required to range-gate each photomultiplier. The range gating will gate the photomultiplier off during the time the ground backscatter is received. Range gating will be required only when the lidar is pointed downward. The gating will be done by connecting a high voltage MOSFET to dynode 2 of the photomultiplier. The application of a logic pulse (5 volts) to the gate will clamp dynode 2 (and dynode 1) to ground in 200 nsec, with zero volts between the cathode, dynode 1, and dynode 2. With the dynode 1 and 2 extraction voltages gated off, the cathode photocurrent will be cutoff by the cathode space charge.

The location of the range gate will be controlled through the uplink command system. The PMT will be shut off for a period of 50 μsec corresponding to the range gate. A 10 Hz clock will increment the range gate, in or out as selected by command, with respect to the laser synchronization pulse.

Receiver data are listed in Table 8-3 and the PCM data budget is summarized in Table 8-4. Commands and power requirements are in Tables 8-5 and 8-6.

TABLE 8-3

RECEIVER DATA

	T/M Link Number	Resolution (Bits)	Sampling Frequency (Hz)
353 nm Gain Status	1	2	10
1064 nm Gain Status	1	2	10
353 nm PCM Data	1	(See Table 8-4)	
1064 nm PCM Data	1		
353 nm Detector H/V Monitor	2	10	1
1064 nm Detector H/V Monitor	2	10	1
353 nm Detector Temperature Monitor	2	10	1
1064 nm Detector Temperature Monitor	2	10	1
1064 nm Detector Press Monitor	2	10	1
353 nm Filter Temperature Monitor	2	10	1
1064 nm Filter Temperature Monitor	2	10	1
353 nm Range Gate Location	1	10	10
1064 nm Range Gate Location	1	10	10
353 nm Range Gate Enable	1	1	10
1064 nm Range Gate Enable	1	1	10

TABLE 8-4

PCM DATA BANDWIDTH SUMMARY

	2 Detectors	All Detectors Total (kbps)
Signal/Detector 8 Bits/Sample x 400 Range Bins x 10 pps = 32 kbps/Detector		64.00
Background/Detector 8 Bits/Sample x 128 Range Bins x 10 pps = 10.24 kbps/Detector		20.48
Digitizer Switch Position 8 Bits/Sample x 1 Sample/Frame x 10 pps		.16
Digitizer dc Offset 8 Bits/Sample x 1 Sample/Frame x 10 pps		.16
Range Gate Position 10 Bits/Sample x 1 Sample/Frame x 10 pps		.20
	Synchronization	10.00
	Unassigned	5.00
		100.00 kbps

TABLE 8-5

RECEIVER COMMANDS

353 nm GPROG0
353 nm GPROG1
353 nm GPROG2
353 nm GPROG3
1064 nm GPROG0
1064 nm GPROG1
1064 nm GPROG2
1064 nm GPROG3
DETECTOR TEST
353 nm RANGE GATE ENABLE
1064 nm RANGE GATE ENABLE
353 nm RANGE GATE ADJ
1064 nm RANGE GATE ADJ
RANGE GATE IN/OUT
RANGE GATE CLEAR

TOTAL COMMANDS 15

TABLE 8-6

RECEIVER POWER

28 Vdc 6 AMP CONTINUOUS

9.0 POINTING MIRROR SYSTEM

The pointing mirror system, shown in Figure 9.1, is composed of a laser mirror, a cloud monitor mirror, and a receiver mirror all connected rigidly to a commandable motor driven shaft.

The shaft is supported at only two points, one at the gear box bearing and the other at a self aligning ball bearing adjacent to the receiver mirror. beyond this bearing, the shaft supports the cloud monitor and laser mirrors as a cantilever beam. The cantilever has been designed to minimize the deflections of the pointing mirrors. This is accomplished by using the weight of the receiver mirror to counterbalance the deflection of the cantilever beam.

The pointing mirrors will be co-aligned, on the ground at ambient temperature, at a position 45° from the vertical nadir (lidar viewing down). The only other attitude which need be considered for alignment errors is that 60° from the vertical zenith (lidar viewing 30° from zenith). By using a design which compensates for thermal variations of the components, the only errors we have to consider are the tolerance in the bearing's backlash which generates a maximum movement at the laser pointing mirror of 109 μin, and the movement due to the difference in deflection due to variable stiffness of the pointing receiver mirror at 45° and 60°, which is 41 μin. The maximum total movement is therefore 150 μin. Since the distance between the pointing receiver mirror and the pointing laser mirror is 39.37 inches, the angular variation between the two is = 3.8 μradians.

The reflected ray is deflected twice as much or ~8 μradians, which is negligible compared to the 3 milliradian angular field of view of the lidar optical system.

The pointing system shaft is centered on the receiver mirror axis, but offset from the laser and cloud monitor axes as shown in Figure 9.2. In the horizontal viewing mode, the laser and cloud monitor mirrors are out of the field of view. The obscuration of the receiver pointing mirror when in the horizontal mode is approximately 10%. This is less than the reflection losses of the mirrors when the pointing system is used in the zenith and nadir modes. The mirror coatings are the same as used on the receiver telescope (See Section 8.2).

Positioning of the mirrors will be controlled and indicated by cams and switches. The shaft is driven by an ac motor with a gear head. The shaft bearings must operate over the required temperature range (down to -50°C). Table 9-1 lists the purchase parts of the pointing mirror system.

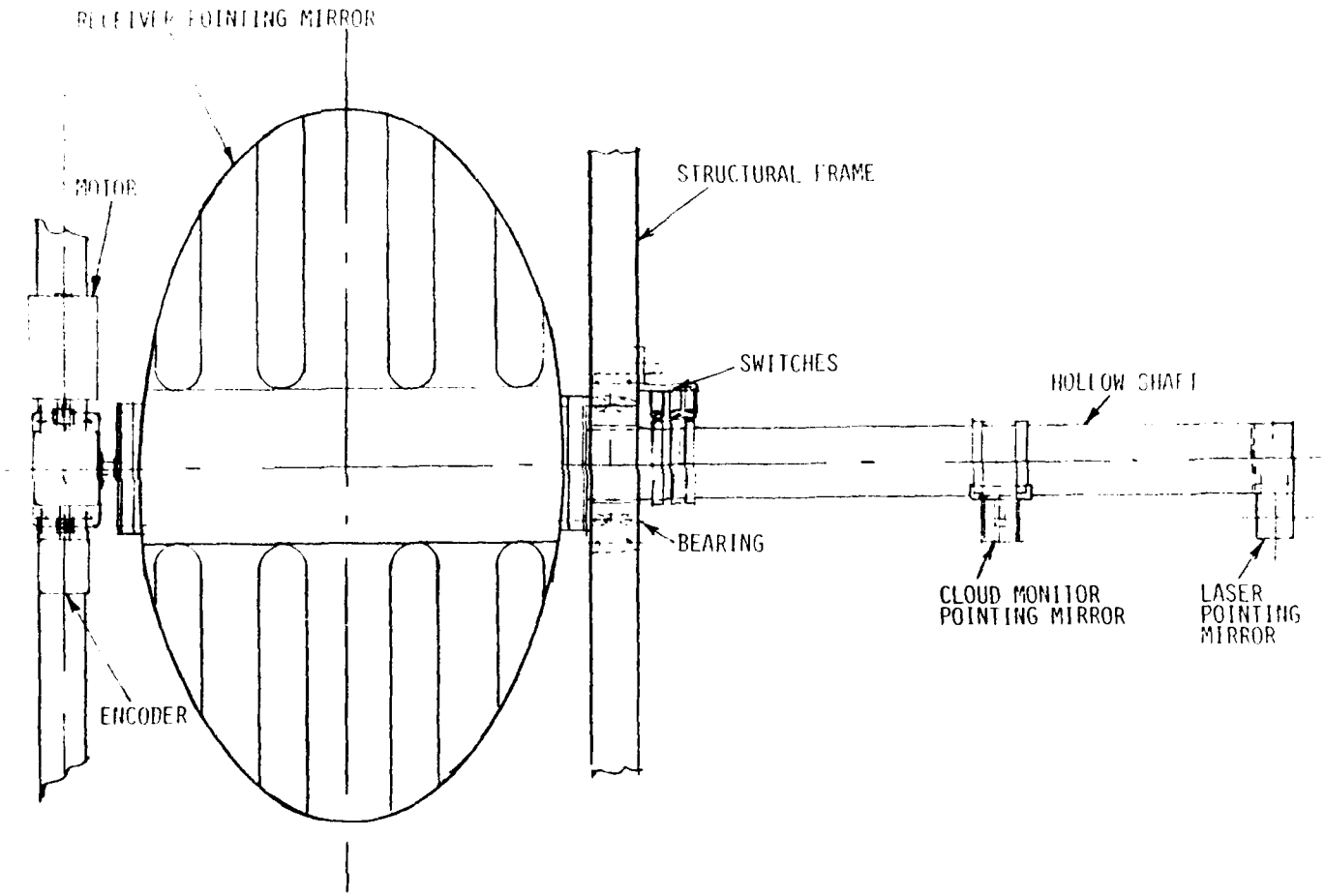

Figure 9.1 Pointing Mirror System

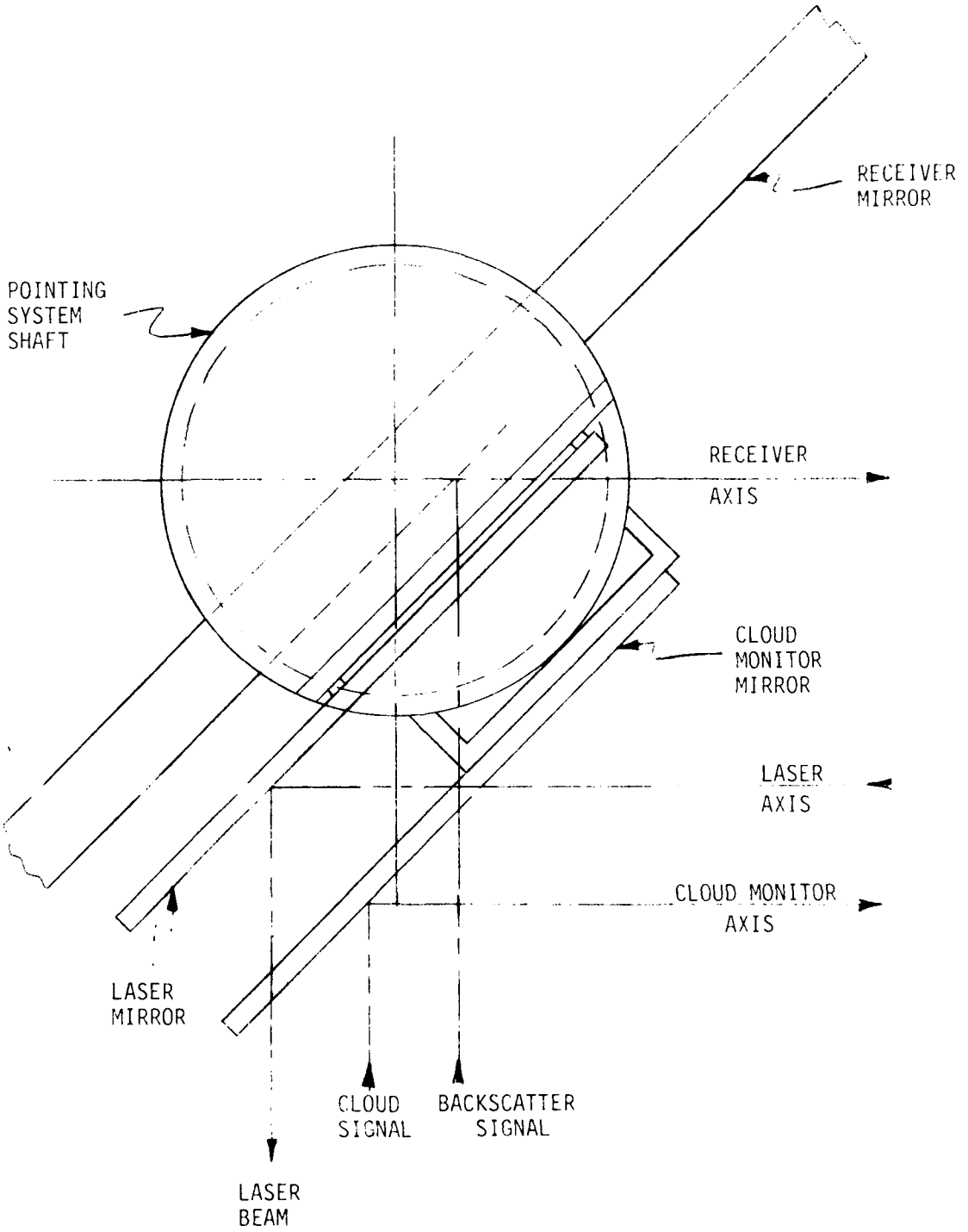

Figure 9.2 Pointing Mirror Positions, Nadir Operation

TABLE 9-1

POINTING SYSTEM PURCHASE PARTS

Item	Qty	Description	Manufacturer	Comments
1	1	AC. Motor 400 Hz -83A108-	TRW Globe	
2	1	Bevel Gear Drive Page 147 PT353-78 AD 3	Hub City	Test for -65°F Operation
3	1	Potentiometer Model 3465 2" dia.	Burns	
4	4	Switches 1 SX T2 Terminal	Microswitch	
5	2	Clamps 3 1/2 Dia. 9/16 S/S	Ideal Corporation Brooklyn, NY	
6	1	Self Aligning Ball Bearing 2305	SKF	To be checked for cold operation.
7	1	Pillow Block	SKF	
8	1	Bellows S/S 4.OD.	Standard Thomson	
9	1	Bellows Neoprene LDF-5-263-4-4 Catalog page 30	Latex Products Hawthorne, NJ	

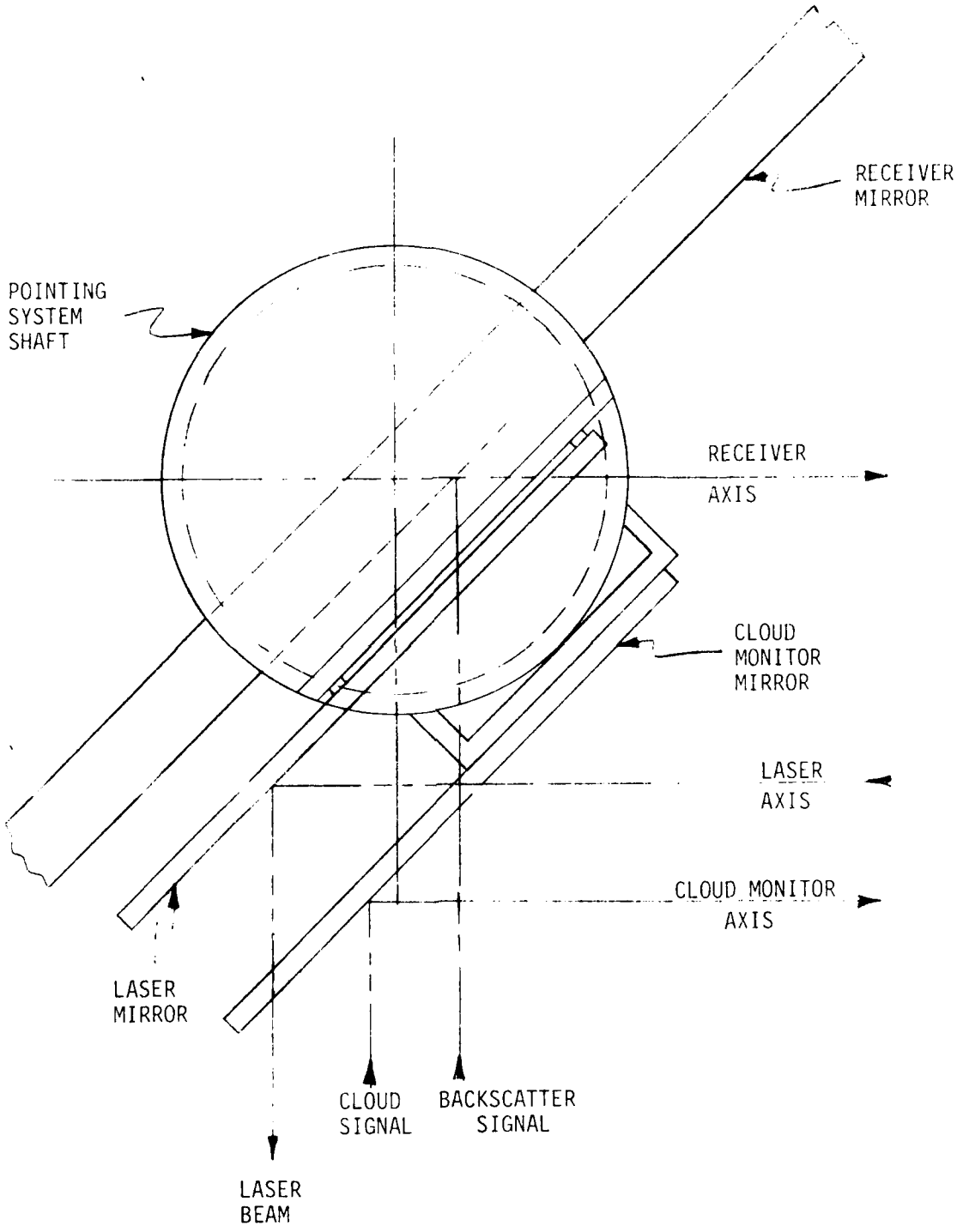

Figure 9.2 Pointing Mirror Positions, Nadir Operation

TABLE 9-1

POINTING SYSTEM PURCHASE PARTS

Item	Qty	Description	Manufacturer	Comments
1	1	AC. Motor 400 Hz -83A108-	TRW Globe	
2	1	Bevel Gear Drive Page 147 PT353-78 AD 3	Hub City	Test for -65°F Operation
3	1	Potentiometer Model 3465 2" dia.	Burns	
4	4	Switches 1 SX T2 Terminal	Microswitch	
5	2	Clamps 3 1/2 Dia. 9/16 S/S	Ideal Corporation Brooklyn, NY	
6	1	Self Aligning Ball Bearing 2305	SKF	To be checked for cold operation.
7	1	Pillow Block	SKF	
8	1	Bellows S/S 4.OD.	Standard Thomson	
9	1	Bellows Neoprene LDF-5-2ó3-4-4 Catalog page 30	Latex Products Hawthorne, NJ	

A block diagram of the motor drive pointing mirror electronics is shown in Figure 9.3. An 8-bit microprocessor is used to define and control the motor drive logic. A laser fire inhibit is generated whenever the pointing mirror is not in the commanded position. The pointing mirror data is in Table 9-2, the commands in Table 9-3, and the power requirements in Table 9-4.

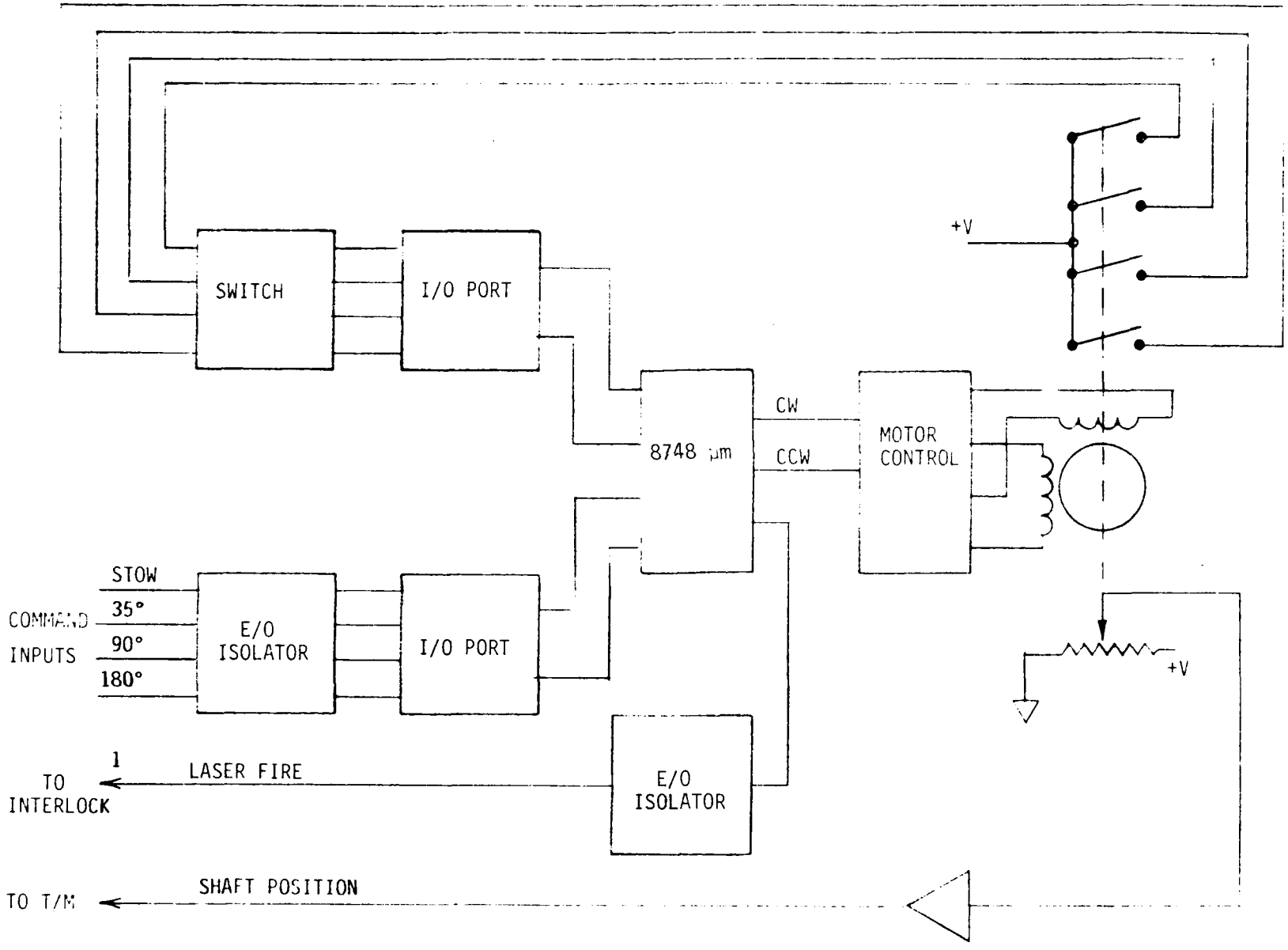

Figure 9.3 Motor Drive Electronics

TABLE 9-2

POINTING MIRROR DATA

MIRROR ANGLE	T/M LINK NUMBER	RESOLUTION (BITS)	SAMPLING FREQUENCY (Hz)
STOW	2	10	1
$+35^{o}$	1	1	10
$+85^{o}$	1	1	10
$+180^{o}$	1	1	10
DRIVE CW	1	1	10
DRIVE CCW	2	1	1
	2	1	1

TABLE 9-3

POINTING MIRROR COMMANDS

STOW	
+ 35°	
+ 85°	
+ 180°	
TOTAL	4

TABLE 9.4

POINTING MIRROR POWER REQUIREMENTS

28 Vdc	2 AMP	UPON COMMAND
28 Vdc	0.1 AMP	STANDBY

10.0 CLOUD MONITOR

When the lidar system is to be used in the nadir-looking mode of operation, it is desirable to determine in advance the type of cloud cover in the field of view. We have specified a monitor to operate in the 10-13 μm region of the infrared, where the clear atmosphere is essentially transparent. Specifications of the cloud monitor are given in Table 10-1.

Thick clouds are good blackbodies and their emission is, of course, dependent on their temperature. Figure 10.1 shows the spectral radiances from a downward-looking satellite system.[15] Also shown are blackbody spectral radiance curves for several temperatures. If we assume the clouds are optically thick and at the approximate temperature of the ambient at the given altitude,[16] then their spectral radiance at 10 μm would be as shown in Figure 10.2.

The cloud monitor has its own mirror in the pointing mirror system (See Section 9.0). It is coated with the same protected aluminum as the other mirrors. The pointing mirror system design limits the use of the cloud monitor to the nadir-looking mode only, which is the only mode of interest.

The cloud temperature will be determined from the detector signal corresponding to the temperature difference between the clouds in the field of view and the chopper. The chopper temperature will be monitored with a temperature sensor. This temperature will be passively maintained at approximately 300°K by appropriate thermal packaging. The 90 Hz chopped signal from the detector amplifier will be synchronously demodulated, filtered, and sent to telemetry.

The cloud monitor data, command, and power requirements are given in Table 10-2.

TABLE 10-1

CLOUD MONITOR SPECIFICATIONS

FIELD OF VIEW	4 mr
DETECTOR	
Type	HgCdTe (PV)
Operating Temperature	77°K
Active Area	0.2 mm diameter
D* (λ_{max}, f_{max})	>1 x 10^{10}
FILTER	
Type	Multilayer Interference
Passband	10-13 μm
Transmission	60% (ave.)
LENS	
Material	Germanium, A-R coated
Clear Aperture	2.5 cm diameter
F/no.	F/2.0
CRYOGENICS	
Cryogen	Liquid Nitrogen
Dewar-Hold Time	12 hours
CHOPPING	
Frequency	90 Hz
Chopper Temperature	~300°K

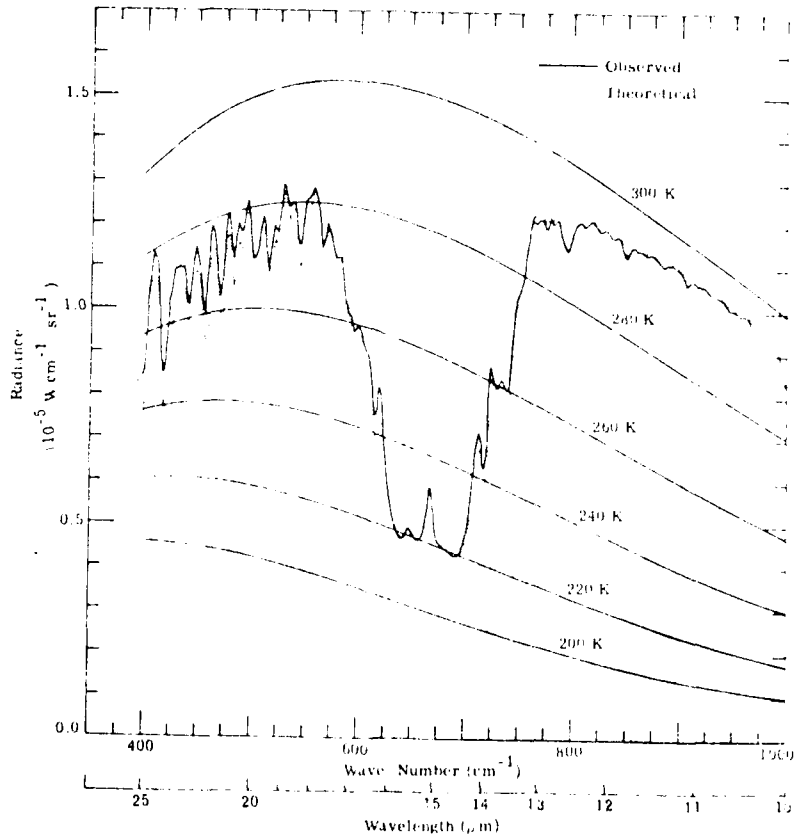

Figure 10.1 Infrared Terrestrial-atmospheric Radiation Satellite Data

AD-A095 366 VISIDYNE INC BURLINGTON MASS F/G 4/1
BALLOONBORNE LIDAR EXPERIMENT.(U)
DEC 80 O SHEPHERD, G AURILIO, R D BUCKNAM F19628-80-C-0094
UNCLASSIFIED VI-577 AFGL-TR-80-0373 NL

2 of 2
AD A 095366

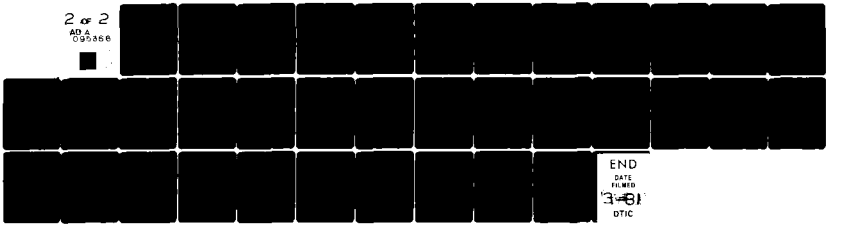

END
DATE FILMED
3-81
DTIC

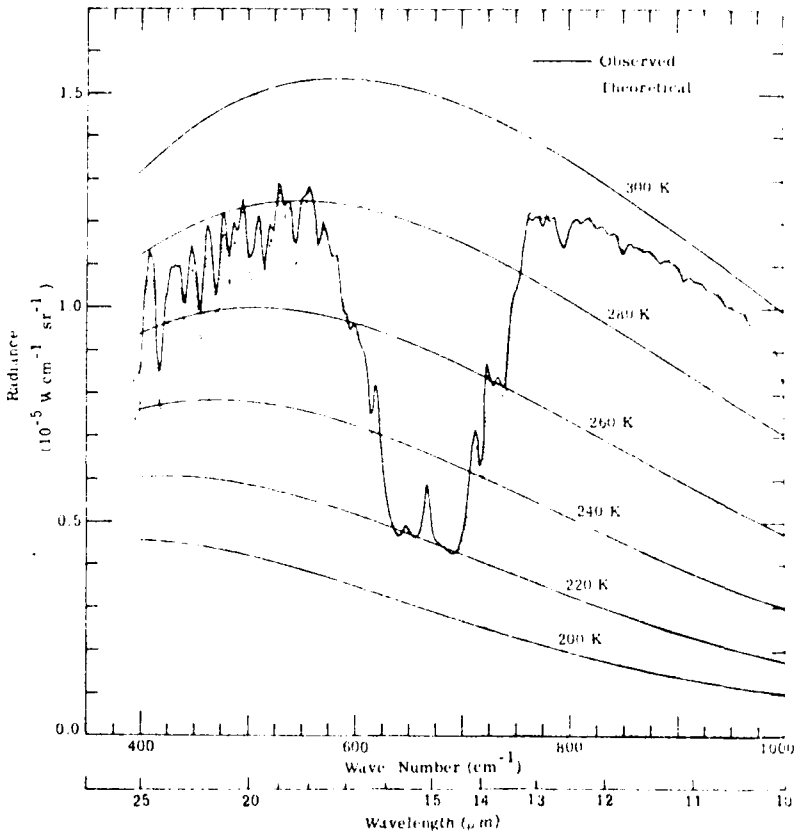

Figure 10.1 Infrared Terrestrial-atmospheric Radiation Satellite Data

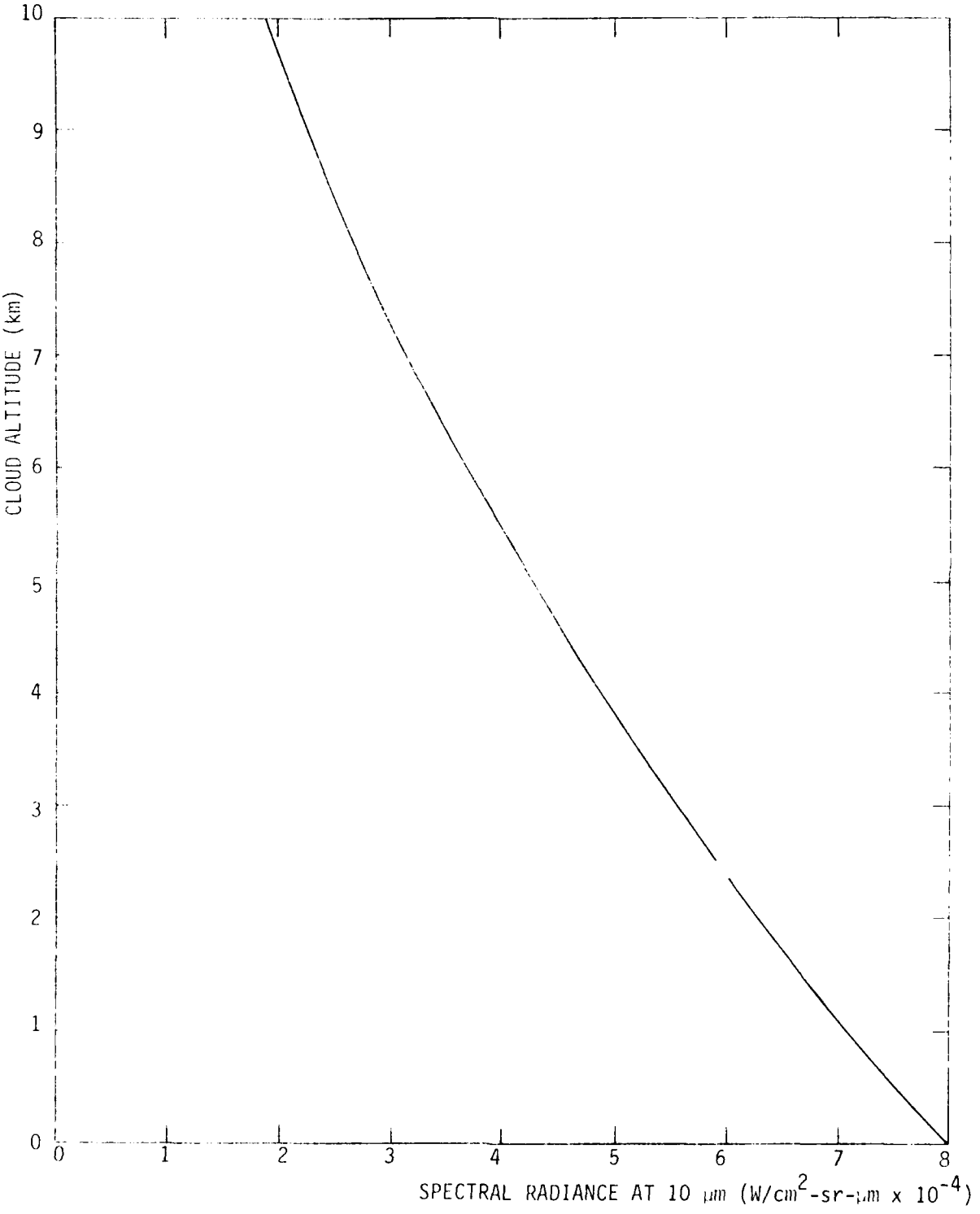

Figure 10.2 Spectral Radiance of Clouds vs Cloud Altitude

TABLE 10-2

CLOUD MONITOR REQUIREMENTS

	T/M Link Number	Resolution (Bits)	Sampling Frequency (Hz)
DATA			
Radiometer Data	2	10	1
Chopper Temperature Monitor	2	10	1
COMMAND			
None Required			
POWER			
28 Vdc 1 Amp.			

11.0 THERMAL CONTROL SYSTEM

11.1 Introduction

The laser and its power supplies generate approximately 1000 watts of heat during operation. This heat must be eliminated from the payload system. The most efficient method to remove the waste heat is by radiation to space. The design of the thermal control system is complicated slightly by the laser requirements for use of a de-ionized cooling fluid.

The selected laser for the lidar payload comes equipped with a cooling system which must be integrated by means of a heat exchanger into a secondary cooling system. This second system then carries the unwanted heat from the laser cooling system to the radiator which radiates the heat to space.

Figure 11.1 shows a schematic of the proposed system.

11.2 Cooling System Parameters

The purpose of this section is to define the parameters for the lidar cooling system. These parameters are as follows:

1. system operating temperatures
2. coolant flow rate
3. types of heat exchanger
4. coolant flow line sizes
5. radiator area.

The laser system must be maintained within certain temperature limits. The maximum allowable temperature is 35°C (95°F). The minimum allowable temperature is 5°C (41°F). The total heat generated by the laser system is 1000 watts. As the laser itself must use de-ionized water with glycol to prevent freezing, a heat exchanger is required between the laser and the radiator. This is to transfer heat from the de-ionized water/glycol system of the laser to the water/glycol mixture of the radiator. The heat exchanger schematic is shown in Figure 11.2.

11.2.1 Heat Exchanger Parameters - The first item of interest is to determine ideally the coolant temperature differences required to remove 1000 watts (3412 BTU/hr) of heat. We have selected a coolant flow rate of 1 gal/min in both the hot and cold sides of the heat exchanger which corresponds to a flow rate of 535 lbsm/hr. Then the heat exchanger temperature differences can be calculated from the following:

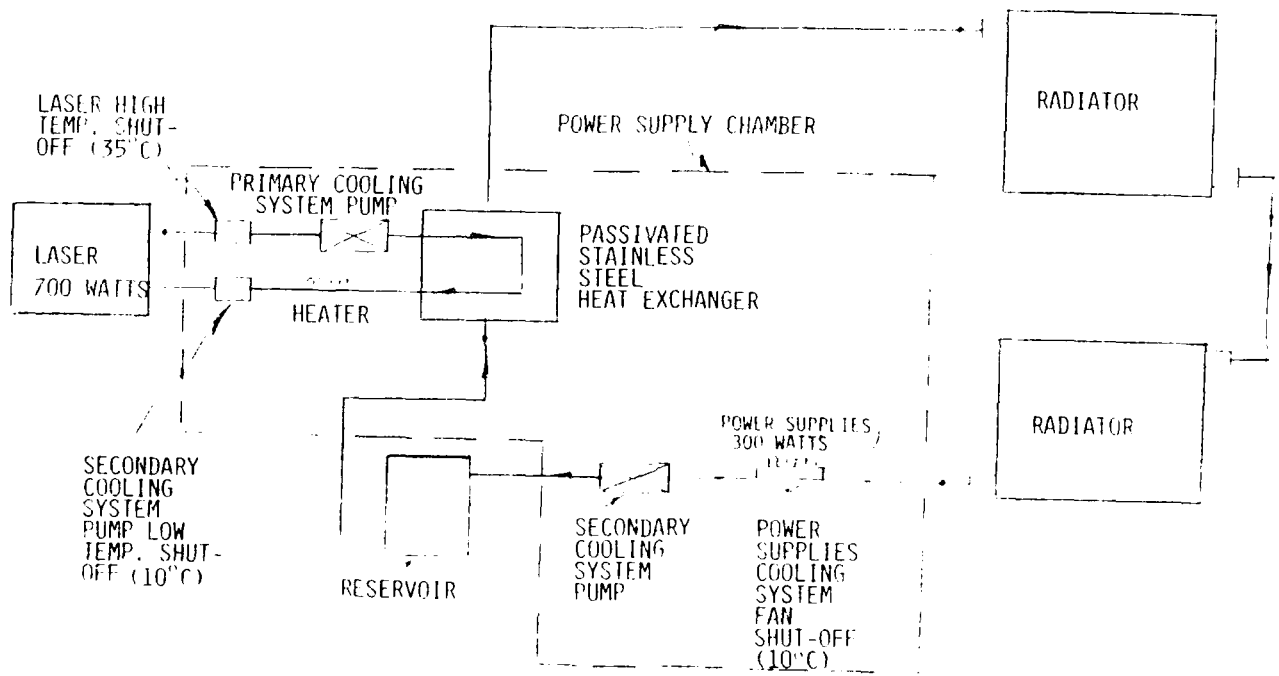

Figure 11.1 Lidar Cooling System

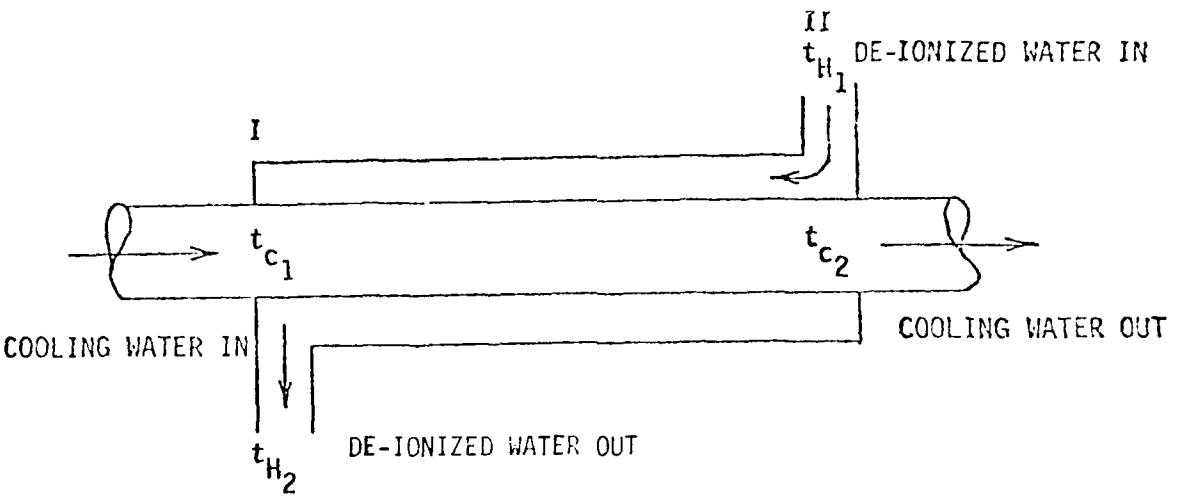

Figure 11.2 Heat Exchanger Schematic

$$q = WC_p\Delta t$$

$$\Delta t = \frac{q}{W C_p} = \frac{3412}{(535)(.9)} \sim = 9^\circ F$$

$q = 3412$ BTU/hr
$W = 535$ lbm/hr
$W_H = 535$ lbm/hr
$C_p = 0.70$ BTU/lbm°F

The laser maximum and minumum allowable temperatures are $t_{H\ MAX} = 95^\circ F$ and $t_{HMIN} = 41^\circ F$.
In order to allow as much margin as possible, the hot side temperature difference of 9°F will be centered between these two temperature extremes such that $t_{H1} = 72^\circ F$ and $t_{H2} = 63^\circ F$. The heat transfer in the heat exhanger is governed by the hot side heat transfer coefficient (h_H) and the cold side heat transfer coefficient (h_c).

For turbulent water flow in straight pipes, the heat transfer coefficient, h, can be defined by the following:[17]

$$h = \frac{0.008\,[1 + 0.011t]G^{0.8}}{D^{0.2}}$$

where t = temperature (°F),
G = mass velocity (lbm/hr ft^2),
and D = tube diameter (ft).

The coolant flow area, A', of the tubing having a .56" outside diameter and a .04" wall is 9.62×10^{-4} ft^2. then the mass velocities are

$$G_c = W_c/A' = 556133 \text{ lbm/hr ft}^2$$

$$G_H = W_H/A' = 556133 \text{ lbm/hr ft}^2$$

and the heat transfer coefficient is:

$$h_H = 1035 \frac{\text{BTU}}{\text{hr ft}^2\text{°F}}$$

$$h_c = 794 \frac{\text{BTU}}{\text{hr ft}^2\text{°F}}$$

The overall heat transfer coefficient, U, in BTU/hr ft^2°F is defined by the following expression:[118]

$$\frac{1}{U} = \frac{1}{h_h} + \frac{x/12}{k} + \frac{1}{h_c}$$

where x = Tube wall thickness (in.)

K = Thermal conductivity of tube wall = 110 (BTU/hr ft_2°F/ft).

Substituting the previously determined values yields an overall heat transfer of 457 BTU/hr ft^2°F.

In order to calculate the length of a single pass counterflow heat exchanger, the following equation will be used:[118]

$$\frac{1}{U} \; LN \frac{\Delta t_{o_{II}}}{\Delta t_{o_I}} = \frac{\Delta t_{o_{II}} - \Delta t_{o_I}}{q} \; A$$

where A = exchanger wall surface area,

$\Delta t_{o_{II}} = t_{H_1} - t_{C_2} = 72-42 = 32$°F

and $\Delta t_{o_I} = t_{h_2} - t_{C_1} = 63-32 = 31$°F

Solving the equation for A and substituting gives an area, A, equal to 36.57 in^2. Then the length, ℓ, of the heat exchanger tubing is simply

$$\ell = A/\pi b = 21.7 \text{ in.}$$

In order to shorten possibly the above single pass counterflow heat exchanger length, a two pass heat exchanger was also examined. The length of a double pass heat exchanger was determined to be 11.5 inches.

11.2.2 Radiator Area and Design - When the average temperature of the radiator is 37°F (3°C), it will reject heat at about 26 watts/ft^2 (89 BTU/ft^2). The radiation area required is then 3412/89 = 38 ft^2. The radiator temperature used here is based upon experimental measurements of a radiator panel on a balloon payload (BAMM) at float altitude.

A radiator system which includes three radiating panels, each measuring 15 ft^2 has been designed. They will be mounted on three vertical sides of the payload structure excluding the fourth side where the mirror pointing system is mounted. Losses due to the roll bars being in the radiating field of view will be more than made up by the additional radiation from the difference between the actual total plate area of 45 ft^2 and the required area of 36 ft^2.

Radiation into space of the heat generated by electronic equipment and telemetry transmitters has been used on another balloonborne payload designed by Visidyne.[19] This radiator was constructed using a special technique for bonding the aluminum radiating panels to the coolant tubing. This technique is described in the following paragraphs.

The radiating plate of .125" thick aluminum received the heat input through an array of rectangular tubing 1" x 1/2" outside dimensions. The tubing was held in place against the aluminum plate by means of mechanical brackets spaced evenly along the plate. The plates were connected to a manifold on the input side which in turn connected to a pumping system of two pumps in parallel. On the output side, each tube was welded to a round piece of tubing able to accept a 1/2" quick-disconnect fitting which connected each loop to the appropriate electronic instrument to be cooled.

In order to enhance heat transfer between the rectangular tubing and the radiating panel, a conductive epoxy (Allied Resin Corporation AKCON T 516 A epoxy tooling material) was used. The epoxy was poured between the tubing and the plate in a way that the gap between the two was filled with the first pass. The second pass formed a fillet on one side and a third pass formed a fillet on the other side, thus affording the best heat path between the tubes and the plate.

The radiation of the panels will be enhanced by a coat of special Nextel Velvet Coating manufactured by Decorating Products Division of 3M Company. This paint has an absorptivity of the sun's rays of 0.2 and an emissivity at the radiator temperature of 0.85.

The laser chamber and the laser power supply chambers will be fitted with external fiberglass insulation to minimize the heat flow through the chamber walls.

The laser system must be capable of continuous operation both in-flight and on the ground. To prevent overheating during ground operation, an auxilliary liquid air heat exchanger will be mounted in the laser chamber. During ground operation, cooling water will be circulated through the auxilliary heat exchanger to remove the excess heat from inside the laser chamber.

The thermal control data are in Table 11-1, the commands in Table 11-2, and power in Table 11-3. The system operational interlocks are summarized in Table 11-4.

TABLE 11-1

THERMAL CONTROL DATA

	T/M Link Number	Resolution (Bits)	Sampling Frequency (Hz)
Temperature			
Primary Coolant Reservoir	2	10	0.1
Secondary Coolant Reservoir	2	10	0.1
Radiator 1	2	10	0.1
Radiator 2	2	10	0.1
Radiator 3	2	10	0.1
Laser Optical Bench	2	10	0.1
Laser Optical Bench	2	10	0.1
Laser Power Supply	2	10	0.1
Liquid-Liquid Heat Exchanger	2	10	0.1
Secondary Coolant Pump ON	2	1	1
Power Supply Heat Exchanger Fan ON	2	1	1
Primary Coolant Heater ON	2	1	1
Optical Bench Heater ON	2	1	1
Secondary Coolant Flow	2	1	1

TABLE 11-2

THERMAL CONTROL COMMANDS

Secondary Coolant Pump ON
Secondary Coolant Pump OFF
Secondary Coolant Pump AUTO

Total Commands 3

TABLE 11-3

THERMAL CONTROL POWER

Primary Coolant Pump	Included in Laser Power Budget
Secondary Coolant Pump	2 amps
Primary Coolant Reservoir Heater	1 amp
Laser Optical Bench Heater	2 amps
Heat Exchanger Fan	1 amp
Electronics	1 amp

NOTE: Heaters and secondary coolant pump will not normally be operated simultaneously.

TABLE 11-4

THERMAL CONTROL SYSTEM OPERATIONAL INTERLOCKS

Temperature of Primary Coolants Greater than 35°C	Laser Shuts Down
Temperature of Primary Coolants Less than 10°C (Secondary pump is auto-mode)	Secondary Coolant Pump Shuts Off Primary Coolant Heater Turned On
Power Supply Heat Sink Temperature Less than 10°C	Liquid to Air Heat Exchanger Fan is Shut Off
Laser Optical Bench Less than 20°C	Optical Bench Strip Heater is Turned On

12.0 PAYLOAD ELECTRONICS

12.1 Power

The prime power source of the payload will be Ag-Zn batteries. The payload will be capable of being easily setup to be powered by laboratory power supplies for ground testing.

The payload battery requirements are summarized in Table 12-1.

12.2 Telemetry

The payload telemetry will consist of two independent links of PCM data. Link 1 will carry the primary scientific data while Line 2 will carry the engineering diagnostic and monitoring data. A summary of the payload telemetry requirements is in Table 12-2.

12.3 Command

The experiment design has been based on the assumption that all commands will be in the form of contact closures at command distribution. All command functions are electro-optically isolated within the experiment. A summary of the payload command requirements is given in Table 12-3.

12.4 Interface

The initial requirements for payload cabling and interconnections have been established.

12.5 Compass

The balloonborne lidar payload will use a simple compass as a heading reference. The compass will be the Model 101 Marine Heading Sensor made by DigiCourse, Inc., in New Orleans, Louisiana. This sensor is an opto-electronically read magnetic compass that transmits heading information via a five-conductor cable to a Model 250 Interface Unit.

The internal gimballing accommodates plus or minus 70 degrees in pitch and roll. The binnacle contains compensation magnets mounted at each end of two plated brass rods that run at 90 degrees to each other across the binnacle near the bottom. Should deviation influences in the guidance package be too great to be fully corrected by the standard magnets, all four magnets can be replaced by a set of stronger magnets supplied by the manufacturer. Table 12-4 gives detailed specifications for the compass.

TABLE 12-1

PAYLOAD BATTERY REQUIREMENTS

Battery	Amp-Hrs.	System
A	80	Laser
B	80	Laser
C	80	Laser
D	80	Laser
E		Telemetry
F	80	Lidar Receiver
G	80	Thermal Control
H		Housekeeping

TABLE 12-2

TELEMETRY

Link Number	Function	Data Rate
1	Scientific	100 kbps
2	Engineering	

TABLE 12-3

COMMAND SUMMARY

System	Number of Commands
Laser	14
Receiver	15
Thermal Control	3
Cloud Monitor	0
Pointing Mirror	4
Unassigned	9
Total Commands	45

TABLE 12-4

SPECIFICATIONS FOR THE MODEL 261A MARINE HEADING SENSOR

Diameter of Spherical Housing including flanges	6.5 inches
Height, including Binnacle	7.0 inches
Weight, including Binnacle	4.5 lbs.
Shock	Capable of meeting MIL-S-901C
Vibration	Capable of meeting MIL-STD-167B
Movement	Two spring-backed sapphire bearings, osmium-tipped pivots
Gimballing	±70° roll and pitch
Resolution	1°
Electronics Description	Infrared LED illuminated phototransistors through Gray coded card. Custom CMOS integrated circuits converts optically coded signal to serial pulse train.
Power Consumption	Range: 2.5 mW to 50 mW (proportional to sampling rate)
Voltage Requirements	Range: 4.5 Vdc to 5.5 Vdc
Output Format	Serial pulse train, N+1 pulses
Output Signal Frequency	Range: Selectable 0.5 kHz to 50 kHz standard 25 kHz
Data Sampling Rate	Range: Selectable 0.5 Hz to 50 Hz standard 25 Hz
Connections	Input voltage, data output, and ground
Temperature Limitations	Operating -40°C to 70°C Storage -55°C to 85°C
Circuit Protection	Reverse polarity, over-voltage
Housing	Waterproof, U/V stabilized Lexan

The Model 250 interfaces the heading sensor output to telemetry. This unit accepts the serial pulse train from the heading sensor and converts it to one of several selectable outputs, as shown in the specifications given in Table 12-5.

TABLE 12-5

SPECIFICATIONS FOR THE MODEL 250 HEADING SENSOR INTERFACE UNIT

Electronics Description	Solid state electronics converts heading sensor data to selected output format through use of CMOS circuitry.
Selectable Outputs	Static parallel binary (9 bit) Static parallel BCD (10 bit) Serial binary Serial BCD True or complement parallel binary or BCD
Output Selection	Selection made by external jumper or switch
Output	Digital, buffered with CMOS type 4050 buffer, analog, zero to 3.59 Vdc
Voltage Requirements	7 Vdc to 20 Vdc
Current	6 milliamps (constant)
Housing Dimensions	7.5" x 4.7" x 2.0"

13.0 GROUND SUPPORT EQUIPMENT

The lidar payload has been designed to permit full operation in a stand-alone mode. Laser operation is monitored and controlled at the Laser Control Panel on the payload. Receiver analog signals can be monitored at BNC connectors on each receiver chamber. Receiver digitized data can be monitored at the connectors on the front panel of the digitizer. Since the PCM encoded data is in a standard IRIG format, range telemetry systems will be used to decode this data.

The in-flight data readout and display system will require a computer system capable of graphics and hard-copy printout. A recommended system is shown in Figure 13.1. This system would have the capability to display the density data, in near real-time in the formats shown in Section 3.0. The software requirements of this system are listed in Table 13-1.

TABLE 13-1
REQUIRED SOFTWARE

RT-11 OPERATING SYSTEM

FORTRAN IV

PLOT 10

LIDAR CODE MODIFIED TO INPUT PCM DATA

A listing of ground support equipment required for launch field support is in Table 13-2. It should be noted that a clean room facility will be required at the payload building area for final laser alignment, assembly, and testing.

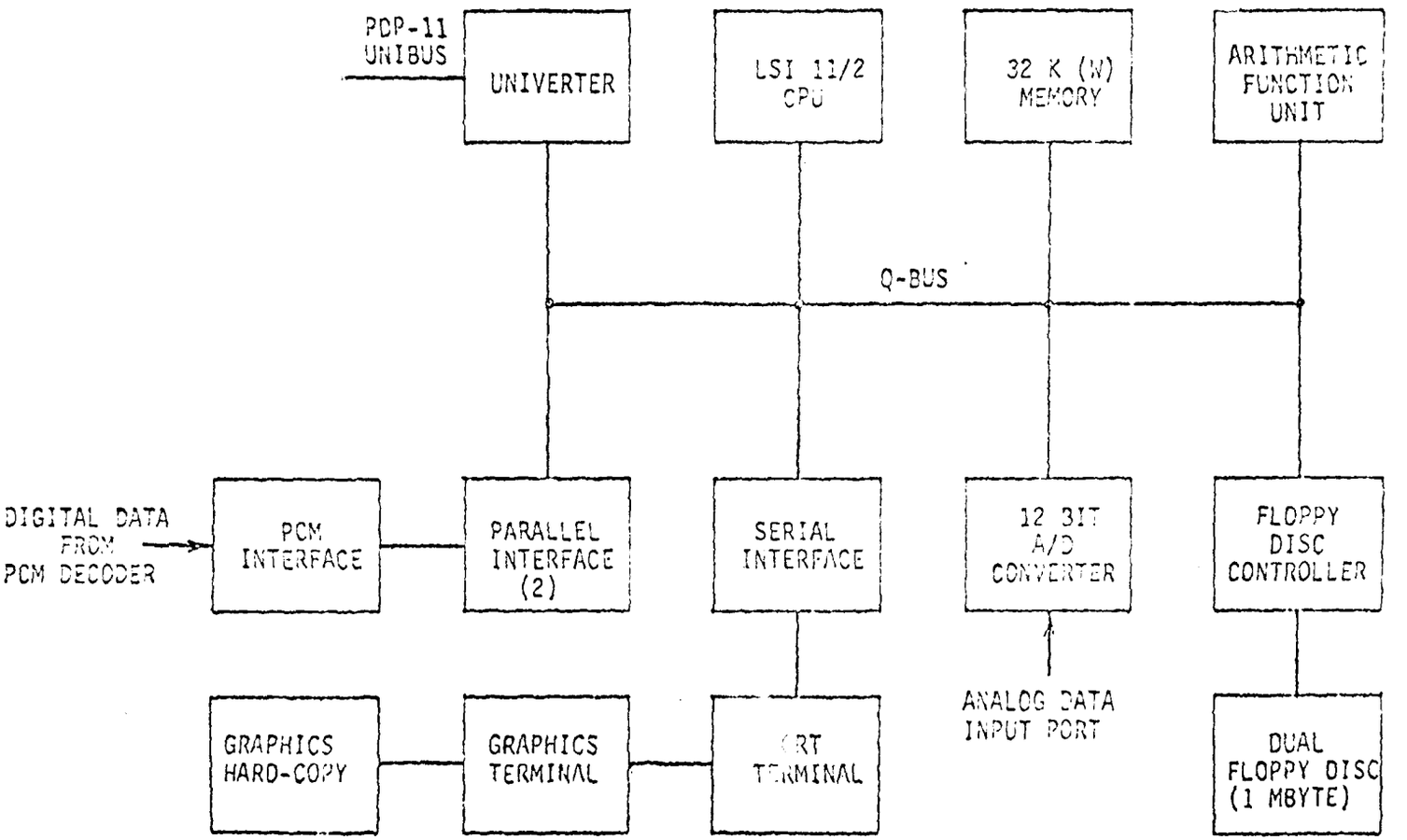

Figure 13.1 Recommended Lidar Data System

TABLE 13-2

GROUND SUPPORT EQUIPMENT

Battery Charging Power Supplies and Cables

EG&G 581 Laser Radiometer

Auto Collimator

Diffusing Screen

2 Meter Optical Bench

2-75 mm Corner Cube Reflector

2-One Kilometer Spool Fiber Optic Communication Cable

1 Theodolite

2 Sets Neutral Density Filters

12 Sets Laser Eye Safety Glasses

6 LS-160 LN_2

1 Small Freezer for VPM-164 Storage

1 Telephone Dialer Alarm

Clean Room Materials as Required

1 ILS Cooling System

1 ILS Line Converter

14.0 TEST PLANS

The following sections describe various test techniques which will be used to calibrate and checkout the lidar system.

14.1 Laser Calibration

A laboratory test plan for the laser is outlined in Table 14-1.

The absolute calibrations of the laser will be done using a standard detector having a radiometer calibration traceable to N.B.S. An EG&G Model 561 Laser Radiometer will be used. The calibration will consist of comparing the absolute output of the laser in joules at each wavelength to the output voltage from the laser radiant power monitor detector.

The 355 and 1064 nm components of the laser output will be separated by dichroic beamsplitters of the same type as used in the receiver optics. The reflected 1064 nm radiation would be incident on one detector and the transmitted 355 nm on another. Studies to determine the effects of beam polarization will be made by rotating the beamsplitters in the laser beam and relocating the detectors accordingly.

Beam homogeneity can be measured at various points along the laser beam axis by using blue line biazo paper or IR-sensitive photographic film and firing the laser. These provide a permanent record of beam homogeneity. The homogeneity should be determined for each of the wavelengths of interest and as a function of the number of pulses fired in the sequence. Measurement of beam homogeneity in the far field, where it enters the receiver field-of-view, is somewhat of a problem. The laser beam (divergence of 2 mr) and the receiver field-of-view first become coincident at a range of about 65 meters, and they are 89% coincident at a range of about 2000 meters. An experiment set-up having a range of 50 meters would not be difficult to attain. At that range, the beam diameter is still only about 10 cm. With a diffuse test target and multifirings of the laser, time exposure (length of exposure to be determined experimentally) photographs should provide all the information required. As the range increases to longer and longer paths, inhomogeneities in the atmosphere will have an increasing effect over the beam uniformity and studies of this effect should be reviewed (Ref. Section 5.4.3.).

The divergence of the beam for each wavelength, will be determined by using suitable filters and scanning the beam with a detector.

TABLE 14-1

TEST PLAN FOR LIDAR LABORATORY CALIBRATION

LASER

- ABSOLUTE RADIANCE PER PULSE AS A FUNCTION OF RADIANT POWER MONITOR AT THREE WAVELENGTHS
- BEAM HOMOGENEITY
- BEAM DIVERGENCE AT THREE WAVELENGTHS
- PULSE AMPLITUDE STABILITY
- PULSE WIDTH
- PULSE TIME JITTER
- LASER TEMPERATURE STABILITY

TABLE 14-2

TEST PLAN LABORATORY LIDAR CALIBRATION

RECEIVER

- OPTICAL ALIGNMENT
- FIELD OF VIEW

LIDAR

- RECEIVER ABSOLUTE CALIBRATION
- RECEIVER TIMING CALIBRATION
  OPTICAL DELAY LINE

Tests will be performed to confirm that the radiating wavelengths of the laser are within the passbands of the receiver interference filters. To do this, the laser will be fired into the detector-beamsplitter set-up described above and filters with passbands identical to those in the receiver inserted one at a time between the laser output and the beamsplitter. The detector readings with the filters in the beam path would then be compared to the appropriate readings taken when the laser was fired without the filter in the beam path. If the difference in the readings is consistent with the peak transmission values, then it can be concluded that the laser is radiating at the proper wavelengths.

14.2 Lidar Calibration

The test plan for the lidar calibration is summarized in Table 14-2. The field-of-view of the receiver will be mapped by using a test photomultiplier in place of one of the flight photomultipliers in the receiver. By using a modulated, collimated point source and securing the receiver section on an X-Y axes mount, the response of receiver as a function of its pointing angles can be measured and the results plotted.

The absolute calibration of the receiver will be done using the calibrated lidar laser as a test source. A transmitting prism with a slight wedge will be placed in the laser beam to deflect the beam axis of the laser to make it coincident with the axis of the receiver at some convenient distance (transmission of the prism to be measured at the wavelengths of interest). A near ideal diffusing surface, made of Eastman White Reflectance Paint, will be positioned in, and normal to, the laser beam path at this distance. When the laser is fired, the photon flux will be incident on a screen which acts as a Lambertian surface.

Because this backscattered flux is many orders of magnitude greater than that predicted to be observed during the flight, it will be necessary to attenuate the received photon flux. Stacks of N.D. 2.0 filters will be mounted in front of the receiver photomultiplier tubes for this calibration.

When the laser is fired, both the laser power monitor signals and the two detector data signals are recorded. The receiver sensitivity constant, K, is the following:

$$K \text{ (photons/count)} = \frac{P \; A_c}{\pi \, \ell_{cal}^2} \alpha \frac{1}{V_{cal}}$$

where P = number of photons radiated in the wavelength lines of interest by the laser during a single pulse as determined from the laser power monitor data.

A_c = receiver telescope collecting area

ℓ_{cal} = distance from defocusing screen to payload

α = neutral density filter attenuation factor

V_{cal} = measured data counts

The receiver sensitivity constant, K, is then used to convert data counts to corresponding intensity values through the above equation.

An advantage of this calibration technique is that it can easily be repeated in the field during payload testing. Thus, complete experiment operational capability can be fully demonstrated at the latest possible time prior to launch. Another advantage of this calibration technique is that it includes and compensates for any timing, spectral, or optical geometry effects in the system.

In addition and in conjunction with throughput testing, the system will be subjected to RFI and light leak testing. For these tests, the neutral density filters are completely blocked and the laser fired. The high gain data signals are monitored on an oscilloscope for any detectable signals.

14.3 Optical Alignment

The nominal alignment requirement is that the optical axis of the receiver be parallel to the laser beam in azimuth and in elevation to 0.2 milliradians or better. The 0.2 milliradians is considered to be an appropriate alignment tolerance because it is small compared to the required system resolution of 2 milliradians but, on the other hand, it is large enough to be readily achievable in practice.

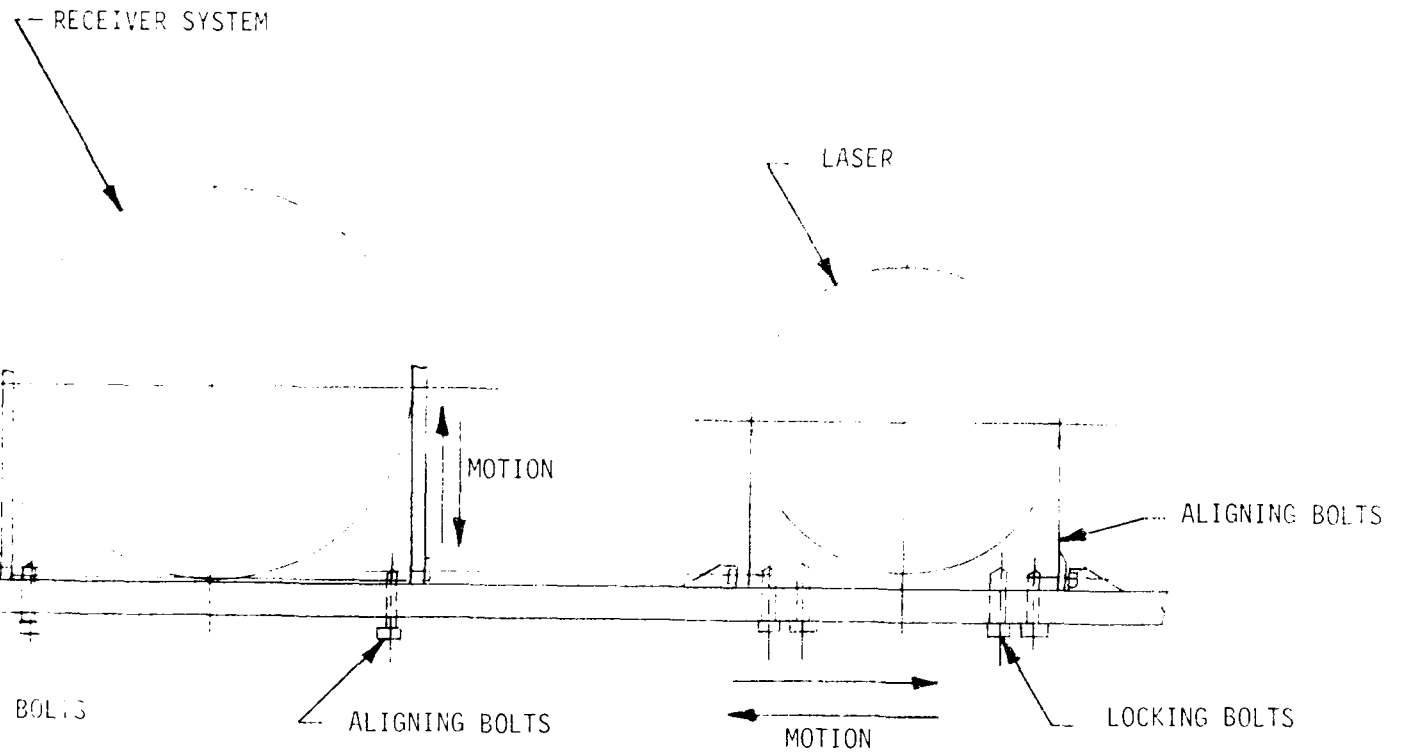

Figure 14.1 Optical Axis Alignment System

The technique for mechanically aligning the optical axes of the lidar transmitter and receiver is shown in Figure 14.1. The transmitter is fastened to the optical deck by eight bolts, which allow side motion parallel to the optical deck to be imparted to the transmitter by adjusting screws at the four corners of the laser container. The receiver is able to be rotated about a horizontal axis through the field stop of the primary mirror.

A pin holds the receiver in place and a set of screws locks it while two adjusting screws change its position in a direction orthogonal to the optical deck.

The procedure for co-aligning the laser beam and the optical axis of the receiver uses a theodolite, a pair of pentaprisms, and a corner cube retro-reflector. This procedure, shown in Figure 14.2, consists of the following steps:

1. As shown in the left half of Figure 14.2, the theodolite (with protective filter) is placed to intercept the laser beam. The base of the theodolite is accurately leveled using a sensitive bubble level. The telescope of the theodolite is then adjusted in elevation until the laser beam is centered on the reticle, as shown. The elevation adjustment of the theodolite is then locked.

2. As shown in the right half of this figure, the theodolite is moved to the vicinity of the axis of the receiver, and the base is again leveled. Two pentaprisms and a cube corner retro-reflector are then positioned to relay the laser beam into the theodolite, as shown. The beam entering the theodolite will be parallel, in the plane of the diagram, to the beam exiting the laser because of the constant 90° deviation property of the pentaprisms and the retro-reflecting property of the cube corner. The pentaprism on the right is then rotated about axis A-A until the laser beam is again centered in elevation on the theodolite reticle. The beam entering the theodolite is now parallel to the beam exiting the laser in the plane perpendicular to the diagram, as well as in the plane containing the diagram.

3. The retro-reflector is now removed, and the laser beam is allowed to enter the receiver optics. Using the degree of freedom shown in Figure 14.1, the system is now adjusted until the image of the laser beam formed by the receiver optics is centered on the field stop. The laser and receiver are now co-aligned.

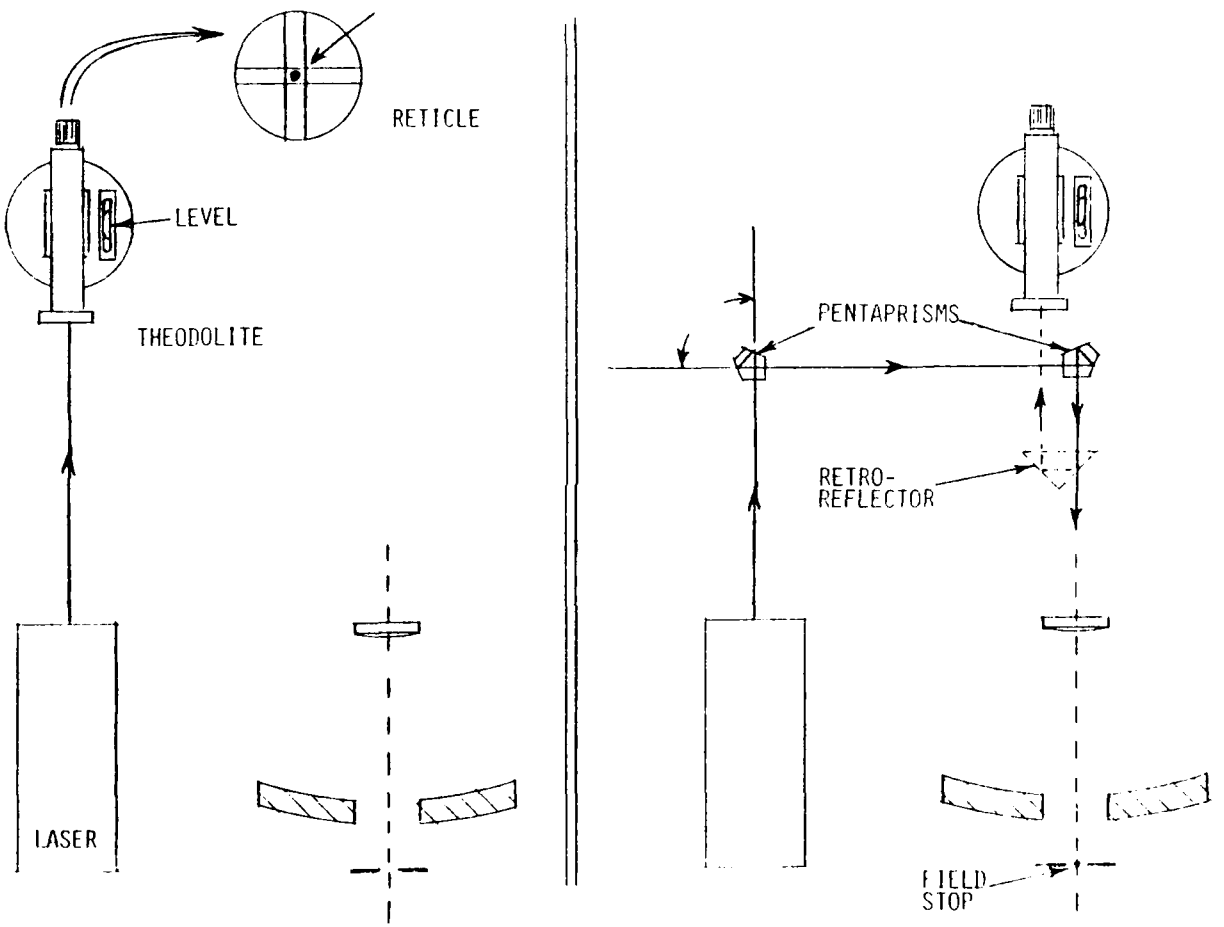

Alignment in the plane of the diagram relies on the constant 90° ray deviation of the pentaprisms.
Alignment perpendicular to the plane of the diagram uses the theodolite and level as references.

Figure 14.2 Optical Alignment of the Laser and the Receiver

14.4 Lidar System Tests

In order to check out the operation of the lidar system, tests are needed in which the laser is fired, the laser radiation enters the receiver optics after a suitable time delay, and resulting signal from the receiver is processed and displayed.

Such tests would check, among other things, the relative timing of the various systems, the wavelength compatability of the transmitter radiation with the receiver passbands, the relative signal levels, and the amount of RF interference between the major sub-systems. Ideally, such tests should also verify correct optical alignment between the receiver and transmitter. Three end-to-end system tests, two of which will verify the state of alignment, will be made.

In the first test technique, a long coil of low-loss optical fiber will be used to transmit a small portion of the laser pulse from the transmitted beam to the entrance aperture of the receiver, with the length of the coil determining the time delay. Coil lengths of one and two kilometers will provide realistic delay times. With this technique, checks could be made of laser operations, receiver operations, relative signal levels, timing and ranging, and wavelength compatability. However, the technique would not verify the state of alignment.

In the second test technique to be studied, the atmopshere will be used as a target by aiming the lidar upward into the night sky. This would verify the operation of all systems except ranging. However, isolated data points to verify the ranging accuracy could be found by aiming the lidar into an overcast sky, providing that the height to the bottom of the overcast could be independently measured.

The third test will use a controlled horizontal range of at least 2 km over which the laser can be fired. By locating two corner cube reflectors at known ranges from the lidar, an absolute calibration of range will be established.

14.5 Pre-flight Tests

A number of the tests and calibration steps previously described will be repeated in the field in preparation for launch. These include measurement of the laser pulse energy with the calibrated detector, measurement of the receiver sensitivity, and verification of proper alignment between

the transmitter and receiver. Also, one of the end-to-end checks will be repeated to verify timing and wavelength compatibility.

Immediately before launch, one of the end-to-end checks will be performed to verify proper operation of the entire lidar system. The most appropriate one is the test using the optical fiber delay line. A light-tight cover containing the optical fiber coil will be fitted over the front of the transmitter and receiver. The laser will then be fired and the various system parameters monitored. This final test will be performed on the runway within an hour of two of launch.

14.6 Engineering Tests

The integration test plan is outlined in Figure 14.3. The environmental test plan is in Table 14-3 and lidar thermovac test plan is outlined in Table 14-4.

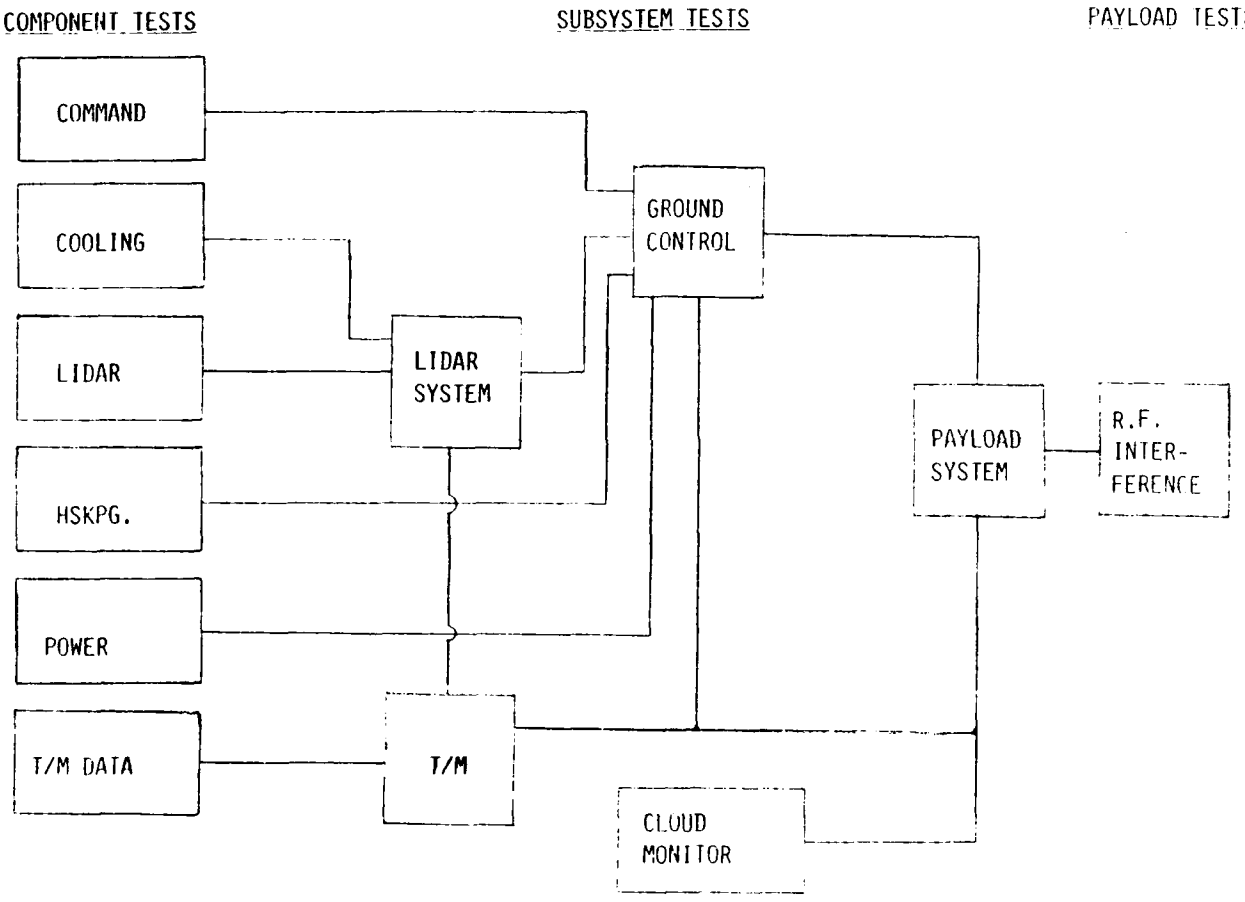

Figure 14.3 Integration Testing

TABLE 14-3

LIDAR ENVIRONMENTAL TEST PLAN

- GROUND TEST AT AMBIENT CONDITIONS OF COMPONENTS.
- COMPONENT TEST UNDER LOW PRESSURE (140,000 FT) CONDITIONS.
- SYSTEM TEST AT AMBIENT CONDITIONS.
- SYSTEM QUALIFICATION TESTING AT AMBIENT CONDITIONS.
- SYSTEM TEST UNDER SIMULATED FLIGHT CONDITIONS - THERMO-VAC.

TABLE 14-4

LIDAR THERMO-VAC TEST PLAN

- SYSTEM CHECK-OUT UNDER AMBIENT CONDITIONS IN ENVIRONMENTAL CHAMBER SIMULATING PRE-LAUNCH CHECK-OUT.

- SIMULATED LAUNCH, PAYLOAD ASCENT AND FLOAT.
  OPERATION OF LIDAR SYSTEM DUPLICATING AN ACTUAL LAUNCH.

- BALLOON LIDAR SYSTEM OPERATION UNDER FLOAT CONDITIONS OF TEMPERATURE AND PRESSURE.

- RECOVERY

15.0 SUMMARY

The purpose of this report is to outline the design of a lidar experiment for the measurement of atmospheric density from a balloon platform. This design includes not only the optical, electronic and mechanical design of the balloonborne lidar but includes overall system and experiment plans. An in-depth study was done of the in-flight eye safety problems to be encountered and safe operational criteria established.

This design is for a state-of-the-art balloonborne instrumentation system in which the following technologies have been applied in order to achieve the experimental goals:

1. Optics
2. Electronics
3. Mechanical structures and pressure vessels
4. Heat transfer
5. Microprocessors
6. Cryogenics

The application of these technologies in the fabrication, assembly, test, calibration, and flight of this experiment will require expertise and craftsmanship in these fields. This design, although complete, will require additional breadboard development of selected components and/or sub-systems and practical hardware engineering will be required in the assembly and test phases of the experiments.

The implementation of this lidar experiment will result in a major advancement in the knowledge of the upper atmospheric density profile.

16.0 REFERENCES

1. "RCA Electro-Optics Handbook", Technical Series EOH-11, RCA Corporation, Harrison, N.J., (1974).
2. "Safety Rules and Recommendations" in Laser Focus Buyers' Guide (1980).
3. Shepherd, O., J.W. Carpenter, W.P. Reidy, W.H. Sheehan, and T.F. Zehnpfennig, "The Design and Flight Test of a 30 kW Rocketborne Electron Accelerator Module (EXCEDE II TEST) HAES Report No. 11, "Final Report, Contract F19628-75-C-0015, AFCRL-TR-75-0379, Visiydne, Inc., 15 July 1975.
4. "American National Standard for the Safe Use of Lasers", ANSI Z136.1-1976 (1976).
5. Brehm, W.F., and J.L. Buckley, "Design Study of a Laser Radar System for Spaceflight Application", G.E. Space Division, AFGL-TR-79-0264 (Dec. 1979).
6. Zuev, V.E., "Propagation of Visible and Infrared Radiation in the Atmosphere", John Wiley and Sons, New York (1974).
7. Hall, F.F., "Atmospheric Effects-Transmission of Optical Radiation Through the Atmosphere", Electro-Optical Systems Analysis Course Notes (C. 1975).
8. Fried, D.L., G.E. Meyers, and M.P. Keister, Jr., Journal of the O.S.A., 57, (1967), 787.
9. Shipley, S.T., and E.V. Browell, "Effect of Scintillation on Eye Safety for Shuttle and Aircraft Borne Lidars (Presented at the 10th International Laser Radar Conference)" NASA Langely Research Center, (October 1980).
10. Shannon, R.R., Smith, W.S., Ceccon, C., Metheny, W. and Philbrick, R.: Atmospheric Phase Distortions, AD-B-03530L, (1978).
11. Hufnagel, R.E.: Propagation through Atmospheric Turbulence, from the Infrared Handbook, Eds. Wolfe, W.L. and Zissis, G.J., Office of Naval Research, Ch. 6, (1978).
12. Drummeter, L.F., Jr., and Hass, G., p. 305 in G. Hass and R.E. Thun (eds), "Physics of Thin Films", Vol. 2, Academic New York, (1964).
13. Denton Vacuum, Inc., Brochure.

14. "Effects of the Variation of Angle of Incidence and Temperature on Infrared Filter Characteristics", OCLI Inc., Technical Report.
15. ANSI/IEEE Std. 583-1975, IEEE Standard Modular Instrumentation and Digital Interface System (CAMAC)
16. IRIG Telemetry Standard, 106-80
17. Conrath, B.J., et al., J.G.R. 75, (1970), 5821.
18. "U.S. Standard Atmosphere", NOAA-S/T 76-1562, Washington, D.C., "October 1976).
19. "Kent's Mechanical Engineers' Handbook, Power Volume", J.K. Salisbury, (editor), John Wiley & Sons, Inc., New York (1957).
20. "Heat Transmission", W.H. McAdams, McGraw-Hill Book Co., Inc., New York, (1954).
21. Brooke, R.W., G. Aurilio, R.D. Bucknam, A.G. Hurd, W.H. Sheehan and O. Shepherd, "Balloon Altitude Mosaic Measurements (BAMM)", Final Report, Contract No. F19628-78-C-0086, AFGL-TR- , Visidyne, Inc., 26 November 1980.

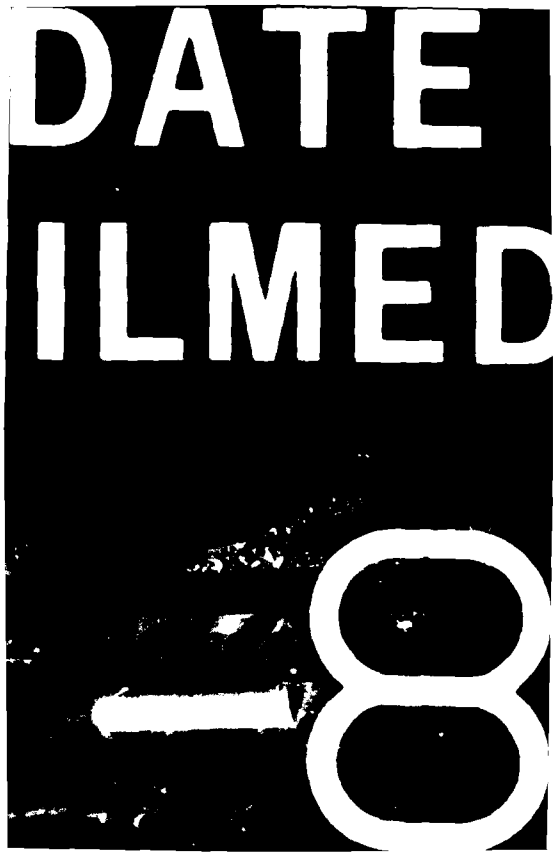
DATE
ILMED
8